

MASTER

MIMO controller design for a respiratory module

Geeven, M.J.E.F.

Award date:
2019

[Link to publication](#)

Disclaimer

This document contains a student thesis (bachelor's or master's), as authored by a student at Eindhoven University of Technology. Student theses are made available in the TU/e repository upon obtaining the required degree. The grade received is not published on the document as presented in the repository. The required complexity or quality of research of student theses may vary by program, and the required minimum study period may vary in duration.

General rights

Copyright and moral rights for the publications made accessible in the public portal are retained by the authors and/or other copyright owners and it is a condition of accessing publications that users recognise and abide by the legal requirements associated with these rights.

- Users may download and print one copy of any publication from the public portal for the purpose of private study or research.
- You may not further distribute the material or use it for any profit-making activity or commercial gain



EINDHOVEN UNIVERSITY OF TECHNOLOGY
DYNAMICS AND CONTROL GROUP

MECHANICAL ENGINEERING

MIMO controller design for a respiratory module

MASTER'S THESIS
D&C NUMBER: DC 2019.092

M.J.E.F. GEEVEN
1020646

Supervisors: ir. J.M.F. Reinders DEMCON and TU/e
dr. ir. S.J.L.M. van Loon DEMCON
dr. ir. T.A.E. Oomen TU/e
prof. dr. ir. N. van de Wouw TU/e

November 26, 2019

Abstract

This thesis describes the design process of a feedback and feedforward control strategy for a multi-input multi-output mechanical ventilation system with expiration valve. A mechanical ventilation system is used to assist patients who are not able to breathe sufficiently on their own. When applied to a patient, the mechanical ventilation system is used to achieve a desired pressure and flow control objective for the lungs of the patient. Pressure tracking performance is important in mechanical ventilation systems, and a poor performance can easily over-extend the patient's lungs and cause ventilation-induced lung injuries. Flow control is used to achieve a refreshing flow inside the mechanical ventilation system to wash out CO_2 -rich air. Strong coupling effects between pressure and flow are present in the mechanical ventilation system. The state-of-practice controller for the mechanical ventilation system does not take these coupling effects into account, and achieves a sub-optimal performance using a complex control structure.

In this thesis, a feedback and feedforward control strategy are designed to improve the pressure and flow tracking performance, while also achieving a more insightful controller design which is easy-to-use for control engineers. The main strategy for the controller design is to base the feedforward controller on known and fixed components of the ventilation system, i.e., the hose system, ventilation module, and expiration valve. Thereafter, a feedback controller is designed which attenuates unknown disturbances, such as, model uncertainties, a coughing patient, or a twisted breathing hose.

The feedforward controller is designed using a parametric model of the ventilation module, expiration valve, and patient. Using the steady-state characteristics of this model, it is possible to design a patient-independent feedforward controller. A feedback controller is designed on the basis of system identification experiments to characterize the plant dynamics, because of the significant model uncertainty and non-linearities of the parametric model. The feedback controller is designed using a decentralized multi-input multi-output control structure.

An experimental case-study of the derived control strategy has shown that the controller is not yet suitable to outperform the state-of-practice controller of the ventilation system. The reason for this is that unknown highly non-linear dynamics of the patient and expiration valve deteriorate the pressure and flow tracking performance. Undesired pressure and flow overshoot is observed. Although the desired performance is not yet achieved, the designed controller is more insightful compared to the state-of-practice controller and provides a suitable foundation for performance improvements in future research for this application.

Acknowledgments

First of all, I would like to thank my TU/e supervisors prof. dr. ir. Nathan van de Wouw and dr. ir. Tom Oomen for the academic guidance throughout my Master graduation project. The strong discussions at the university taught me to be more critical about my research and helped me to complete this graduation project. I would also like to thank Joey Reinders and Bas van Loon of DEMCON Macawi, for the day-to-day support at DEMCON Macawi, and also for providing me with the mechanical ventilation set-up, which allowed me to experimentally verify my research goals. At DEMCON I was also able to experience an actual working environment with many motivating colleagues that were always available for advice.

I would like to thank my parents and sister for constantly motivating me during this intense Master graduation project. Finally, I thank my girlfriend Fabienne who helped me to relieve my doubts during the more difficult parts of this project.

Contents

Abstract	I
Acknowledgments	II
1 Introduction	1
1.1 Mechanical ventilation system description	2
1.2 Pressure-controlled ventilation cycle	3
1.3 Control problem	4
1.3.1 Control challenges	5
1.3.2 State-of-the-art solutions	5
1.3.3 High-level control strategy	6
1.4 Research objectives	7
1.5 Report layout	8
2 System modeling	9
2.1 Patient-hose-valve model	9
2.1.1 Patient model	9
2.1.2 Patient-hose model	10
2.1.3 Expiration valve	11
2.1.4 Derivation of a patient-hose-valve state-space model	13
2.2 Open-loop stability for bounded inputs	14
2.3 Output switching condition	15
2.4 Summary	16
3 Feedforward controller design	17
3.1 Feedforward design motivation	17
3.1.1 High-level controller design	18
3.2 Constant steady-state solution of the patient-hose-valve system	19
3.3 Expiration valve look-up table	20
3.4 Limitations of the feedforward controller	22
3.5 Frequency domain alternative strategy	22
3.6 Summary	23
4 Feedback controller design	24
4.1 Decentralized feedback control motivation	24
4.1.1 Control limitations of the non-linear state-space model	24
4.1.2 Motivation for a decentralized solution	27
4.2 System identification	28
4.2.1 Experimental set-up	28
4.2.2 Obtaining a MIMO FRF	28
4.2.3 Interaction analysis	30
4.3 Decentralized feedback controller design	32
4.3.1 Decentralized controller tuning	32
4.3.2 MIMO stability	33
4.4 Stability under switched output signals	36

4.4.1	Linearized closed-loop dynamics	36
4.4.2	Switching scenarios	37
4.5	Summary	38
5	Simulations and experimental verification	39
5.1	Performance measure and use-case description	39
5.2	Verification of the feedforward controller	40
5.2.1	Feedforward controller: simulation results	40
5.2.2	Feedforward controller: experimental results	41
5.3	Verification of the feedback controller	43
5.3.1	Feedback controller: simulation results	43
5.3.2	Feedback controller: experimental results	44
5.4	State-of-practice control compared to the proposed controller design	46
5.5	Summary	47
6	Conclusions and Recommendations	48
6.1	Conclusions	48
6.2	Recommendations	50
6.2.1	Improved model accuracy	50
6.2.2	Reset integrator for C_{1fb}	50
6.2.3	Pressure bound for C_{2fb}	52
	Bibliography	55
	Appendix A Steady-state solution	56
	Appendix B LUT experiment for the expiration valve	57
B.1	Purpose	57
B.2	Set-up	57
B.3	Method	57
B.4	Limitations	58
	Appendix C TU/e Code of Scientific Conduct	59

Chapter 1

Introduction

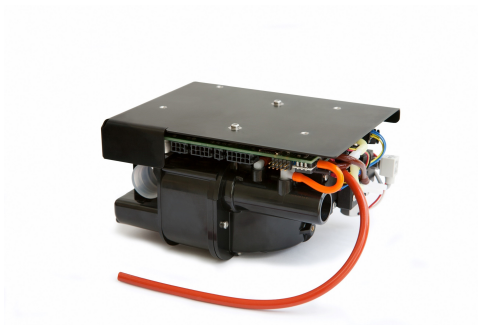
Many patients on the Intensive Care Unit (ICU) or during hospital transportation are unable to breathe sufficiently on their own. Hence, they require the assistance of a mechanical ventilation system. Mechanical ventilation systems can be used to take over the full respiratory cycle, which is often done for patients who are in a coma or during surgery. In less severe conditions, mechanical ventilation systems can partially take over the breathing efforts of the patient, for instance, during the recovery period after a surgery. Mechanical ventilation systems are widely used in practice and can apply many different breathing modes to suit the need of every patient. Fig. 1.1a shows an example of a mechanical ventilation system in an ICU setting.

Mechanical ventilation systems generate a positive pressure near the airway of the patient, which results in an air flow to the lungs. For this research project, a blower-driven mechanical ventilation system is considered, which compresses ambient air from the surrounding area. Fig. 1.1b shows a typical ventilation module for a mechanical ventilation system, which is produced by Macawi [1]. The mechanical ventilation system can be used with a variety of oxygen mixtures corresponding to the needs of each patient. Positive pressure ventilators use a hose system to guide the air from the blower to the patient. Every hose system requires an air leak to refresh CO_2 -rich air, thereby preventing the patient from inhaling his/her previously exhaled air. For this project, the leak is actively regulated by means of an expiration valve.

Control plays an important role in mechanical ventilation systems, in particular lung pressure control. A lung pressure overshoot leads to over-extension of the patient's lungs, which is recognized as one of the main causes of Ventilation Induced Lung Injuries (VILI) [2]. In addition, if the lung pressure drops too far, an alveolar collapse can occur which causes shear stress lung damage in a relatively short time span [3]. It is concluded that tight pressure control is an important aspect in mechanical ventilation. Furthermore, the mechanical ventilator controller must also be



(a) Example of a mechanical ventilation system in practice.



(b) Macawi ventilation module used in mechanical ventilation systems.

Fig. 1.1. A mechanical ventilation system in use and a ventilation module produced by Macawi [1].

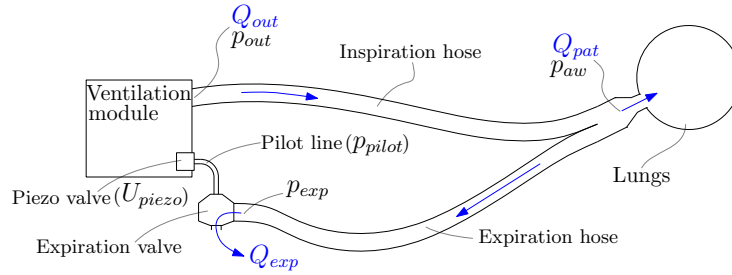


Fig. 1.2. Schematic visualization of the mechanical ventilation system with patient.

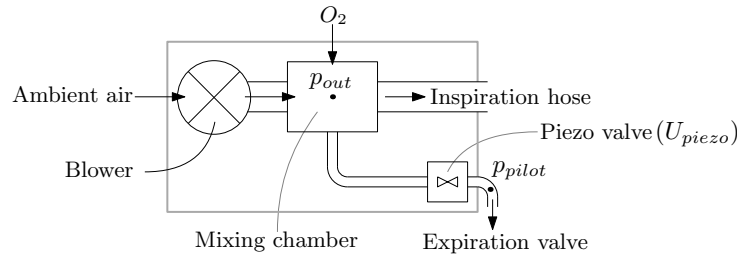


Fig. 1.3. Detailed schematic of the ventilation module and its main components.

robust for unknown disturbances, such as, a coughing patient or a twisted breathing hose. The mechanical ventilation system must be applicable for a large variety of patients, which requires state-of-the-art control solutions. The focus of this thesis is on improving and simplifying an existent control solution for a mechanical ventilation system with expiration valve.

First, in Section 1.1, the main components of the mechanical ventilation system are described. Thereafter, in Section 1.2, the breathing cycle and the main purpose of the mechanical ventilation system in this cycle is explained. The control problem and the main challenges for this research project are defined in Section 1.3. Thereafter, the challenges are combined to a well-defined research objective in Section 1.4. Finally, in Section 1.5, the layout of this thesis is provided.

1.1 Mechanical ventilation system description

This section describes the main components of the mechanical ventilation system. The blower, hose system, and expiration valve are all part of the mechanical ventilation system. Fig. 1.2 shows the most important components and parameters of the mechanical ventilation system with patient. **The blower** uses ambient air to generate a blower outlet pressure, i.e., p_{out} . Additional oxygen can be added in a mixing chamber if required. However, in this thesis this is not considered. The pressure generated by the blower results in an airflow Q_{out} , which enters the beginning of the **inspiration hose**, see Fig. 1.2. The generated O_2 -rich airflow propagates through this hose towards the patient during inspiration. The flow entering or leaving the patient is called the patient flow Q_{pat} and the pressure just before the patient is called the patient airway pressure p_{aw} . After the gas exchange inside the lungs, the CO_2 -rich air leaves the patient and enters the **expiration hose**. This hose connects the patient with the expiration valve, and is used to direct CO_2 -rich air out of the patient during expiration.

The **expiration valve** is located at the end of the expiration hose, and controls the expiration flow Q_{exp} leaving the hose system. The pressure just before the expiration valve is denoted as p_{exp} . The expiration valve is pressure controlled and can be actuated using the pressure inside a pilot line, i.e., p_{pilot} . Fig. 1.3 shows a more detailed schematic of the ventilation module, which shows the location of the blower, piezo valve, and the mixing chamber. The pressure inside the pilot line originates from the pressure inside the mixing chamber. This pressure is guided through the piezo valve, which uses a voltage U_{piezo} to adapt p_{out} to the desired pressure p_{pilot} . This pressure is then used to open and close the expiration valve, and, therewith, control the flow going through

the expiration valve. As a result, the airflow through the expiration valve is determined by both p_{out} and U_{piezo} . In the next section, the pressure-controlled ventilation cycle for the mechanical ventilation system and patient in Fig. 1.2 is explained.

1.2 Pressure-controlled ventilation cycle

This section describes the pressure-controlled ventilation cycle, which is considered in this thesis. The mechanical ventilation system is equipped with a large variety of ventilation modes. However, this work only focuses on the Continuous-Mandatory Ventilation (CMV) mode with a pressure-controlled ventilation cycle, see [4] and [5]. Pressure-controlled ventilation focuses on applying the correct air pressure to a patient which results in a patient flow. In this mode, spontaneous effort of the patient is not taken into account, which means that it is also not in scope for this research. In addition, this work only focuses on ventilation of adult patients, which means that neonates and pediatric patients are not considered as well.

Fig. 1.4a shows a set of pressure-controlled ventilation cycle graphs for a mechanical ventilation system with expiration valve. The first graph shows the pressure target p_{target} (dashed black) and a typical response of the airway pressure p_{aw} (solid red) to that target. This airway pressure p_{aw} is measured just before the mouth of the patient. The lower pressure target for the airway pressure is called the Positive End Expiratory Pressure (PEEP) which ensures that the patient experiences a certain minimum lung pressure to prevent collapsing of the lung. The Inspiratory Positive Airway Pressure (IPAP) is used as an upper pressure target. The values for IPAP and PEEP are typically set by hospital personnel, depending on the patient. The second graph shows the patient flow Q_{pat} that enters and leaves the patient, and the third graph shows the blower flow Q_{out} that is going through the inspiration hose. The fourth graph shows the expiration flow Q_{exp} that leaves the hose system through the expiration valve. The following four phases are defined during a pressure-controlled breathing cycle:

- I. **Inspiration phase 1,**
- II. **Inspiration phase 2,**
- III. **Expiration phase 1,**
- IV. **Expiration phase 2.**

Inspiration phase 1 (I) in Fig. 1.4a indicates the pressure build-up from PEEP to IPAP. This increase in pressure results in an air flow entering the lungs of the patient. During this phase, the expiration valve is slightly opened to allow some flow from the blower to circulate through the hose system. This flow is called the 'baseflow', and is used to refresh the hose and to wash out the CO_2 -rich air present in the system. The baseflow target is indicated as Q_{bf} in Fig. 1.4a. Fig. 1.4b shows in red where and when baseflow is present in the hose system. The patient flow is indicated in blue.

Inspiration phase 2 (II) starts when the patient is filled with O_2 -rich air and the IPAP pressure is achieved. During this phase the airway pressure p_{aw} is kept constant while the same baseflow Q_{bf} is provided by the blower and expiration valve. Notice that there is no patient flow during this period, the baseflow goes completely through the expiration valve. The constant pressure and zero patient flow allows for gas exchange inside the lungs which is the main purpose of mechanical ventilation.

In **Expiration phase 1 (III)**, the airway pressure drops from IPAP to PEEP which results in a negative patient flow, i.e., the patient is breathing out the CO_2 -rich air. This patient flow is guided through the expiration hose towards the expiration valve. During this phase, the expiration valve is operated to a more open position, such that the CO_2 -rich patient air can leave the system. Due to the more open position of the expiration valve, the patient experiences a minimal breathing resistance. During this phase, the baseflow level Q_{bf} is still maintained near the blower, i.e., $Q_{out} = Q_{bf}$.

Finally, in **Expiration phase 2 (IV)**, the breathing cycle is finished. The mechanical ventilation system controls pressure at PEEP level and sustains a baseflow through the complete hose system. During this phase, the patient flow is zero and a new breathing cycle can be initiated depending on the ventilation mode.

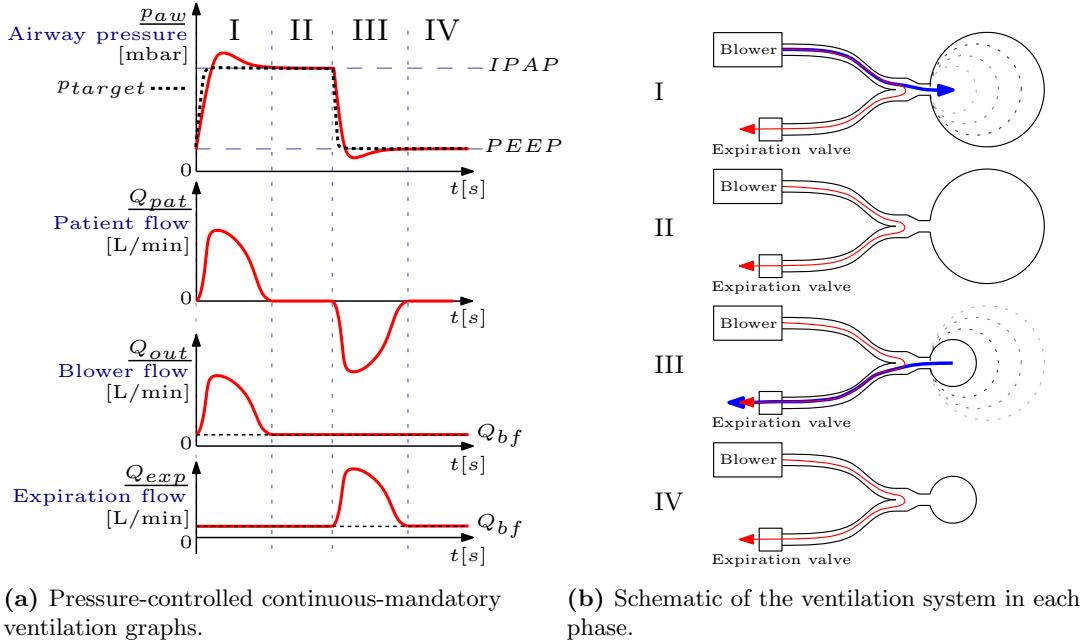


Fig. 1.4. The pressure-controlled breathing cycle is divided in four phases. The red lines in b represent the baseflow and the blue lines the patient flow.

1.3 Control problem

This section describes the high-level control problem for the mechanical ventilation of a patient during the pressure-controlled ventilation cycle. To fully carry out the pressure-controlled ventilation cycle, the mechanical ventilation system has a pressure and a flow tracking objective.

The pressure tracking objective is defined for the airway pressure p_{aw} . As shown in Fig. 1.4a, the airway pressure p_{aw} should track the pressure target p_{target} during each phase of the breathing cycle. The flow tracking objective is defined for the baseflow requirement of the pressure-controlled breathing cycle. The baseflow target is defined as Q_{bf} in the bottom two figures of Fig. 1.4a. It is observed that baseflow is present at Q_{out} during phase II, III, and IV, and at Q_{exp} during phase I, II, and IV. Notice that baseflow target Q_{bf} is not always maintained by Q_{exp} or Q_{out} . During phase I, for instance, it is impossible for Q_{out} to maintain the baseflow target, because this would conflict with the inspiration flow towards the patient, see Fig. 1.4a and 1.4b. During phase III, it is physically impossible to maintain baseflow at Q_{exp} , because this would conflict with the flow leaving the patient during expiration.

From the bottom two figures in Fig. 1.4a it is concluded that there is always a baseflow present somewhere in the hose system. However, this baseflow cannot be observed at one location during the whole breathing cycle. As a result, the baseflow target Q_{bf} is achieved using a combination of Q_{exp} and Q_{out} . To summarize, the pressure and flow tracking objectives are defined as:

1. The airway pressure p_{aw} should track the pressure target p_{target} .
2. The baseflow target Q_{bf} is maintained during each phase of the breathing cycle using a combination of Q_{exp} and Q_{out} .

To achieve the airway pressure and baseflow objective, the mechanical ventilation system uses the following two inputs:

1. The blower outlet pressure p_{out} .
2. The piezo valve voltage U_{piezo} .

As a result, the pressure-controlled ventilation cycle is considered a Multi-Input Multi-Output (MIMO) control problem.

To reach the desired objectives, several control challenges arise regarding the mechanical ventilation system and patient. In the next section, the main control challenges for this project are defined. After that, in Section 1.3.2, state-of-the-art control solutions for mechanical ventilation systems are presented. Finally, in Section 1.3.3, the high-level control strategy for the mechanical ventilation system is defined.

1.3.1 Control challenges

This section describes the control challenges that are encountered to achieve the desired objectives from the previous section. The following control challenges are defined:

1. Multi-variable input-output coupling is present between p_{out} and U_{piezo} and the two control objectives. The blower pressure p_{out} is used to generate pressure inside the hose system. In addition, p_{out} and the piezo valve voltage U_{piezo} together control the expiration valve, and thus the expiration flow leaving the hose system. As a result, both inputs are coupled to the expiration valve and opening the expiration valve influences both control objectives at the same time. It is concluded that input-output coupling is present in the system, which makes this MIMO control problem challenging.
2. Robustness for varying-load dynamics. The main objective of a mechanical ventilation system is to ventilate the patient, which means that the patient dynamics are part of the system to be controlled. The mechanical ventilation system is applied to a large variety of patients. The dynamics differ from patient to patient, and can even be slowly varying when a patient is healing or deteriorating. Consequently, this induces a significant amount of model uncertainty and unknown disturbances to the control problem.
3. Incomplete definition of the baseflow target. The baseflow target Q_{bf} is not fully defined in each phase of the breathing cycle for one single output. Although it is concluded that there is a baseflow present somewhere in the hose system during each phase, the baseflow target cannot be maintained at one location during the whole breathing cycle. As a result, it is not possible to use a single output to control the baseflow target Q_{bf} during the complete breathing cycle.

These control challenges are encountered when solving the control problem. In the next section, state-of-the-art control solutions for mechanical ventilation systems are shown and it is argued that they do not solve the above mentioned control challenges.

1.3.2 State-of-the-art solutions

The state-of-the-art control of mechanical ventilation systems is explored in this section. Even though the use of mechanical ventilation systems is applied on a world-wide scale, the number of relevant papers on control applied to ventilation are limited. Possible reasons include, the relatively straight-forward PID control structures that are often used in practice, or due to company confidentiality. Model-based control strategies are often used for mechanical ventilation systems and require the derivation of a dynamical model. This can either be done by fitting a Frequency Response Function (FRF) measurement, or by developing a parametric model which captures the dynamics of the system.

A few approaches on parametric modeling for the hose system, expiration valve, and patient dynamics have been developed in literature. In [6], many methods are described for linear and non-linear models for lung dynamics, which include the airway resistance and lung compliance, i.e., the inverse of stiffness. In [7], one specific strategy from [6] is emphasized, which models the patient and hose system using the knowledge and lay-out of an electrical circuit. Modeling strategies for expiration valves are also presented in literature. In [8], for example, the modeling process of a voice coil actuated expiration valve is presented, which is used for simulations of a complete mechanical ventilation system. A different valve model is suggested in [9], which models a voice coil expiration valve as a mass-spring-damper system. [10] applies the same strategy, and introduces a force balancing method which also applies for pressure-actuated expiration valves. A flow-based model is presented in [11], which describes a fluid-flow analytical model for several

critical locations around the expiration valve. The model shows a high accuracy compared to a finite element model. The patient models in [6] and [7] are suitable for control. However, the expiration valve models in [8]-[11] are mainly applied as simulation tools for flow analysis. The application in actual control strategies for mechanical ventilation systems is limited.

A few suitable control designs for mechanical ventilation systems can be found in literature. In [12], for instance, a model-based control design is applied which uses a linear lung and hose model. Spontaneous breathing effort is estimated using a disturbance observer. However, this method focuses on one specific patient type and requires identification of each patient beforehand to achieve the desired performance. In a different approach, [13] describes a variable-gain controller which switches between a high-gain and low-gain controller to distinguish between two conflicting control goals, i.e., a short pressure rise time and limited flow oscillations.

To improve performance of feedback control strategies for mechanical ventilation systems, additional learning and estimation-based control strategies have been studied which incorporate unknown dynamics and resistances. An Iterative Learning Control (ILC) approach is applied by [14], this work takes into account unknown lung and hose parameters. This control technique uses information from previous breathing cycles to improve the performance of the next cycle. When this ILC control strategy is applied, the unknown repeating errors are almost completely eliminated and very high pressure tracking performance can be achieved. However, ILC is only applicable in the case of a repetitive breathing stroke. Disturbances, such as, a coughing patient, a twisted hose, and other non-repeating disturbances are not taken into account using ILC and slow down the learning rate of the controller, and thus its performance. A different approach is applied by [15], who uses an adaptive controller with estimator which compensates for the unknown pressure drop along the hose system. Although this adaptive control design does not show an increased performance compared to an ILC design, it can perform well without a repetitive breathing pattern and it guarantees robustness against spontaneous breathing efforts.

Although these control strategies show great performance improvements for mechanical ventilation systems, they are mainly focused on ventilators that require only one control objective, for instance, pressure or flow tracking. Additionally, they only use one input to control the system, which is either an inspiration/expiration valve or the blower pressure p_{out} . The involvement of multiple actuators and control objectives for mechanical ventilation systems is not yet investigated. To conclude, the current state-of-the-art control solutions are not suitable, or require more research, to apply for this MIMO control problem. In the next section, a high-level control strategy is derived for the control problem.

1.3.3 High-level control strategy

This section presents the considered high-level control strategy for the MIMO control problem, taking into account the control challenges from Section 1.3.1. As discussed, the mechanical ventilation system consists of a ventilation module, hose system, and expiration valve. In addition, the patient is also part of the control system, see Fig. 1.2. The control strategy for this control system is to derive a MIMO feedforward and feedback control strategy to achieve the two objectives that are presented at the beginning of Section 1.3. This control strategy also aims to tackle the control challenges stated in Section 1.3.1. The high-level control strategy is visualized in Fig. 1.5, in which C_{ff} represents the feedforward controller, C_{fb} represents the feedback control strategy, and G represents the hose system, expiration valve, unknown patient dynamics, and the ventilation module.

The first control challenge, i.e., the input-output coupling problem, is tackled by deriving a dynamical model of the mechanical ventilation system. Using this model, it is possible to describe the coupling between the inputs and outputs. Next, a feedforward controller is derived which incorporates these coupling effects. The main idea of the feedforward controller is to compensate for all system components that are fixed and known, i.e., the inspiration hose, expiration hose, ventilation module, and the expiration valve characteristics. These components do not change over time which means that they can be compensated for by means of a feedforward control strategy.

Thereafter, a feedback controller is designed to tackle the second challenge, i.e., to attenuate unknown disturbances, e.g., a coughing patient, a twisted hose, and modeling uncertainty due to the large variety of unknown patient dynamics. The third challenge, i.e., the incomplete definition

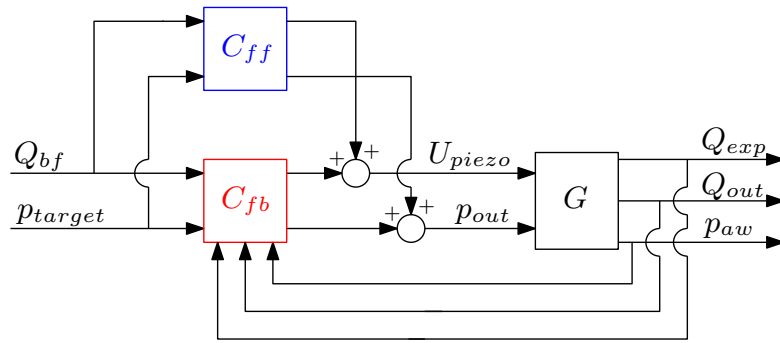


Fig. 1.5. High-level control block scheme. C_{fb} is the feedback controller, C_{ff} is the feedforward controller, and G represents the hose system, expiration valve, ventilation module, and the patient dynamics.

of the baseflow target Q_{bf} , is tackled using a switching algorithm, which is explained in Chapter 2. The design of the feedforward and feedback controller is presented in Chapter 3 and Chapter 4, respectively. In the next section, the research objectives and sub-objectives are presented for this project.

1.4 Research objectives

This section provides the research objectives for this project. The state-of-practice controller that is currently running on the mechanical ventilation system, is designed without the use of a parametric model. As a result, the cause of the coupling effects between flow and pressure are not fully understood, and are therefore not incorporated in the controller design, which results in a sub-optimal performance. To partially improve this sub-optimal performance, the state-of-practice controller design is expanded with multiple ventilation-related events, such as, triggers, gain scheduling, and resets, that over-complicate the controller design.

Given the complexity of the state-of-practice controller design and its sub-optimal performance, the main objective for this research project is defined as:

Design a controller for a mechanical ventilation system with expiration valve to improve both pressure and baseflow tracking performance, by taking into account the coupling between pressure and flow in the design process.

This objective can be achieved by splitting up the main objective in several smaller sub-objectives:

- *Derive a dynamical model of the breathing hose system, expiration valve, and patient, which is suitable for a controller design.*
- *Using the dynamical model, establish a well-defined feedforward control strategy which takes the pressure and flow coupling into account.*
- *Design a feedback controller that controls the large variety of unknown patient dynamics, and attenuates unknown disturbances. Minimize the use of triggers, resets, and gain scheduling to obtain a controller design which is insightful and easy-to-use for control engineers.*
- *Experimentally test the designed controllers.*

These sub-objectives are used again in Chapter 6 to draw conclusions about the findings of this work. In the next section, the layout of this thesis is provided.

1.5 Report layout

This thesis is structured as follows; First, in Chapter 2, a dynamical model is derived for the patient-hose-valve system. After that, in Chapter 3, a feedforward controller is designed based on the dynamical model from Chapter 2. In Chapter 4, a feedback controller is designed to increase the robustness against unknown disturbances, such as a coughing patient or modeling errors. Thereafter, in Chapter 5, the feedforward and feedback controller are verified using simulations and an experimental case-study. Finally, in Chapter 6, the main conclusions are presented which are compared to the research objectives of Section 1.4. In addition, recommendations for future research are also provided in Chapter 6.

Chapter 2

System modeling

In this chapter, the dynamical model of the considered patient-hose-valve system is derived as described in the first sub-objective of Section 1.4. The model consists of the patient dynamics, inspiration hose, expiration hose, and expiration valve. This model is used to gain insight in the system dynamics. Furthermore, the obtained model is used to derive a steady-state feedforward strategy in Chapter 3. First, in Section 2.1, the patient-hose-valve model is derived. In Section 2.1.4, the derived model is rewritten as a non-linear state-space model. Stability of the open-loop system with bounded inputs is analyzed in Section 2.2. An output switch is defined in Section 2.3, which deals with the incomplete baseflow definition. Finally, the main conclusions are summarized in Section 2.4.

2.1 Patient-hose-valve model

In this section, the model for the patient-hose-valve system is derived. First, the patient model is derived in Section 2.1.1. Then, the hose system is added to the patient model in Section 2.1.2. Thereafter, the system is extended by adding the expiration valve to the model. The complete patient-hose-valve model is rewritten as a non-linear state-space model in Section 2.1.4.

2.1.1 Patient model

This section describes the process of deriving a patient model which consists of patient's lungs and the airway. In this work, a linear one-compartmental lung model is considered as described in [6]. A first-order differential equation is used to describe the lung dynamics as

$$p_{lung}(t) = \frac{1}{C_{lung}} \int Q_{pat} dt \quad \rightarrow \quad \dot{p}_{lung}(t) = \frac{1}{C_{lung}} Q_{pat}, \quad (2.1)$$

where p_{lung} is the lung pressure in mbar, \dot{p}_{lung} describes the time derivative of the lung pressure, Q_{pat} is the patient flow, i.e., the flow going in and out of the lungs in L/min, and C_{lung} is the lung compliance, i.e., inverse of stiffness, in L/mbar. A schematic visualization of the lung and its most relevant parameters is shown in Fig. 2.1. The patient's airway is added to the lung model, which connects the lungs to the patient's mouth. The patient flow Q_{pat} , that enters and leaves the lung, flows through the airway. The patient flow depends on the airway resistance, and

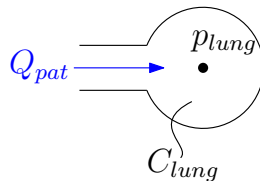


Fig. 2.1. Schematic visualization of the lung.

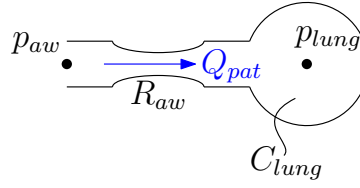


Fig. 2.2. Schematic visualization of the lung and the airway with the relevant parameters.

the pressure difference between the lung pressure and the pressure just before the airway. This relation is described by

$$Q_{pat} = \frac{p_{aw} - p_{lung}}{R_{aw}}, \quad (2.2)$$

where p_{aw} is the pressure at the start of the patient's airway, i.e., the airway pressure, and R_{aw} is the airway resistance in mbar s/L. Fig. 2.2 shows a schematic representation of the lung and the airway with the relevant parameters. The first-order lung differential equation in (2.1) is extended to the full patient model by substituting (2.2) in (2.1), which results in

$$\dot{p}_{lung} = \frac{p_{aw} - p_{lung}}{C_{lung}R_{aw}}. \quad (2.3)$$

2.1.2 Patient-hose model

This section describes the process of obtaining a model for the inspiration and expiration hose, which is combined with the patient model. The inspiration hose connects the patient's airway with the ventilation module. The total airflow through the inspiration hose depends on the hose resistance, and the the pressure difference between the pressure at the beginning of the inspiration hose, i.e., p_{out} , and the pressure at the end of the inspiration hose, i.e. p_{aw} . A similar flow-pressure relation as in (2.2) is derived for the inspiration hose, which is

$$Q_{out} = \frac{p_{out} - p_{aw}}{R_{hose1}}, \quad (2.4)$$

where Q_{out} is the flow through the inspiration hose, p_{out} is the pressure generated by the blower at the beginning of the inspiration hose, and R_{hose1} is the inspiration hose resistance in mbar s/L. Besides the inspiration hose, there is also an expiration hose, which is used to guide the exhaled CO_2 -rich air away from the patient. The expiration hose attaches to the patient's airway and the expiration valve. The flow through the expiration hose is denoted as Q_{exp} in L/min. This flow depends on the expiration hose resistance, in combination with the pressure difference between the patient's airway and the pressure just before the expiration valve, i.e., p_{exp} in mbar. The resulting equation for the expiration flow Q_{exp} is defined as

$$Q_{exp} = \frac{p_{aw} - p_{exp}}{R_{hose2}}, \quad (2.5)$$

where R_{hose2} is the expiration hose resistance. Fig. 2.3 shows the complete model of the patient-hose system, which includes the patient, the inspiration hose, and the expiration hose. The system is considered to have no leaks, hence, conservation of flow gives the following relation:

$$Q_{pat} = Q_{out} - Q_{exp}. \quad (2.6)$$

In other words, the difference between Q_{out} and Q_{exp} gives the patient flow Q_{pat} . Flow can only be generated by the blower, and can only leave the system through the expiration hose, i.e., $Q_{out} \geq 0$ and $Q_{exp} \geq 0$. The constraint $Q_{out} \geq 0$ is established mechanically by means of a check valve in the ventilation module. The constraint $Q_{exp} \geq 0$ is automatically imposed, because the patient can only breath in through the inspiration hose, and breath out through the expiration hose. These constraints are insightful, but they are not incorporated in the patient-hose model.

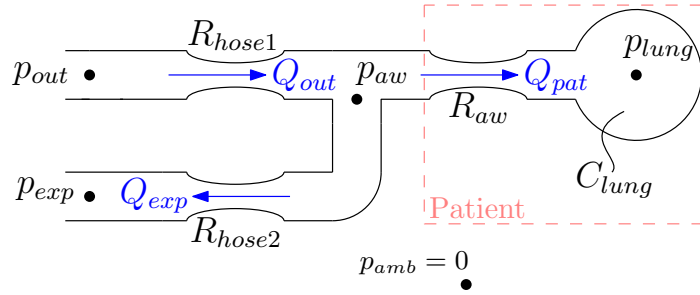


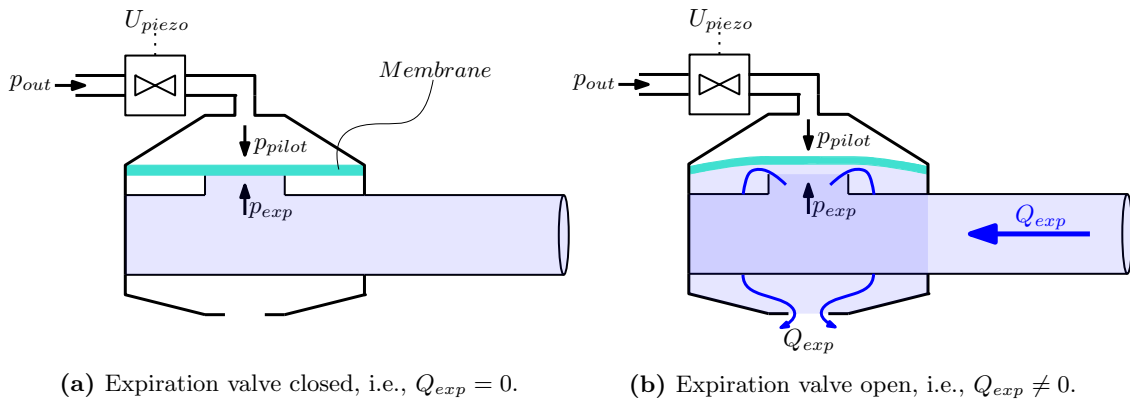
Fig. 2.3. Schematic drawing of the patient-hose system.

The blower that generates the pressure p_{out} is equipped with an internal controller. This internal blower controller is used to control p_{out} to the desired pressure set-point $p_{control}$. This controller reduces the error made as a result of the blower actuator dynamics. Given the focus of this research project, the blower dynamics and internal controller are not taken into account. As a result, the blower dynamics are assumed to be perfectly controlled by the internal controller, i.e., $p_{control} = p_{out}$.

2.1.3 Expiration valve

This section describes a technique to model the expiration valve as a variable resistance. To derive the full model of the patient-hose-valve system, an expiration valve model is added to the patient-hose model. The expiration valve is shown schematically in a closed and open position in Fig. 2.4a and 2.4b, respectively. As described in Section 1.1, the valve is pressure actuated by p_{pilot} . This pilot pressure is generated by the blower, i.e., p_{out} . To achieve the desired p_{pilot} , p_{out} is scaled using a piezo valve. By changing the voltage to the piezo valve, i.e., U_{piezo} , the desired pilot pressure p_{pilot} is obtained. The piezo valve voltage is set between -24V and 24V. Thus, -24V means that the piezo valve is completely closed, i.e., $p_{pilot} = 0$. 24V means that the piezo valve is completely open, i.e., $p_{pilot} = p_{out}$. The scaled pressure propagates through the pilot line to actuate the expiration valve. Inside the expiration valve, the pressure p_{pilot} exerts a force to the top side of a membrane, see Fig. 2.4. The expiration pressure p_{exp} exerts a force to the bottom side of the membrane in opposite direction. The force difference results in a deflection of the membrane, which allows air to flow through. Using this knowledge, the expiration valve is modeled as a variable resistance R_{exp} , which depends on p_{pilot} and p_{exp} , i.e.,

$$R_{exp} := R_C(p_{pilot}, p_{exp}), \quad (2.7)$$



(a) Expiration valve closed, i.e., $Q_{exp} = 0$.

(b) Expiration valve open, i.e., $Q_{exp} \neq 0$.

Fig. 2.4. Schematic of the pressure actuated expiration valve in an open and closed position.

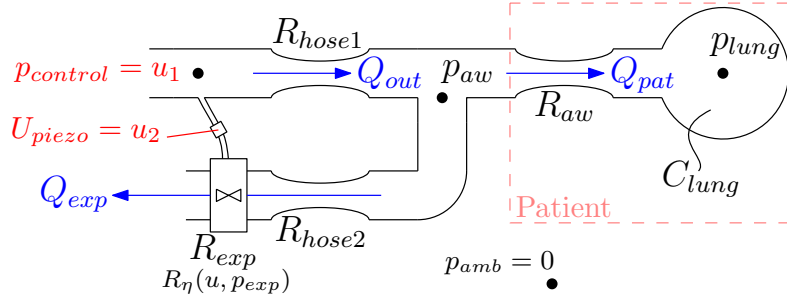


Fig. 2.5. Schematic drawing of patient-hose-valve system, with the new input notation and variable expiration valve resistance R_{exp} .

in which $R_{\zeta}(p_{pilot}, p_{exp})$ is an unknown function for R_{exp} , expressed by p_{pilot} and p_{exp} . Since the pressure p_{pilot} depends on both U_{piezo} and p_{out} , (2.7) becomes

$$R_{exp} := R_{\eta}(p_{out}, U_{piezo}, p_{exp}). \quad (2.8)$$

As discussed in Section 2.1.2, the blower dynamics are not taken into account for this project, which means that p_{out} is renamed $p_{control}$ for the remainder of this work. The expiration valve resistance is then defined as

$$R_{exp} := R_{\eta}(p_{control}, U_{piezo}, p_{exp}). \quad (2.9)$$

In Section 1.3, the inputs of the control system are defined as the blower pressure and the piezo valve voltage. Consequently, $p_{control}$ and U_{piezo} are renamed as u_1 and u_2 , respectively. The input vector u is defined as

$$u = \begin{bmatrix} u_1 \\ u_2 \end{bmatrix} = \begin{bmatrix} p_{control} \\ U_{piezo} \end{bmatrix}. \quad (2.10)$$

With this new input notation, the function for R_{exp} in (2.9) is simplified to

$$R_{exp} = R_{\eta}(u, p_{exp}). \quad (2.11)$$

Force balancing models for expiration valves are presented in [8] and [10]. However, due to the unpredictable highly non-linear behavior of the expiration valve, these methods are deemed not accurate enough for this particular type of expiration valve. In Chapter 3, more details are presented about this non-linear behavior of the expiration valve and an experimental model is obtained. For now, the function R_{η} in (2.11) is sufficient to derive the full patient-hose-valve system.

The additional resistance R_{exp} at the end of the expiration hose changes the expiration flow equation in (2.5). To define a new equation for Q_{exp} , the pressure difference is now taken between the airway pressure p_{aw} and the ambient pressure p_{amb} . In this work, all pressures are expressed with respect to the ambient pressure, i.e., $p_{amb} = 0$. The new equation for Q_{exp} is

$$Q_{exp} = \frac{p_{aw}}{R_{exp} + R_{hose2}}, \quad (2.12)$$

$$Q_{exp} = \frac{p_{aw}}{R_{\eta}(u, p_{exp}) + R_{hose2}}. \quad (2.13)$$

The new input notation (2.10) and the variable resistance R_{exp} in (2.11) are added to the patient-hose model. Fig. 2.5 shows the new patient-hose-valve model schematically, in which the expiration valve is located at the end of the expiration hose. The pilot line with piezo valve connects u_1 ($p_{control}$) with the expiration valve. In the next section, a non-linear state-space model of the patient-hose-valve system is derived.

2.1.4 Derivation of a patient-hose-valve state-space model

This section describes the derivation of a non-linear state-space model for the patient-hose-valve model described in the previous sections. The differential equation in (2.3) is extended by deriving a more detailed expression for p_{aw} . This is achieved by exploiting the conservation of flow in (2.6), in combination with the flow-pressure relations, i.e., (2.2), (2.4), and (2.13). These relations are substituted in (2.6), resulting in

$$\frac{p_{aw} - p_{lung}}{R_{aw}} = \frac{u_1 - p_{aw}}{R_{hose1}} - \frac{p_{aw}}{R_{\eta}(u, p_{exp}) + R_{hose2}}. \quad (2.14)$$

This is rewritten, to obtain an expression for p_{aw} , which results in

$$p_{aw} \left(\frac{1}{R_{aw}} + \frac{1}{R_{hose1}} + \frac{1}{R_{\eta}(u, p_{exp}) + R_{hose2}} \right) = \frac{u_1}{R_{hose1}} + \frac{p_{lung}}{R_{aw}}, \quad (2.15)$$

$$p_{aw} = \frac{\frac{u_1}{R_{hose1}} + \frac{p_{lung}}{R_{aw}}}{\left(\frac{1}{R_{aw}} + \frac{1}{R_{hose1}} + \frac{1}{R_{\eta}(u, p_{exp}) + R_{hose2}} \right)}. \quad (2.16)$$

Rewriting this equation results in

$$p_{aw} = \frac{R_{hose1}(R_{hose2} + R_{\eta}(u, p_{exp}))p_{lung} + R_{aw}(R_{hose2} + R_{\eta}(u, p_{exp}))u_1}{R_{sum}(u, p_{exp})}, \quad (2.17)$$

in which

$$R_{sum}(u, p_{exp}) = R_{hose1}(R_{hose2} + R_{\eta}(u, p_{exp})) + R_{aw}(R_{hose1} + R_{hose2} + R_{\eta}(u, p_{exp})). \quad (2.18)$$

Next, (2.17) is substituted in (2.1). This results in the following first-order differential equation:

$$\dot{p}_{lung} = - \underbrace{\frac{R_{hose1} + R_{hose2} + R_{\eta}(u, p_{exp})}{C_{lung}R_{sum}(u, p_{exp})}}_{\mathbf{A}(u, p_{exp})} p_{lung} + \underbrace{\frac{R_{hose2} + R_{\eta}(u, p_{exp})}{C_{lung}R_{sum}(u, p_{exp})}}_{\mathbf{B}(u, p_{exp})} u_1. \quad (2.19)$$

This differential equation consists of a state matrix $\mathbf{A}(u, p_{exp})$ and an input matrix $\mathbf{B}(u, p_{exp})$. However, p_{exp} is also influenced by the state p_{lung} , which means that the expiration valve resistance R_{exp} in (2.11) also depends on the state p_{lung} . Furthermore, if both inputs u_1 and u_2 are known, and the state p_{lung} is known, then the patient-hose-valve system is fully defined. As a result, p_{exp} is a redundant variable, which means that R_{exp} can be fully defined as

$$R_{exp} := R_{\psi}(u, p_{lung}). \quad (2.20)$$

As a result, $R_{\eta}(u, p_{exp})$ in (2.19) is replaced with $R_{\psi}(u, p_{lung})$, which results in

$$\dot{p}_{lung} = - \underbrace{\frac{R_{hose1} + R_{hose2} + R_{\psi}(u, p_{lung})}{C_{lung}R_{sum}(u, p_{lung})}}_{\mathbf{A}(u, p_{lung})} p_{lung} + \underbrace{\frac{R_{hose2} + R_{\psi}(u, p_{lung})}{C_{lung}R_{sum}(u, p_{lung})}}_{\mathbf{B}(u, p_{lung})} u_1. \quad (2.21)$$

It can be observed that the inputs u_1 and u_2 , and the state p_{lung} are present in the state matrix $\mathbf{A}(u, p_{lung})$ and input matrix $\mathbf{B}(u, p_{lung})$. This phenomena couples the inputs and the state in a non-linear manner. To complete the state-space model, the output equations are derived for p_{aw} , Q_{exp} , and Q_{out} . The output equation for p_{aw} is obtained by rewriting (2.17) as

$$p_{aw} = \underbrace{\frac{R_{hose1}(R_{hose2} + R_{\psi}(u, p_{lung}))}{R_{sum}(u, p_{lung})}}_{\mathbf{C}_p(u, p_{lung})} p_{lung} + \underbrace{\frac{R_{aw}(R_{hose2} + R_{\psi}(u, p_{lung}))}{R_{sum}(u, p_{lung})}}_{\mathbf{D}_p(u, p_{lung})} u_1, \quad (2.22)$$

in which $\mathbf{C}_p(u, plung)$ and $\mathbf{D}_p(u, plung)$ are the output matrix and feedthrough matrix for p_{aw} , respectively. The output equation for Q_{exp} is obtained by substituting (2.22) in (2.13), which results in

$$Q_{exp} = \underbrace{\frac{R_{hose1}}{R_{sum}(u, plung)}}_{\mathbf{C}_{Q_{exp}}(u, plung)} plung + \underbrace{\frac{R_{aw}}{R_{sum}(u, plung)}}_{\mathbf{D}_{Q_{exp}}(u, plung)} u_1. \quad (2.23)$$

The output equation for Q_{out} is obtained by substituting (2.22) in (2.4), which results in

$$Q_{out} = -\underbrace{\frac{R_{hose2} + R_\psi(u, plung)}{R_{sum}(u, plung)}}_{\mathbf{C}_{Q_{out}}(u, plung)} plung + \underbrace{\frac{R_{aw} + R_\psi(u, plung) + R_{hose2}}{R_{sum}(u, plung)}}_{\mathbf{D}_{Q_{out}}(u, plung)} u_1. \quad (2.24)$$

A full non-linear state-space model is obtained by combining (2.21), (2.22), (2.23), and (2.24). The state-space model for the patient-hose-valve system is defined as

$$\begin{aligned} \dot{plung} &= \mathbf{A}(u, plung)plung + [\mathbf{B}(u, plung) \quad 0] u, \\ \begin{bmatrix} p_{aw} \\ Q_{exp} \\ Q_{out} \end{bmatrix} &= \begin{bmatrix} \mathbf{C}_p(u, plung) \\ \mathbf{C}_{Q_{exp}}(u, plung) \\ \mathbf{C}_{Q_{out}}(u, plung) \end{bmatrix} plung + \begin{bmatrix} \mathbf{D}_p(u, plung) & 0 \\ \mathbf{D}_{Q_{exp}}(u, plung) & 0 \\ \mathbf{D}_{Q_{out}}(u, plung) & 0 \end{bmatrix} u \end{aligned} \quad (2.25)$$

with

$$\mathbf{A}(u, plung) = \left[-\frac{R_{hose1} + R_{hose2} + R_\psi(u, plung)}{C_{lung} R_{sum}(u, plung)} \right], \quad (2.26)$$

$$\mathbf{B}(u, plung) = \left[\frac{R_{hose2} + R_\psi(u, plung)}{C_{lung} R_{sum}(u, plung)} \right]. \quad (2.27)$$

In these matrices, $R_{sum}(u, plung)$ is defined as in (2.18). The combined $\mathbf{C}(u, plung)$ matrix is defined as

$$\mathbf{C}(u, plung) = \begin{bmatrix} \mathbf{C}_p(u, plung) \\ \mathbf{C}_{Q_{exp}}(u, plung) \\ \mathbf{C}_{Q_{out}}(u, plung) \end{bmatrix} = \begin{bmatrix} \frac{R_{hose1}(R_{hose2} + R_\psi(u, plung))}{R_{sum}(u, plung)} \\ \frac{R_{hose1}}{R_{sum}(u, plung)} \\ -\frac{R_{hose2} - R_\psi(u, plung)}{R_{sum}(u, plung)} \end{bmatrix} \quad (2.28)$$

and the combined $\mathbf{D}(u, plung)$ matrix is defined as

$$\mathbf{D}(u, plung) = \begin{bmatrix} \mathbf{D}_p(u, plung) & 0 \\ \mathbf{D}_{Q_{exp}}(u, plung) & 0 \\ \mathbf{D}_{Q_{out}}(u, plung) & 0 \end{bmatrix} = \begin{bmatrix} \frac{R_{aw}(R_{hose2} + R_\psi(u, plung))}{R_{sum}(u, plung)} & 0 \\ \frac{R_{aw}}{R_{sum}(u, plung)} & 0 \\ \frac{R_{aw} + R_\psi(u, plung) + R_{hose2}}{R_{sum}(u, plung)} & 0 \end{bmatrix}. \quad (2.29)$$

The state-space model in (2.25) describes the complete patient-hose-valve system. Although the state-space model can be used to gain insight in the system dynamics, the derived state-space structure has several interesting characteristics. The input u_2 is only present in the state-space model through the expiration valve resistance $R_\psi(u, plung)$. It is concluded that $R_\psi(u, plung)$ induces a non-linear coupling between both inputs and the state $plung$. As a result of this coupling, analyzing the input-output behavior and the state behavior is challenging.

It is important to analyze the open-loop stability of the non-linear system with bounded inputs. If a system is open-loop stable for bounded inputs, it is always possible to apply a feedforward controller without destabilizing the system. Moreover, it allows for open-loop identification measurements without the process of designing a stabilizing controller first. Open-loop stability of the patient-hose-valve system with bounded inputs is analyzed in the next section.

2.2 Open-loop stability for bounded inputs

In this section, an open-loop stability analysis for the patient-hose-valve system is provided. This analysis is used to show that the state-space model in (2.25)-(2.29) is open-loop stable for bounded

inputs. In addition, it is shown that for these bounded inputs, the system has a unique asymptotically stable solution.

Let us first analyze the system without inputs, i.e., $u = 0$. Although the system is non-linear, the open-loop stability analysis is relatively straight-forward due to the one-dimensional nature of the system dynamics, i.e., $\mathbf{A}(u, p_{lung}) \in \mathbb{R}^{1 \times 1}$, and the physical properties of R_{exp} . The expiration valve resistance $R_{exp} := R_{\psi}(u, p_{lung})$ operates in the following range:

$$R_{min} < R_{\psi}(u, p_{lung}) \leq \infty, \quad (2.30)$$

in which $R_{min} > 0$ is the minimal resistance of the expiration valve, which occurs when the valve is completely open. An infinitely large resistance occurs when the valve is closed, which allows no flow to pass through the valve. $R_{\psi}(u, p_{lung})$ is never negative, because this would indicate that air flows from a low pressure point to a high pressure point, which is physically impossible. Using (2.30), it is concluded that $R_{exp} := R_{\psi}(u, p_{lung})$ is strictly positive. As a result, all parameters in $\mathbf{A}(u, p_{lung})$, i.e., C_{lung} , R_{aw} , $R_{\psi}(u, p_{lung})$, R_{hose1} , and R_{hose2} are all strictly positive. From (2.26), it is then concluded that the matrix $\mathbf{A}(u, p_{lung})$ is always strictly negative, independent of the value of $R_{\psi}(u, p_{lung})$. Although negative definiteness of all switching state matrices does not guarantee asymptotic stability in general, see [16, p. 7], it is sufficient for this scalar system. In more detail, as long as $\mathbf{A}(u, p_{lung}) < 0$ then it is guaranteed that for any value of p_{lung} , \dot{p}_{lung} is always pointing in the opposite direction which yields global asymptotic stability (GAS) of the open-loop non-linear system without inputs. In addition, it is concluded that $p_{lung} = 0$ is the only equilibrium point of the system without inputs.

To prove asymptotic stability of the system with inputs, it is sufficient to check if $\mathbf{B}(u, p_{lung})$ is bounded $\forall R_{\psi}(u, p_{lung})$ in (2.30). For $R_{\psi}(u, p_{lung}) \neq \infty$ it is concluded that $\mathbf{B}(u, p_{lung})$ in (2.27) is always bounded, because C_{lung} , R_{aw} , and R_{hose1} are all strictly positive. However, for the closed valve position, i.e., $R_{\psi}(u, p_{lung}) = \infty$, it is important to verify that $\mathbf{B}(u, p_{lung})$ is also bounded. This is analyzed by solving $\lim_{R_{\psi} \rightarrow \infty} \mathbf{B}(u, p_{lung})$:

$$\lim_{R_{\psi} \rightarrow \infty} \mathbf{B}(u, p_{lung}) = \frac{1}{C_{lung}(R_{aw} + R_{hose1})}. \quad (2.31)$$

From (2.31), it is concluded that $\mathbf{B}(u, p_{lung})$ is bounded $\forall R_{\psi}(u, p_{lung})$ in (2.30). This result in combination with GAS of the state matrix $\mathbf{A}(u, p_{lung})$, concludes that the patient-hose-valve system with bounded inputs is open-loop GAS $\forall R_{\psi}(u, p_{lung})$ in (2.30). In addition, it is concluded that any solution is GAS, because the unperturbed system only has one asymptotically stable equilibrium point. This characteristic is later used to design a feedforward controller for the system in Chapter 3.

2.3 Output switching condition

This section describes an output switch for the state-space model in (2.25)-(2.29), which is applied to solve the incomplete definition of the baseflow target. As described in Section 1.3, the baseflow target Q_{bf} is partially defined for the expiration flow Q_{exp} and partially for the blower outlet flow Q_{out} . The corresponding output equations have been defined in (2.23) and (2.24), respectively. To achieve a fully defined target during each phase of the breathing cycle, a straight-forward solution is to switch the baseflow target between Q_{exp} and Q_{out} .

The desired output switch is defined as follows: during phase I in Fig. 1.4a, Q_{exp} is used as an output, and during phase II, III, and IV, Q_{out} is used as an output. To achieve this, the following switching condition is defined:

$$\mu = \begin{cases} Q_{exp} & \text{if } Q_{out} > Q_{bf} \wedge p_{target} \neq PEEP, \\ Q_{out} & \text{otherwise.} \end{cases} \quad (2.32)$$

During phase I in Fig. 1.4a, the blower outlet flow Q_{out} is larger than Q_{bf} , and the pressure target p_{target} is at *IPAP* level. This means that, according to the switching algorithm in (2.32), Q_{exp} is used as an output. During phase II, the blower outlet flow Q_{out} decreases to the baseflow level. Consequently, the output switch is enabled and switches to the output Q_{out} , because $Q_{out} = Q_{bf}$.

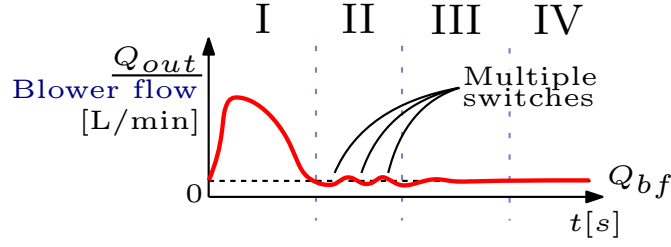


Fig. 2.6. Multiple switches due to flow oscillations.

During phase III and IV, it is not possible to switch back to Q_{exp} because of the condition $p_{target} \neq PEEP$.

However, during phase II, the baseflow might oscillate around the baseflow level Q_{bf} due to disturbances. These oscillations cause a chattering effect for the output switch in (2.32). In other words, for every flow oscillation around Q_{bf} during phase II, the output switch μ is triggered, which is undesired. To prevent this chattering effect, a third boolean condition b^+ is derived for the switching algorithm in (2.32), which is defined as

$$b^+ = \begin{cases} 1 & \text{at the start of the mandatory inspiration of the breathing cycle,} \\ 0 & \text{when the output switches to } Q_{out} \text{ for the first time.} \end{cases} \quad (2.33)$$

In more detail, $b^+ = 1$ as soon as a mandatory inspiration is initiated at the start of a breathing cycle. This happens when $PEEP$ changes to $IPAP$, i.e., at the start of phase I, see Fig. 1.4a. The boolean in (2.33) switches to $b^+ = 0$ when the output is switched from Q_{exp} to Q_{out} for the first time in the breathing cycle. This boolean ensures that only one switch is allowed during phase II. In other words, when the output switches from Q_{exp} to Q_{out} , it only switches back to Q_{exp} at the the end of the breathing cycle. This prevents the chattering effect of the switching condition μ .

A new switching condition ϕ is defined which combines the old switching condition μ in (2.32) with the boolean condition b^+ in (2.33), which results in

$$\phi = \begin{cases} Q_{exp} & \text{if } Q_{out} > Q_{bf} \quad \wedge \quad p_{target} \neq PEEP \quad \wedge \quad b^+ = 1, \\ Q_{out} & \text{otherwise.} \end{cases} \quad (2.34)$$

This switching condition ensures that the output switch occurs only once from Q_{exp} to Q_{out} at the transition from phase I to phase II, and only once from Q_{out} back to Q_{exp} at the end of the breathing cycle, during the transition from phase IV to phase I. The switching condition ϕ in (2.34) applies to the non-linear state-space model in (2.25)-(2.29), and is later analyzed during the feedback controller design process in Chapter 4.

2.4 Summary

In this chapter, a state-space model for the patient-hose-valve system has been derived. First, a first-order differential equation is used to describe the patient's airway and lung dynamics. Thereafter, the inspiration hose and expiration hose have been modeled. Then, the expiration valve is modeled as a variable resistance $R_{exp} := R_{\psi}(u, p_{lung})$, which depends on both inputs and the state p_{lung} . The separate models have been combined to a non-linear state-space model, which is proven to be open-loop globally asymptotically stable for bounded inputs, which has a unique steady-state solution. This property allows for separate designs of a feedback and feedforward control strategy. Finally, an output switch is defined for Q_{exp} and Q_{out} to deal with the incomplete definition of the baseflow target Q_{bf} . In the next chapter, the state-space model in (2.25)-(2.29) is used to derive a feedforward controller for the patient-hose-valve system using a steady-state solution.

Chapter 3

Feedforward controller design

This chapter describes the design process of a feedforward controller for the patient-hose-valve system in (2.25)-(2.29). This feedforward controller design is the second sub-objective of Section 1.4. As described in Section 1.3.3, the feedforward design is based on all known components of the state-space model. Thereafter, in Chapter 4, a feedback controller is designed to deal with unknown disturbances and modeling uncertainties.

This chapter describes the feedforward controller design and is structured as follows. First, in Section 3.1, the use of a constant steady-state feedforward controller is motivated. Thereafter, in Section 3.1.1, the high-level feedforward controller design is presented. In Section 3.2, a constant steady-state solution of the state-space model is derived which is used for the feedforward controller design. After that, in Section 3.3, the constant steady-state solution is extended with an experimental model for the expiration valve resistance R_{exp} . Furthermore, in Section 3.4, the limitations of the feedforward control strategy are investigated. In Section 3.5, an alternative feedforward strategy is briefly explained. Finally, the chapter is summarized in Section 3.6.

3.1 Feedforward design motivation

In this section, the use of a constant steady-state feedforward controller for the patient-hose-valve system in (2.25)-(2.29) is motivated. In an ideal setting, the feedforward controller is designed as the exact inverse of the state-space model in (2.25)-(2.29). However, an exact plant inverse is only possible when all system parameters are known, which is not the case for the considered system, e.g., patient parameters R_{aw} and C_{lung} are unknown. As a result, an exact plant inverse is not available.

As explained in Section 1.3.3, a suitable strategy is to base the feedforward controller on the system components that are fixed and known, i.e., the hose system and expiration valve. This control strategy is achieved by designing the feedforward controller using the constant steady-state solution of the state-space model. Fig. 3.1 shows the patient-hose-valve system in a constant steady state. A constant steady state is achieved by setting u_1 and u_2 to a constant value, i.e.,

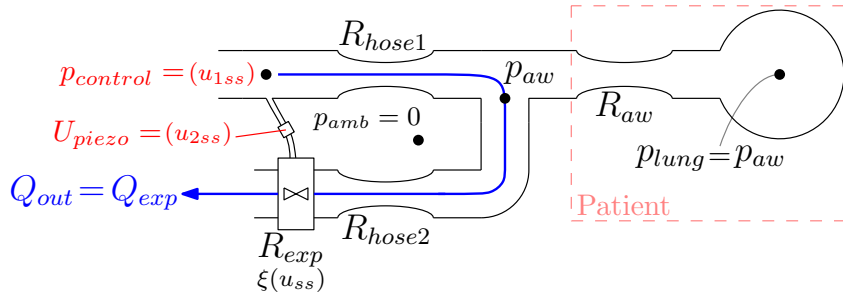


Fig. 3.1. Schematic drawing of the patient-hose-valve system in a constant steady state.

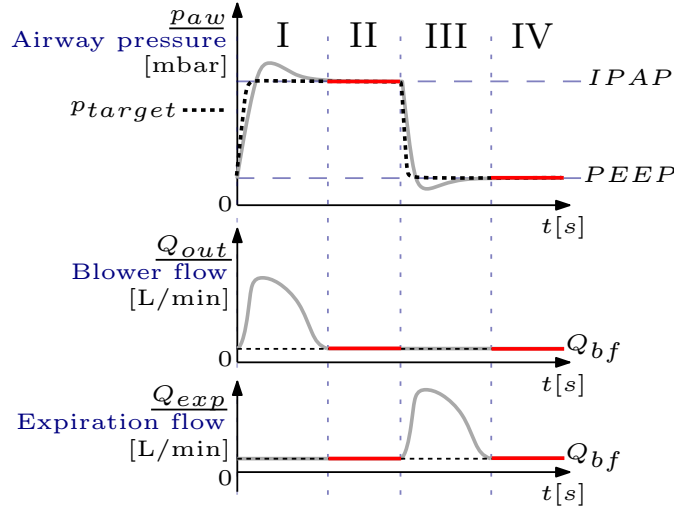


Fig. 3.2. The pressure-controlled breathing cycle with the constant steady-state phases indicated in red.

u_{1ss} and u_{2ss} . As explained in Section 2.2, the open-loop system with constant inputs is globally asymptotically stable and has a unique steady-state solution. This ensures that the system reaches a constant steady state and does not diverge. In a constant steady state, the airway pressure and lung pressure are equal, i.e., $p_{aw} = p_{lung}$. Consequently, no flow enters or leaves the patient, i.e., $Q_{pat} = 0$, which means that all flow generated by the blower leaves through the expiration valve, i.e., $Q_{out} = Q_{exp}$, and the constant steady-state solution is independent of the patient parameters R_{aw} and C_{lung} . In addition, the expiration valve resistance R_{exp} is also constant and patient independent. This means that the R_{exp} only depends on the constant inputs u_{1ss} and u_{2ss} , i.e., $R_{\psi}(u, p_{lung})$ in (2.20) changes to a new constant function $R_{\xi}(u_{ss})$ for R_{exp} . These steady-state characteristics are supported using the non-linear state-space model in Appendix A.

Fig. 3.2 shows the pressure-controlled breathing cycle with the output targets p_{target} and Q_{bf} . Phase II and IV of the pressure-controlled breathing cycle are both examples of the system in a constant steady state and are indicated with a red line in Fig. 3.2. The exact value of p_{aw} , Q_{exp} , and Q_{out} during phase II and IV depends on the value of the constant steady-state inputs u_{1ss} and u_{2ss} , and the hose and valve parameters.

The main concept of the constant steady-state feedforward controller is that for constant targets of p_{target} and Q_{bf} , it is always possible to find constant inputs u_{1ss} and u_{2ss} which achieve $p_{aw} \rightarrow p_{target}$, $Q_{exp} \rightarrow Q_{bf}$, and $Q_{out} \rightarrow Q_{bf}$, as the system reaches a constant steady state. In other words, using the asymptotically stable characteristic and the unique steady-state solution of the system, it is possible to find suitable constant inputs such that the system response will converge to the desired constant steady state during phase II and IV. The constant steady-state inputs u_{1ss} and u_{2ss} can therefore be used as feedforward inputs u_{1ff} and u_{2ff} , respectively. Note that this also means that the feedforward controller does not require the output switch (2.34), described in Section 2.3, because during the constant steady state $Q_{out} = Q_{exp}$. In the following section, a high-level description of the feedforward controller design is presented.

3.1.1 High-level controller design

In this section, a step-by-step description of the feedforward controller is presented. The feedforward inputs, u_{1ff} and u_{2ff} , are derived using the following three steps:

1. The constant steady-state input u_{1ss} and the desired constant expiration valve resistance $R_{exp} := R_{\xi}(u_{ss})$ are calculated directly by solving the state-space model (2.25)-(2.29) in a constant steady state. To achieve this, R_{hose1} , R_{hose2} , p_{target} , and Q_{bf} are required. Note that the parameters R_{hose1} and R_{hose2} are typically obtained through calibration. The constant steady-state solution of the system is derived in Section 3.2.

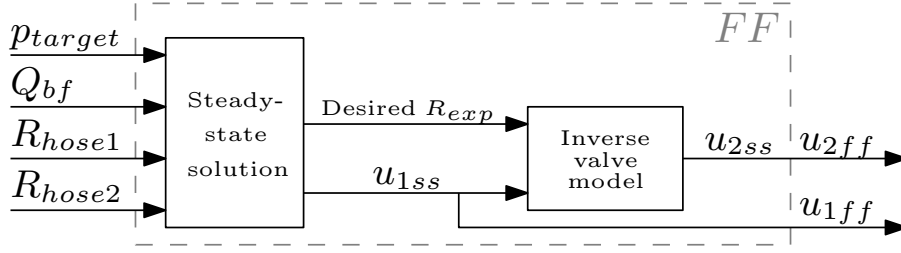


Fig. 3.3. Feedforward controller block scheme.

2. Using the solution of u_{1ss} and the desired R_{exp} , the constant steady-state piezo voltage u_{2ss} is obtained using an inverse model of the expiration valve. This expiration valve model is obtained by means of a Look-Up Table (LUT). In Section 3.3, it is described how this LUT is obtained and implemented.
3. The values for u_{1ss} and u_{2ss} are now used as feedforward inputs u_{1ff} and u_{2ff} , respectively.

Fig. 3.3 visualizes the feedforward calculation process using a block scheme. In the following section, the constant steady-state solution for step one of the feedforward controller is derived.

3.2 Constant steady-state solution of the patient-hose-valve system

In this section, the constant steady-state solution of the patient-hose-valve system in (2.25)-(2.29) is derived. This constant steady-state solution is used to derive the input u_{1ss} and the desired constant valve resistance $R_{\xi}(u_{ss})$. The constant steady-state solution is achieved by setting $\dot{p}_{lung} = 0$. As a result, the state equation part of (2.25) is defined as

$$\bar{p}_{lung} = -\mathbf{A}^{-1}(u_{ss})\mathbf{B}(u_{ss})u_{1ss}, \quad (3.1)$$

in which \bar{p}_{lung} is the constant lung pressure, $\mathbf{A}(u_{ss})$ is the state matrix in a constant steady state, and $\mathbf{B}(u_{ss})$ is the input matrix in steady-state. Note that the matrices no longer depend on the state p_{lung} , because $R_{\psi}(u, p_{lung})$ is now $R_{\xi}(u_{ss})$. The equation in (3.1) describes the constant steady-state solution of the lung dynamics. This solution is extended to a constant steady-state output solution. The output solution is described by

$$\begin{bmatrix} p_{aw} \\ Q_{bf} \end{bmatrix} = \begin{bmatrix} \mathbf{C}_P(u_{ss}) \\ \mathbf{C}_Q(u_{ss}) \end{bmatrix} \bar{p}_{lung} + \begin{bmatrix} \mathbf{D}_P(u_{ss}) \\ \mathbf{D}_Q(u_{ss}) \end{bmatrix} u_{1ss}, \quad (3.2)$$

in which p_{aw} and Q_{bf} are the constant steady-state outputs during phase II and IV. The output equation Q_{bf} can either be the desired baseflow level for Q_{exp} or Q_{out} in (2.23) and (2.24), respectively. The reason for this is that the constant steady-state values of Q_{exp} and Q_{out} are the same during phase II and IV, see Fig. 3.2. In more detail, this means that $\mathbf{C}_Q(u_{ss})$ and $\mathbf{D}_Q(u_{ss})$ are either $\mathbf{C}_{Q_{exp}}(u_{ss})$ and $\mathbf{D}_{Q_{exp}}(u_{ss})$, or $\mathbf{C}_{Q_{out}}(u_{ss})$ and $\mathbf{D}_{Q_{out}}(u_{ss})$. This choice is trivial and does not change the outcome whatsoever. Substituting the constant steady-state lung dynamics from (3.1) in (3.2) results in

$$\begin{bmatrix} p_{aw} \\ Q_{bf} \end{bmatrix} = \begin{bmatrix} \mathbf{C}_P(u_{ss}) \\ \mathbf{C}_Q(u_{ss}) \end{bmatrix} (-\mathbf{A}^{-1}(u_{ss})\mathbf{B}(u_{ss})u_{1ss}) + \begin{bmatrix} \mathbf{D}_P(u_{ss}) \\ \mathbf{D}_Q(u_{ss}) \end{bmatrix} u_{1ss}, \quad (3.3)$$

$$\begin{bmatrix} p_{aw} \\ Q_{bf} \end{bmatrix} = \left(\begin{bmatrix} \mathbf{C}_P(u_{ss}) \\ \mathbf{C}_Q(u_{ss}) \end{bmatrix} (-\mathbf{A}^{-1}(u_{ss})\mathbf{B}(u_{ss})) + \begin{bmatrix} \mathbf{D}_P(u_{ss}) \\ \mathbf{D}_Q(u_{ss}) \end{bmatrix} \right) u_{1ss}. \quad (3.4)$$

Then, the complete constant steady-state output response is calculated by substituting the state-space matrices (2.26)-(2.29) into (3.4). Then, (3.4) is inverted to derive u_{1ss} and $R_\xi(u_{ss})$, which results in

$$u_{1ss} = p_{aw} + Q_{bf} R_{hose1}, \quad (3.5)$$

$$R_\xi(u_{ss}) = \frac{p_{aw}}{Q_{bf}} - R_{hose2}. \quad (3.6)$$

A physical explanation for (3.5) is relatively simple, because it is a rewritten version of the pressure drop equation in (2.4). Correspondingly, (3.6) is a rewritten version of (2.13).

The hose resistances R_{hose1} and R_{hose2} are constant and are typically estimated by a calibration routine before ventilation starts. From (3.5) and (3.6) it is concluded that, if the desired targets for p_{aw} and Q_{bf} are known, u_{1ss} and the desired valve resistance $R_\xi(u_{ss})$ are computed using (3.5) and (3.6). In this case, the output p_{aw} is then replaced with the desired pressure target p_{target} , see Fig. 3.3. This means that step one from Section 3.1.1 is now fulfilled. In step two, the input u_{2ss} is obtained by deriving a LUT of $R_\xi(u_{ss})$. In the following section, this LUT is derived and its function in the feedforward controller is explained.

3.3 Expiration valve look-up table

This section describes the derivation of a LUT for $R_\xi(u_{ss})$, i.e., the desired R_{exp} in a constant steady state. This LUT is used to obtain the constant steady-state input u_{2ss} , as described in step two of Section 3.1.1. First, experiments are described to generate a LUT for the expiration valve resistance R_{exp} in steady state. Thereafter, it is described how this LUT is used to obtain u_{2ss} .

Fig. 3.4 shows a schematic of the experimental set-up that is used to perform the measurements. The patient side is closed-off, which does not affect the constant steady-state behavior of the system, because $Q_{pat} = 0$ during steady state anyway. The LUT is derived by setting the blower pressure u_1 to a constant value, while slowly ramping the piezo voltage u_2 up and down from 24V to -24V, see Fig. 3.5a. Using this strategy, the expiration valve moves from a completely closed to a completely open position, and vice versa. During this ramp, the expiration flow Q_{exp} is measured, which results in a relation between Q_{exp} and u_2 at a given u_1 . Fig. 3.5b shows one measurement of Q_{exp} while the u_2 ramp is applied and u_1 is kept constant at 20 mbar. $Q_{exp} \uparrow$ is the measured expiration flow when the expiration valve is opening, and $Q_{exp} \downarrow$ is the measured expiration flow when the expiration valve is closing.

In an ideal situation, the opening and closing motion of the expiration valve generates the same flow curve, i.e., $Q_{exp} \uparrow = Q_{exp} \downarrow$. However, a hysteresis curve is observed in Fig. 3.5b. This hysteresis effect is caused by non-linear frictional effects inside the piezo valve. During ventilation of a patient, it is impossible to know on which side of the hysteresis curve the expiration valve is operating, because of the unknown disturbances by the patient. Therefore, picking one side of the hysteresis curve is not a suitable solution and leads to significant model errors when the expiration valve operates on the wrong curve. In more detail, if the expiration valve is modeled at $Q_{exp} \uparrow$

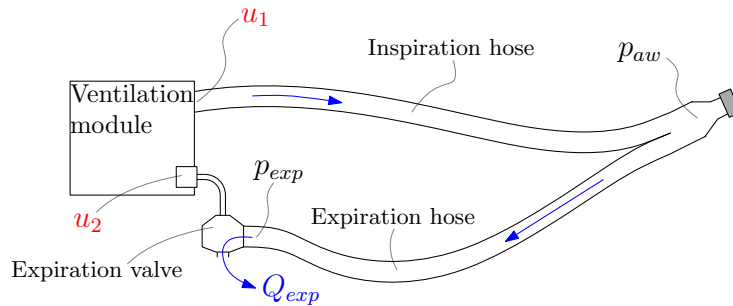
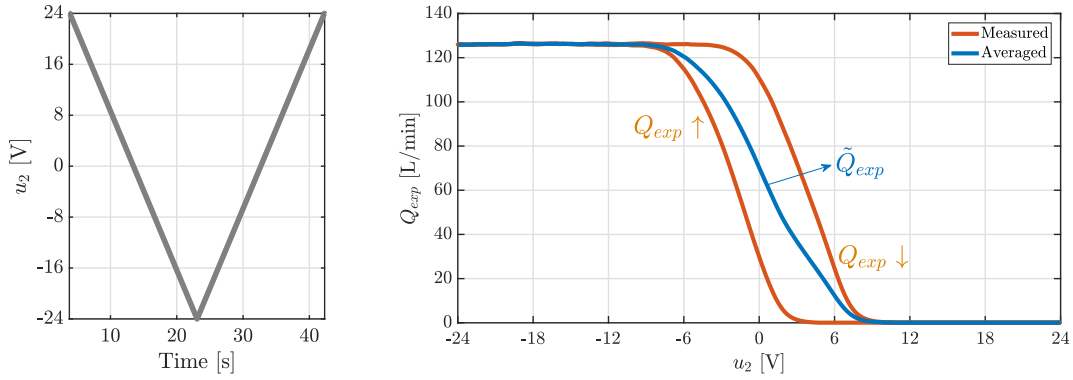


Fig. 3.4. Experimental set-up for LUT measurements.



(a) u_2 voltage ramp input signal.

(b) Measurement of Q_{exp} while a u_2 ramp is applied. u_1 is set constant to 20 mbar.

Fig. 3.5. One of the measurements of Q_{exp} , which is used to derive a LUT for the desired R_{exp} in a constant steady state. The hysteresis effect of the piezo valve is clearly visible in figure b.

while the actual expiration valve operates on $Q_{exp} \downarrow$, this would result in a significant flow error. Take for example $u_2 = 0V$ in Fig. 3.5b, then the Q_{exp} flow error is defined as

$$Q_{exp} \downarrow - Q_{exp} \uparrow = 110 - 30 = 80 \text{ L/min}, \quad (3.7)$$

which is the vertical distance between $Q_{exp} \uparrow$ and $Q_{exp} \downarrow$. The same error occurs when the expiration valve is modeled at $Q_{exp} \downarrow$ while the expiration valve operates at $Q_{exp} \uparrow$. To minimize this modeling error, $Q_{exp} \uparrow$ and $Q_{exp} \downarrow$ are averaged, which results in \tilde{Q}_{exp} , see Fig. 3.5b. The averaging process ensures that the modeling error never reaches the maximal value when the expiration valve operates on the wrong hysteresis curve. Using \tilde{Q}_{exp} , the flow error at $u_2 = 0$ is now defined as

$$Q_{exp} \downarrow - \tilde{Q}_{exp} = \tilde{Q}_{exp} - Q_{exp} \uparrow = 40 \text{ L/min}. \quad (3.8)$$

As a result, the flow error is now limited and is independent of which curve the expiration valve is operating, which also results in a more predictable model error.

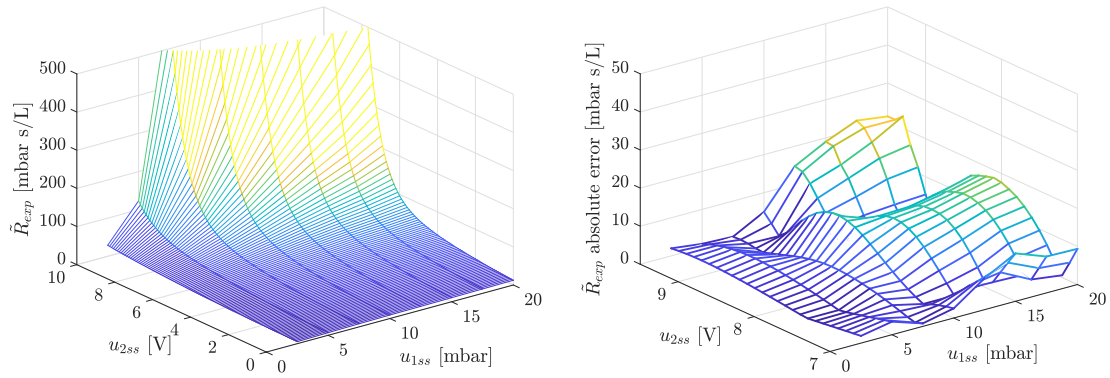
To derive a model for the desired constant R_{exp} , the single measurement of \tilde{Q}_{exp} in Fig. 3.5b is repeated for a variety of constant pressure inputs of u_1 . By doing this, a 3D-surface is created for the average expiration flow \tilde{Q}_{exp} which depends on u_1 and u_2 . During each measurement, the expiration valve pressure p_{exp} is also measured and averaged, i.e., \tilde{p}_{exp} . It is now possible to obtain the average valve resistance \tilde{R}_{exp} using

$$\tilde{R}_{exp} = \frac{\tilde{p}_{exp}}{\tilde{Q}_{exp}}. \quad (3.9)$$

Using (3.9), a 3D-surface is created for the average expiration valve resistance \tilde{R}_{exp} , which is defined for a variety of values of u_1 and u_2 . Fig. 3.6a shows this 3D-surface which functions as a LUT for \tilde{R}_{exp} . The measurements of the LUT are performed sufficiently slow, such that they are valid during a steady state. This means that the inputs u_1 and u_2 are replaced with the constant inputs u_{1ss} and u_{2ss} , respectively. A more detailed description of the measurement process of the LUT experiment is provided in Chapter B.

To fulfill the second step of the feedforward controller in Section 3.1.1, the \tilde{R}_{exp} LUT is used as the expiration valve model in a constant steady state. This model is inverted to derive a LUT for u_{2ss} . However, the LUT in Fig. 3.6a is subject to measurement noise which means that it is not unique, i.e., it is not invertible. To achieve an invertible LUT, a least squares fit is made for the measured \tilde{R}_{exp} LUT, which is monotonically increasing. The fitting function is comprised of the following structure:

$$\tilde{R}_{exp} = \alpha e^{\gamma u_{2ss}} + \beta, \quad (3.10)$$



(a) LUT of the average expiration valve resistance \tilde{R}_{exp} . (b) Error made by using a fit of the LUT. This fit ensures that the LUT is unique.

Fig. 3.6. LUT of the average constant valve resistance \tilde{R}_{exp} , which is achieved by applying the voltage ramp for u_2 for several constant pressures of u_1 .

where α , β , and γ are strictly positive fitting parameters that are used to fit each measurement of \tilde{R}_{exp} , for a constant pressure u_{1ss} . In other words, the fitting parameters α , β , and γ depend on the constant pressure u_{1ss} . Fig. 3.6b shows the fitting error around the constant steady-state operating voltage and pressure of the expiration valve. The fitting equation (3.10) is inverted to obtain a function for u_{2ss} , which results in

$$u_{2ss} = \frac{1}{\gamma} \ln \left(\frac{\tilde{R}_{exp} - \beta}{\alpha} \right). \quad (3.11)$$

This equation for u_{2ss} depends on the average constant valve resistance \tilde{R}_{exp} and u_{1ss} through the parameters α , β , and γ . As a result, the required inverse valve model from step two in Section 3.1.1 can be obtained by filling in the desired \tilde{R}_{exp} and the fitting constants for the desired u_{1ss} . Therewith, step two of the feedforward controller in Section 3.1.1 is fulfilled. As a result, it is now possible to calculate the full feedforward controller inputs u_{1ff} and u_{2ff} using the block scheme in Fig. 3.3, the state-space model in (2.25)-(2.29), and the LUT for the constant expiration valve resistance.

3.4 Limitations of the feedforward controller

Although the feedforward controller is patient independent, it also has some limitations that are explored in this section. First, the feedforward controller uses a LUT of the expiration valve that is based on the average value of a hysteresis curve. As a consequence, the feedforward controller always makes an unavoidable error. Another limitation is that the feedforward controller is designed for the constant steady-state phases II and IV, and not for the transient phases I and III in Fig. 3.2. The only thing that is guaranteed is that the system will eventually converge to the steady-state phase II and IV. However, the transient behavior is not predictable. In addition, feedforward control is an open-loop control strategy, which means that it is not suitable for attenuating unknown disturbances, such as, a coughing patient or a change in hose resistance. Therefore, a feedback controller is designed in Chapter 4. In the next section, the use of a frequency domain based feedforward controller is discussed.

3.5 Frequency domain alternative strategy

This section describes an alternative feedforward strategy based on a frequency domain approach. Note that this feedforward strategy is not applied in this research project, and is mainly explained

as an alternative solution.

From a frequency domain standpoint, it is also possible to design the same constant steady-state feedforward controller using Frequency Response Functions (FRF). For instance, it is possible to derive the static gain of the ventilation system using local FRF measurements of the system. The static gain is the system gain at low frequencies. To achieve a feedforward controller, the static gain is inverted, and used as a feedforward signal. This strategy is also referred to as "steady-state decoupling" in [19]. This feedforward controller is easier to compute in less time compared to the constant steady-state approach in this chapter, because it does not require the derivation of the complete state-space model and the corresponding constant steady-state solution.

Although this steady-state decoupling strategy might seem tempting, it has several disadvantages compared to the state-space strategy:

- The low frequent dynamics of the complete ventilation system are not captured in one single FRF, because they change significantly at different baseflow and airway pressure levels. To obtain a useful FRF based feedforward, a very large variety of measurements is required which is not preferable.
- Using the FRF based feedforward approach, it is unknown how the hysteresis effect of the expiration valve in Section 3.3 affects the constant steady-state behavior.

3.6 Summary

This chapter described the design process of a patient-independent feedforward controller for the non-linear system in (2.25)-(2.29). First, the overall feedforward controller design is introduced which uses the knowledge of all fixed components of the mechanical ventilation system. Thereafter, the required constant steady-state solution of the state-space model is derived for u_{1ss} and the desired expiration valve resistance R_{exp} . This solution automatically provides the first feedforward input u_{1ff} . After that, an experimental model is obtained for R_{exp} which depends on u_{1ss} and u_{2ss} . This model is inverted to obtain a LUT for u_{2ss} , i.e., u_{2ff} . As a result, a feedforward controller is derived for phase II and IV of the breathing cycle, which solely depends on R_{hose1} , R_{hose2} , p_{target} , and Q_{bf} . Moreover, it does not depend on the patient parameters, which is a strong feature. Finally, the limitations of the proposed feedforward controller design are presented. In the next chapter, a decentralized feedback controller is designed for the patient-hose-valve system which is added to the feedforward controller. This feedback controller is used to achieve robustness against unknown patient disturbances and modeling errors.

Chapter 4

Feedback controller design

In this chapter, the design process of a decentralized feedback controller is presented. The design of a feedback controller is part of the third sub-objective of Section 1.4. The feedback controller is used in combination with the feedforward controller from Chapter 3. As explained in Section 1.3.3, the feedback controller is required to attenuate unknown patient disturbances. In addition, the feedback controller is required to compensate for modeling errors and uncertainties, such as the hysteresis effect of the expiration valve in Section 3.3.

In Section 4.1, the use of a decentralized feedback controller is motivated. Thereafter, in Section 4.2, the considered system is identified through experimental identification as a linear MIMO plant. In Section 4.3, the decentralized controllers are derived for the identified system. In addition, the closed-loop stability of the MIMO system is analyzed without the output switch. After that, in Section 4.4, the closed-loop stability of the switched system is discussed. Finally, the chapter is summarized in Section 4.5.

4.1 Decentralized feedback control motivation

This section describes the motivation for a decentralized feedback control strategy for the considered patient-hose-valve system. Fig. 4.1 shows the complete control scheme for the patient-hose-valve system. In this control scheme CG_b represents the internal blower controller and dynamics, G is the patient-hose-valve system, C_{ff} resembles the designed feedforward controller from the previous chapter, and C_{1fb} and C_{2fb} represent the decentralized feedback controllers. The output switch is used to switch between Q_{exp} and Q_{out} to achieve a fully defined baseflow target. The switching condition $\phi(Q_{out}, p_{target})$ is defined in (2.34). As described in Section 2.1.2, the internal blower controller and dynamics are assumed to be under perfect control, i.e., $CG_b = 1$.

As described in [19], a decentralized feedback control strategy uses independent SISO controllers to control the MIMO system. For this system, this means that one controller is designed for the transfer function between p_{aw} and u_1 , and another controller that is suitable for the transfer function between Q_{exp} and u_2 , as well as the transfer function between Q_{out} and u_2 .

First, in Section 4.1.1, the control limitations of the derived state-space model (2.25)-(2.29) are discussed. In addition, the need for system identification experiments for feedback control is explained. After that, in Section 4.1.2, the decentralized control strategy is motivated.

4.1.1 Control limitations of the non-linear state-space model

This section motivates why control strategies, such as, feedback linearization and input-output decoupling, are not suitable for the considered patient-hose-valve model. Many model-based MIMO feedback control strategies have been developed for non-linear state-space models, see [20] and [21]. For example, feedback linearization is often used to control multivariable non-linear systems. By deriving the error dynamics of a non-linear state-space model, it is possible to determine a feedback controller which yields asymptotic tracking of a desired output reference. Using this technique the input-output dynamics of the system are linearized, which allows for

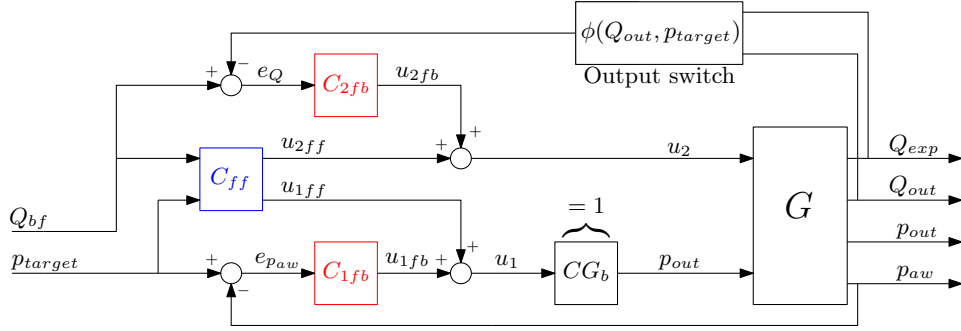


Fig. 4.1. Control scheme of the full system with the feedforward controller C_{ff} from Chapter 3 and the decentralized feedback controllers C_{1fb} and C_{2fb} . The internal blower dynamics and controller CG_b are equal to 1, as explained in Section 2.1.2. The output switch $\phi(Q_{out}, p_{target})$ is applied for the baseflow tracking controller. The switching condition is defined in 2.34.

well-known linear control strategies. Although this method is often applied to a large variety of non-linear systems, it is not suitable for the patient-hose-valve system in (2.25)-(2.29). The reason for this is that feedback linearization methods require a non-linear system which is affine in the input, i.e., the inputs appear linearly in the state-space model [21, p. 163]. This is not the case for the state-space model in (2.25)-(2.29). Moreover, feedback linearization partially aims to linearize the non-linear dynamics, which means that it is important that the state-space model is accurate and all model parameters are known. As described in Section 1.3, this is not the case for this ventilation system, because the patient parameters R_{aw} and C_{lung} are unknown. Furthermore, the outputs of the system, i.e., p_{aw} , Q_{exp} , and Q_{out} , all contain feedthrough terms of both inputs. This also makes it challenging to cancel all unstable dynamics due to multiple couplings between the inputs and the state in each output. This also increases the need for an accurate model. A poorly estimated parameter leads to an incomplete cancellation of the system dynamics, which might result in instability. As a result, a feedback linearization technique is considered not a suitable control solution for this system.

An input-output decoupling technique is also challenging, because of the non-affine input coupling and the feedthrough terms in all outputs. This increases the sensitivity to model uncertainty, which limits the use of such techniques.

A different strategy is to base the feedback controller design on a linearization of the non-linear system around an operating point. The linearized model allows for well-known linear control strategies for the feedback controller design. Linearizing the system in (2.25)-(2.29) results in a linear MIMO state-space model. The linearized model is obtained by calculating the following partial differential equations:

$$\begin{aligned} \mathbf{A}_{lin} &= \left[\frac{\partial \dot{p}_{lung}}{\partial p_{lung}} \right] \Big|_{op}, & \mathbf{B}_{lin} &= \begin{bmatrix} \frac{\partial \dot{p}_{lung}}{\partial u_1} & \frac{\partial \dot{p}_{lung}}{\partial u_2} \end{bmatrix} \Big|_{op}, \\ \mathbf{C}_{lin} &= \begin{bmatrix} \frac{\partial p_{aw}}{\partial p_{lung}} \\ \frac{\partial Q_{exp}}{\partial p_{lung}} \\ \frac{\partial Q_{out}}{\partial p_{lung}} \end{bmatrix} \Big|_{op}, & \mathbf{D}_{lin} &= \begin{bmatrix} \frac{\partial p_{aw}}{\partial u_1} & \frac{\partial p_{aw}}{\partial u_2} \\ \frac{\partial Q_{exp}}{\partial u_1} & \frac{\partial Q_{exp}}{\partial u_2} \\ \frac{\partial Q_{out}}{\partial u_1} & \frac{\partial Q_{out}}{\partial u_2} \end{bmatrix} \Big|_{op}, \end{aligned} \quad (4.1)$$

with the complete linearized system denoted as

$$\mathbf{G}_{lin} = \left[\begin{array}{c|c} \mathbf{A}_{lin} & \mathbf{B}_{lin} \\ \hline \mathbf{C}_{lin} & \mathbf{D}_{lin} \end{array} \right] \quad (4.2)$$

The system is linearized around an operating point, i.e., op . To realize the linearization, the fitted LUT model of the expiration valve in (3.10) is used as a model for R_{exp} in a constant steady state,

i.e., $R_{\xi}(u_{ss})$. As a result, the state-space model is only accurate in steady state. For now, the hysteresis effect of the piezo valve is ignored, because this is deemed out of scope for this research project. The operating point op for linearization is described as

$$op = \begin{bmatrix} u_{1ss} \\ u_{2ss} \\ \bar{p}_{lung} \end{bmatrix} = \begin{bmatrix} p_{aw} + Q_{bf}R_{hose1} \\ LUT \\ -\mathbf{A}^{-1}(u_{ss})\mathbf{B}(u_{ss})u_{1ss} \end{bmatrix} \quad (4.3)$$

where LUT represents the look-up table in Fig. 3.6a, which obtains u_{2ss} using u_{1ss} and the desired R_{exp} . Using the equation in (4.3), it is possible to linearize the system at a desired constant airway pressure p_{aw} and a desired baseflow Q_{bf} , by choosing realistic values for the state-space parameters R_{aw} , C_{lung} , R_{hose1} , and R_{hose2} . The output targets are then translated to the desired inputs using (4.3).

Fig. 4.2 shows a 3×2 MIMO Bode diagram of the linearized system at $p_{aw} = 30$ mbar and $Q_{bf} = 3$ L/min. The lungs are modeled with an airway resistance $R_{aw} = 5$ mbar s/L and a compliance $C_{lung} = 20$ ml/mbar, i.e., an R5C20 lung. R_{hose1} and R_{hose2} are set to 1.02 mbar

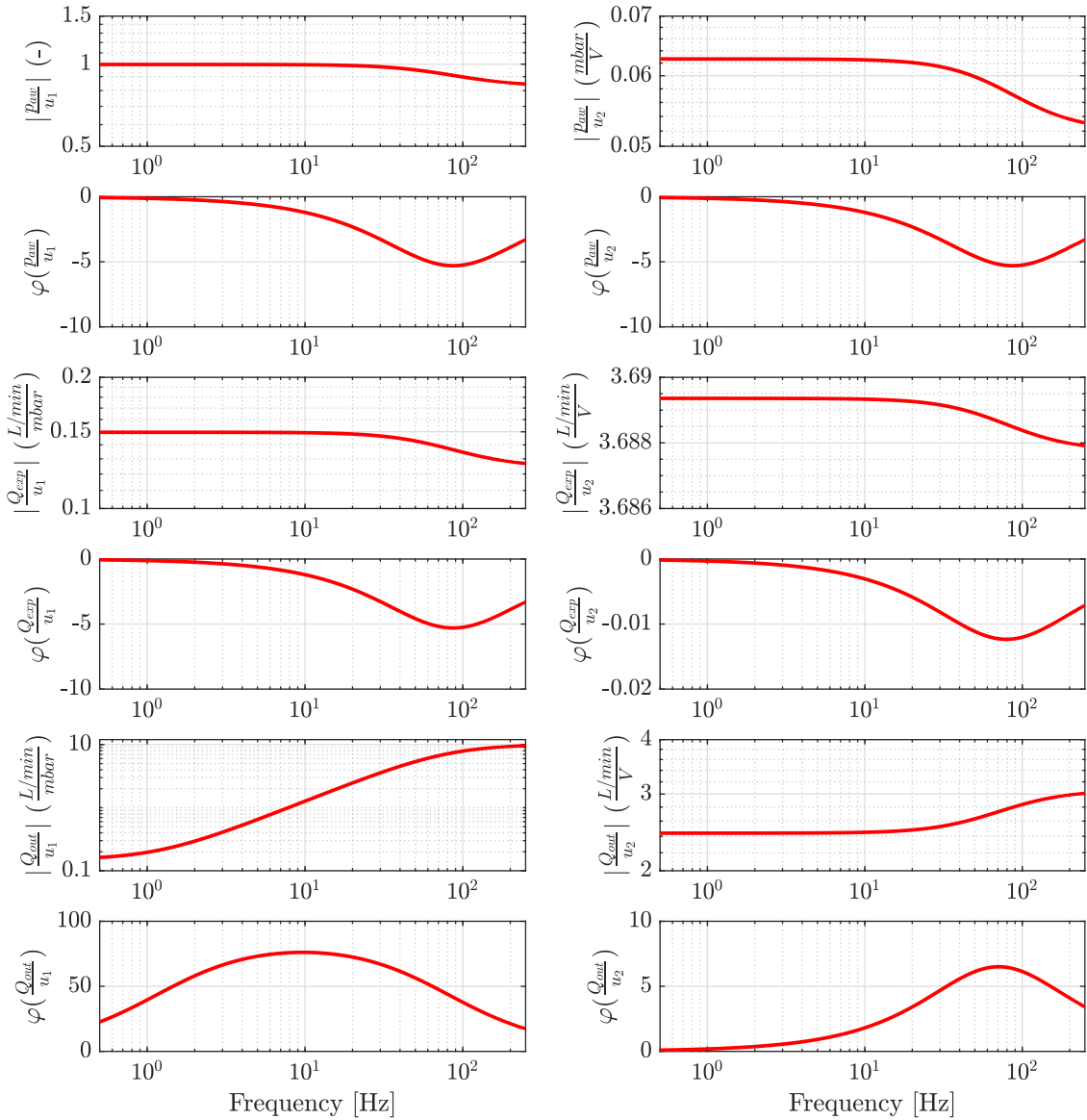


Fig. 4.2. Bode diagram of the linearized state-space model.

s/L. Using these parameters, it is possible to calculate the desired op using (4.3) which results in the required inputs and state $op = [30.051 \quad 7.80 \quad 30]^T$.

It is observed from Fig. 4.2, that only one Bode diagram is dimensionless, i.e., p_{aw}/u_1 . As a result, vertical shifting effects are observed in all Bode diagrams except for p_{aw}/u_1 . The linearized transfer function for p_{aw}/u_1 contains almost no dynamics, i.e., it behaves as a constant gain up until 20 Hz. Only a very slight drop-off is observed at higher frequencies, due to the lung dynamics. This means that an increase in blower pressure is almost one to one proportionate to the response of the airway pressure p_{aw} up until 20 Hz. A similar drop-off effect is observed for the entry p_{aw}/u_2 . Although it has the same drop-off shape as p_{aw}/u_1 , it is shifted vertically due to the unit mismatch. This means that the valve voltage u_2 has a similar effect on p_{aw} as the blower pressure input u_1 . The drop-off is again caused by the high-frequency lung dynamics, which results in more flow entering the lungs. Consequently, the airway pressure p_{aw} drops.

The middle two transfer functions, i.e., Q_{exp}/u_1 and Q_{exp}/u_2 , show a proportionate response at low frequencies. Above 20 Hz, the response of Q_{exp} to both inputs shows a similar drop-off, due to the high-frequency lung dynamics, which causes more air to flow into the lungs and less air to flow through the expiration valve.

The bottom two figures, i.e., Q_{out}/u_1 and Q_{out}/u_2 , show the opposite behavior compared to Q_{exp} at higher frequencies. As explained, more air flows into the lungs at higher frequencies, which also increases the the blower output flow Q_{out} . This explains the gain increase in both bottom figures.

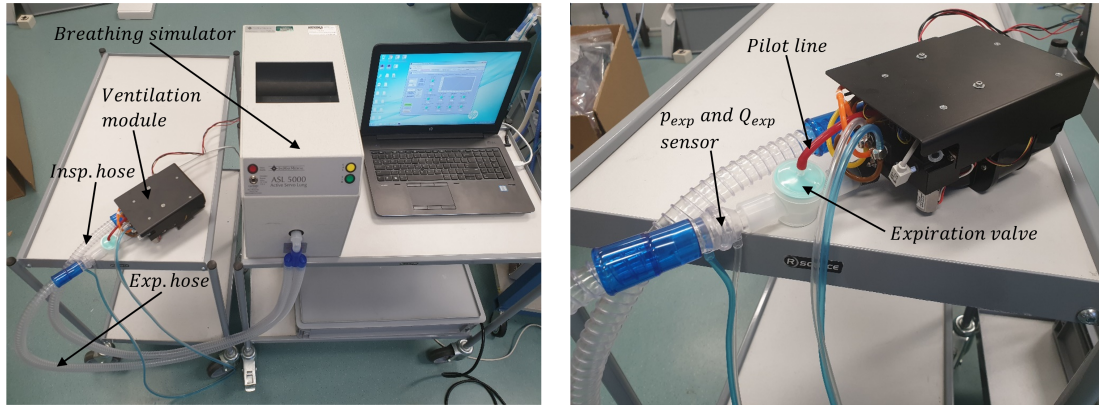
Although the lung dynamics are visible in every transfer function in Fig. 4.2, they only show up at high frequencies above 20 Hz. The reason for this is that the system is linearized around a constant steady state. As discussed in the previous chapter, the constant steady-state phase is independent of the lung dynamics, which means that those dynamics are less visible in the Bode diagrams. In addition, the model for R_{exp} in Section 3.3 is obtained in a constant steady state, which means that it does also not contain any lung dynamics. The remaining dynamics in Fig. 4.2 are governed by static gains and feedthrough terms which only represents the system behavior during a constant steady state. However, the linearized model is not suitable to simulate small perturbations around this constant steady state.

To achieve a suitable MIMO model for the feedback controller design process, the real system dynamics are obtained by means of identification experiments of the actual set-up. Using identification experiments, it is possible to achieve the actual system dynamics for perturbations around a constant steady-state operating point. The identification experiments are performed at various steady-state operating points to fully define the patient-hose-valve system. The identification process is explained in more detail in Section 4.2. Using the identified linear model, a suitable linear MIMO control strategy is applied. The next section motivates the choice for a decentralized feedback controller.

4.1.2 Motivation for a decentralized solution

In this section, the choice for a decentralized controller instead of other MIMO strategies is motivated for the identified linear system. Over the past fifty years, many MIMO feedback control strategies have been developed for coupled linear systems, see [19] and [22]. MIMO control strategies such as Linear Quadratic Guassian (LQG) control and H_∞ control are often used to control multi-variable systems. However, these techniques require an accurate model. The accuracy of each separate model is sufficient. However, due to the large variety in patients, baseflow levels, and pressure levels, picking a nominal model is challenging and might not result in the desired overall performance. In addition, the identification experiments are obtained by perturbing the system around a constant steady-state operating point. As a result, the behavior of the system during the transient phases I and III in Fig. 3.2 is still unpredictable. Other MIMO control strategies, such as decoupling, are also not suitable for this system. A static decoupling is not possible as explained in Section 3.5. Although it is possible to decouple one specific patient type, at a fixed pressure and baseflow level, it will most likely deteriorate the performance for other configurations.

A more suitable solution is to use a decentralized feedback control strategy, which is described in [19]. This is a straight-forward solution, in which each controller can be based on well-known



(a) Experimental set-up for identification measurements.

(b) Close-up of the ventilation module with a sensor just before the expiration valve.

Fig. 4.3. Set-up with all components that were used for the identification experiments.

loop-shaping techniques. The next sections show the complete decentralized feedback controller design process in detail. In Section 4.2, the identification process of a linear MIMO control system is shown. After that, an interaction analysis is performed in Section 4.2.3 to quantify the coupling inside the system. Finally, in Section 4.3, the design process of the decentralized feedback controller is shown.

4.2 System identification

This section describes the process of identifying a linear MIMO system by means of Frequency Response Functions (FRF's) of the real set-up using a predefined set of test lungs. These identified models are later used for the decentralized controller design in Section 4.3. First, in Section 4.2.1, the experimental set-up is introduced which is used to identify the MIMO models. Thereafter, in Section 4.2.2, the measurement procedure for the identification experiments is explained and the obtained MIMO FRF's for several lungs are shown. After that, in Section 4.2.3, an interaction analysis is applied to the obtained MIMO models to quantify the coupling in the system.

4.2.1 Experimental set-up

In this section, the experimental set-up is explained, which is used for the identification experiments. Fig. 4.3 shows the considered set-up, which contains the ventilation module, hose system, breathing simulator, and an expiration valve. The patient's airway and lungs are simulated using the breathing simulator, i.e., the ASL 5000 simulator (IngMar Medical, Pittsburg, PA). This breathing simulator accurately simulates a large variety of linear one-compartmental patients, by setting the resistance R_{aw} and the lung compliance C_{lung} to a desired value. The ASL 5000 is attached to the hose system and the expiration valve. A sensor is located at the end of the expiration hose just before the expiration valve. This sensor measures the expiration flow Q_{exp} going through the expiration valve and the pressure p_{exp} . The response of p_{aw} is estimated using internal measurements Q_{out} and p_{out} . dSPACE software and hardware is used to receive the measured data from the internal and external sensors. In addition, dSPACE is used to control the actuators and computes all required algorithms to actuate the mechanical ventilator. The sampling time for each experiment is set to 500 Hz.

4.2.2 Obtaining a MIMO FRF

This section shows how the MIMO FRF is obtained using the real set-up. To fully describe the non-linear patient-hose-valve system, a large variety of measurements is required at different pressure and flow operating points. The open-loop system is stable for bounded inputs, as described in

Section 2.2. This means that it is possible to use an indirect open-loop identification experiment, as described in [23].

By exciting each input separately, and measuring the output response for each input, it is possible to obtain the MIMO FRF models. This is achieved as follows: first, u_1 and u_2 are set to a constant value, such that the set-up reaches a desired steady state. After that, u_1 is excited and the output response of p_{aw} , Q_{exp} , and Q_{out} are measured. Thereafter, u_2 is excited and the output responses are again measured. A white-noise signal is chosen as an excitation signal, which is filtered through a bandpass filter. This bandpass filter improves the quality of the estimated FRF models for a predefined frequency range and reduces the required measurement time. The bandpass filter consists of a high-pass and a low-pass filter which creates the predefined frequency range for the white-noise signal. The range for the bandpass filter is set between 0.5 and 50 Hz. The identification experiments are performed for five different combinations of lung parameters R_{aw} and C_{lung} , three different p_{aw} pressure levels, and three different baseflow levels Q_{bf} .

Fig. 4.4 shows the obtained MIMO FRF measurements for four different patients, perturbed

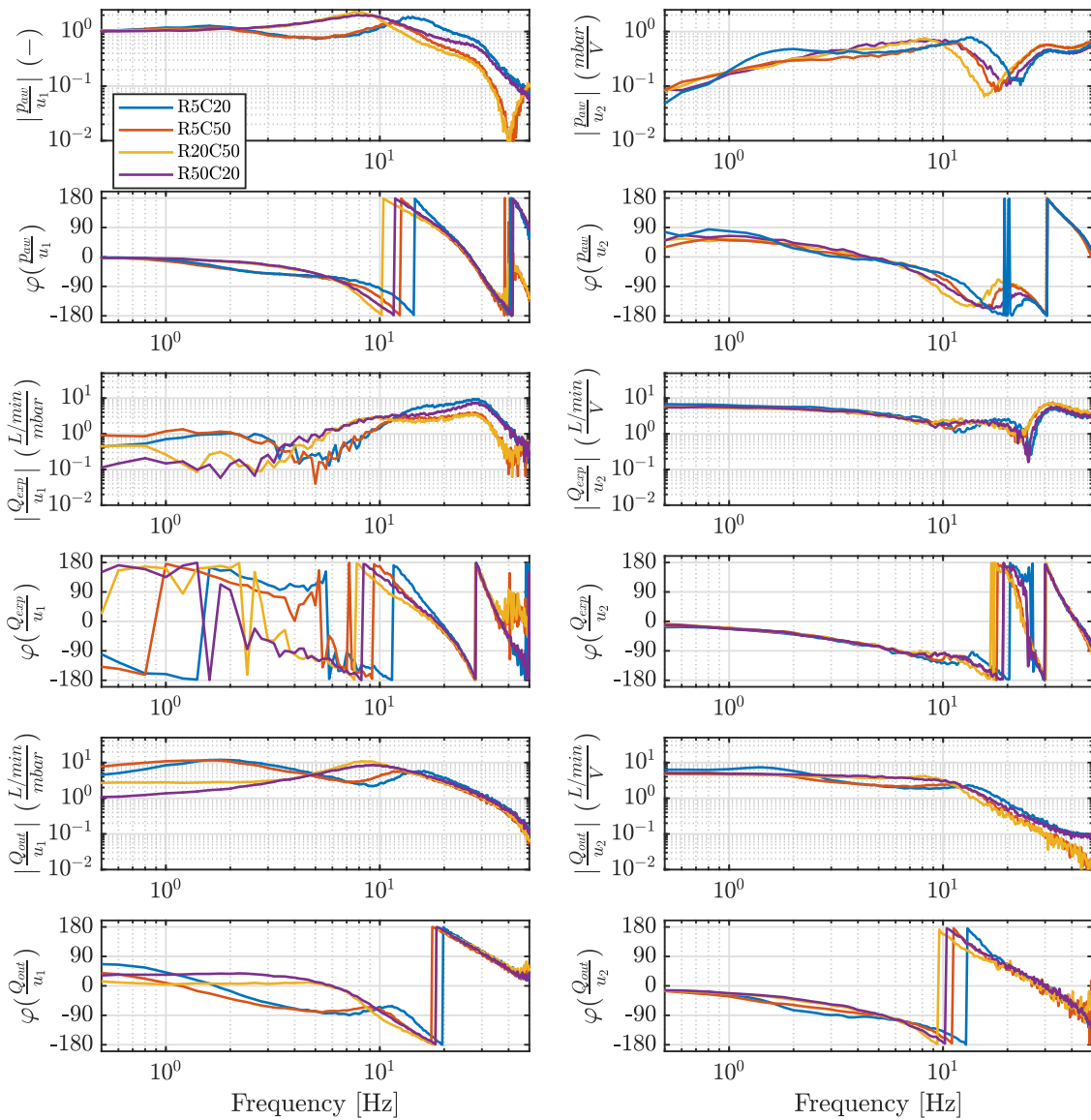


Fig. 4.4. Obtained MIMO FRF of the system for several lung parameters. The measurements are obtained by perturbing the system around a constant steady-state operating point.

around the steady state at $p_{aw} = 30$ mbar and $Q_{bf} = 3$ L/min. This is the same operating point as the one used for the linearized simulation models in Fig. 4.2. In the legend of Fig. 4.4, each lung is expressed using R and C , where $R = R_{aw}$ in mbar s/L and $C = C_{lung}$ in ml/mbar. Although a total of fifteen identification measurements have been performed, Fig. 4.4 only shows the four cases that are the most challenging for stability. In other words, these lungs and settings require the most stabilizing control action. The measured system in Fig. 4.4 represents the system behavior around a steady-state operating point. The measured system is defined as

$$G = \begin{bmatrix} G_{11} & G_{12} \\ G_{21} & G_{22} \\ G_{31} & G_{32} \end{bmatrix} \quad (4.4)$$

in which each matrix entry in G represents the corresponding identified model from Fig. 4.4.

As shown in the figure, the transfer functions are not dimensionless except for p_{aw}/u_1 (G_{11}) in the upper left corner. This transfer function shows that the system behavior between 2 and 10 Hz is mostly determined by the R_{aw} term, because the R5C20 and R5C50 lung show similar behavior up until 10 Hz. The lungs with a higher resistance both show the same behavior as well up until 10 Hz. At high frequencies, i.e., above 30 Hz, the compliance C_{lung} is the dominant term. From the top left figure it is observed that the R5C50 and R20C50 lung show the same behavior above 30 Hz. C_{lung} is more dominant at higher frequencies, because the lung dynamics are excited at higher frequencies. The transfer function p_{aw}/u_2 shows a low gain at frequencies below 1 Hz. This is due to the internal blower controller which ensures that $p_{control}$ is constant at low frequencies, which also keeps p_{aw} constant. In other words, opening and closing the expiration valve has a minimal effect on the airway pressure at low frequencies.

The Q_{exp}/u_2 and Q_{out}/u_2 transfer functions both show the same low-frequency behavior, i.e., a static gain of approximately 4.5 L/min V^{-1} . This corresponds to the constant steady-state behavior of the ventilation system, i.e., $Q_{out} = Q_{exp}$. This constant steady-state effect is not observed between Q_{exp}/u_1 and Q_{out}/u_1 . Instead, Q_{exp}/u_1 shows a noisy signal up to 6 Hz. This is explained by the fact that a pressure perturbation near the blower is almost completely damped out as soon as it reaches the expiration valve. This is mainly due to the long inspiration and expiration hose distance through which the air propagates. Furthermore, the long hose distance also causes a significant phase delay for the transfer function Q_{exp}/u_1 .

It is observed that the identified system in Fig. 4.4 and the linearized model in Fig. 4.4, shows fairly similar constant steady-state behavior for frequencies below 1 Hz. However, the identified system shows much more active lung dynamics up until 10 Hz compared to the linearized model. Therefore, the identified system in Fig. 4.4 is deemed more suitable for the feedback controller design process.

To design the decentralized feedback controllers, it is important to quantify the input-output coupling in the identified MIMO system. The dimensional dependency of each transfer function makes it challenging to compare the magnitude of each MIMO entry with one another. In the next section, an interaction analysis is performed to quantify the coupling between the different FRF's. In addition, this interaction analysis is used to conclude about a suitable controller bandwidth.

4.2.3 Interaction analysis

This section describes an interaction analysis for the measured system G in Fig. 4.4. The interaction analysis is used to motivate the controller bandwidth choice in Section 4.3.1. The unit dependency of the MIMO transfer functions makes it challenging to quantify the coupling in the system. A unitless interaction analysis is used to quantify the coupling using the Relative Gain Array (RGA). The RGA and its characteristics are described in detail in [19]. Due to the output switch in (2.34), it is possible to divide the system in (4.4) as two separate MIMO systems, depending on which output is used. The first MIMO system with Q_{exp} as output is defined as:

$$\begin{aligned} p_{aw} &= G_{11}u_1 + G_{12}u_2, \\ Q_{exp} &= G_{21}u_1 + G_{22}u_2. \end{aligned} \quad (4.5)$$

The second system with Q_{out} as an output is defined as:

$$\begin{aligned} p_{aw} &= G_{11}u_1 + G_{12}u_2, \\ Q_{out} &= G_{31}u_1 + G_{32}u_2. \end{aligned} \quad (4.6)$$

First, the RGA is determined for the case in (4.5) where p_{aw} and Q_{exp} are considered as the output. As discussed in Section 1.3, u_1 is used to control p_{aw} , and u_2 is used to control Q_{exp} . As a result, two different gains can be calculated for the MIMO system. The first gain calculates the transfer function from u_1 to p_{aw} when u_2 is constant, or equivalently pick $u_2 = 0$. The transfer function from u_1 to p_{aw} is then defined as

$$p_{aw} = G_{11}u_1. \quad (4.7)$$

For the second gain, the same transfer function from u_1 to p_{aw} is calculated, but now the loop between u_2 and Q_{exp} is under perfect control, i.e., $Q_{exp} = 0$. The required control action for u_2 to perfectly control $Q_{exp} = 0$ also depends on the first input u_1 , due to interaction. As a result, the perfect control action for u_2 is defined as:

$$u_2 = -\frac{G_{21}}{G_{22}}u_1. \quad (4.8)$$

Note that substituting this u_2 control action into (4.5) results in the desired $Q_{exp} = 0$. To calculate the second gain, (4.8) is substituted in p_{aw} equation of (4.5), which results in

$$p_{aw} = \underbrace{\left(G_{11} - \frac{G_{12}G_{21}}{G_{22}} \right)}_{\hat{G}_{11}} u_1. \quad (4.9)$$

The difference between \hat{G}_{11} and G_{11} shows the change in gain when the loop from u_2 to Q_{exp} is closed. Using this result, the corresponding RGA element is then calculated using

$$\lambda_{11} = \frac{G_{11}}{\hat{G}_{11}}. \quad (4.10)$$

If $\lambda_{11} = 1$, then the gains G_{11} and \hat{G}_{11} are almost equal. This means that the effect of closing an individual feedback loop has a negligible effect on the other loop. In other words, there is no bi-directional interaction between the two loops. The calculation of the RGA element λ_{11} in (4.10) is repeated for the second subsystem in (4.6) using the same strategy.

The RGA element λ_{11} is shown for the MIMO sub-systems (4.5) and (4.6) in Fig. 4.5a and 4.5b, respectively. The four lungs that are shown use the same parameters as the ones shown in

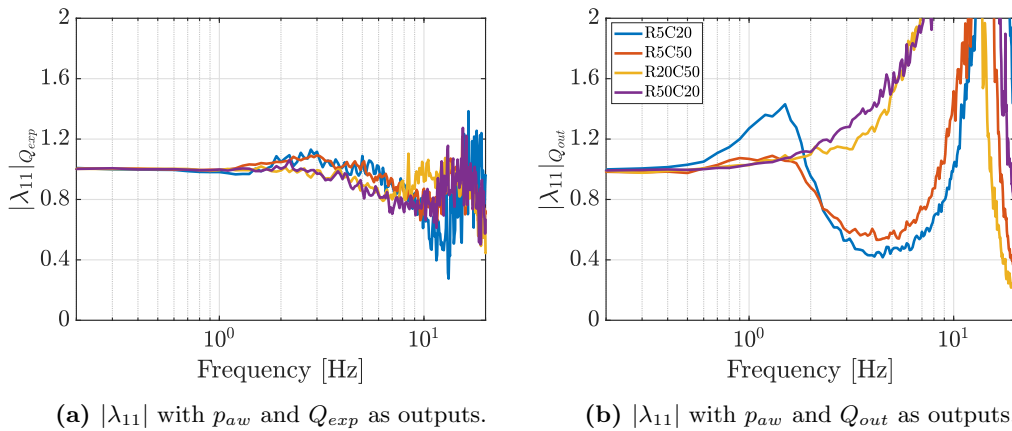


Fig. 4.5. The absolute value of the RGA element λ_{11} shown for the frequency range of interest for both sub-systems in (4.5) and (4.6). The RGA element is calculated for four different lungs.

the MIMO Bode diagrams in Fig. 4.4. If the output switch is applied to Q_{exp} , the RGA element in Fig. 4.5a describes the interaction in the system. If the output switch is applied to Q_{out} , the RGA element in Fig. 4.5b describes the interaction in the system.

From Fig. 4.5a it is concluded that the system with Q_{exp} is decoupled, i.e., $\lambda_{11} \approx 1$, for all lungs up until 6 Hz. After that, λ_{11} deviates too far from 1 which means that strong coupling effects might be observed by closing a feedback loop. For the sub-system with Q_{out} in Fig. 4.5b, the system is only decoupled up until approximately 1 Hz. As a result, it is concluded that the switching system shows coupling effects at frequencies higher than 1 Hz. This characteristic might induce stability problems for the decentralized feedback controller design if the controller bandwidth is chosen higher than 1 Hz. However, a typical breathing cycle in Fig. 1.4a takes four seconds to complete. This corresponds with a periodic reference of 0.25 Hz, which means that a controller bandwidth up to 1 Hz is sufficient for this system.

The next section, the decentralized feedback controller is designed using the obtained knowledge of this interaction analysis.

4.3 Decentralized feedback controller design

This section describes the decentralized feedback controller design process based on the identified MIMO systems from Section 4.2. First, the two independent SISO controllers are tuned in Section 4.3.1. Then, stability of the closed-loop MIMO system is proven in Section 4.3.2.

4.3.1 Decentralized controller tuning

As described in Section 4.1, a decentralized controller consists of a combination of independent SISO controllers. A decentralized controller uses a diagonal structure which is defined as

$$C = \begin{bmatrix} C_{11} & 0 & 0 \\ 0 & C_{22} & 0 \\ 0 & 0 & C_{22} \end{bmatrix}. \quad (4.11)$$

The purpose of this section is to define this diagonal controller C , which is used to control the measured system G in (4.4). The entry C_{11} is tuned for G_{11} , and C_{22} is tuned for both G_{22} and G_{32} . Note that this means that only one feedback controller is tuned for both Q_{exp} and Q_{out} . In theory it is possible to design separate controllers for Q_{exp} and Q_{out} . However, this would introduce a switching controller, which complicates the controller design process and makes it very challenging to guarantee stability of the complete system. To only assess the SISO diagonal control systems, the diagonal system \tilde{G} is defined as

$$\tilde{G} = \begin{bmatrix} G_{11} & 0 \\ 0 & G_{22} \\ 0 & G_{32} \end{bmatrix} \quad (4.12)$$

Using this diagonal model structure, the open-loop system \tilde{L} is defined as

$$\tilde{L} = C\tilde{G}. \quad (4.13)$$

Substituting the matrices G and C from (4.4) and (4.11) results in

$$\tilde{L} = \begin{bmatrix} \tilde{L}_{11} & 0 \\ 0 & \tilde{L}_{22} \\ 0 & \tilde{L}_{32} \end{bmatrix} = \begin{bmatrix} G_{11}C_{11} & 0 \\ 0 & G_{22}C_{22} \\ 0 & G_{32}C_{22} \end{bmatrix}. \quad (4.14)$$

The controllers C_{11} and C_{22} are both designed as cut-off integrators, i.e., PI controllers. The P action is required to shift the Bode diagram vertically to compensate for the offsets due to the unit mismatch. The integral action I is required to eliminate steady-state tracking errors due to model uncertainty that is not taken into account with the feedforward controller. The SISO controllers are defined as

$$C_{11} = \frac{0.1s + 4.398}{s}, \quad C_{22} = 10^{-4} \frac{0.14s + 13.19}{s}. \quad (4.15)$$

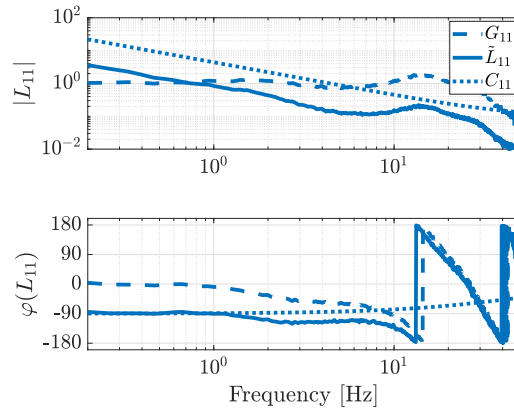
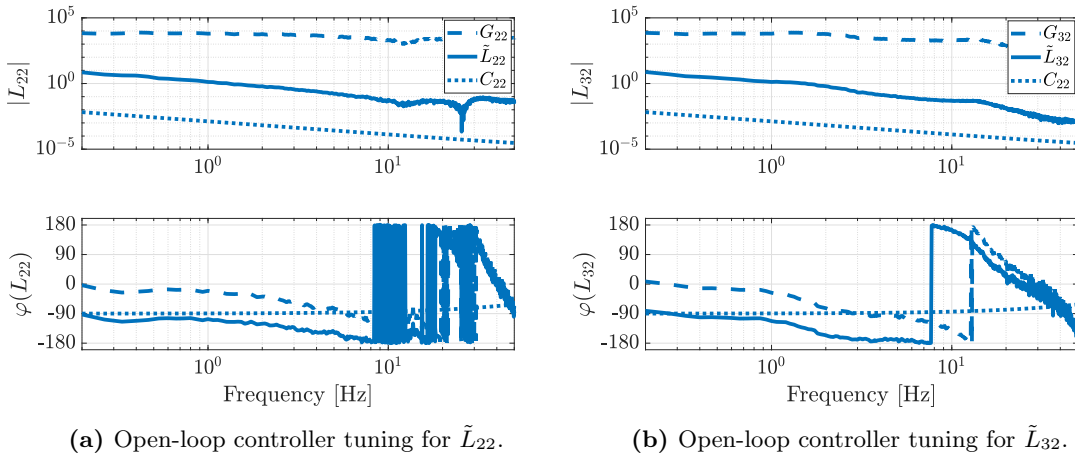


Fig. 4.6. Open-loop controller tuning for \tilde{L}_{11} .



(a) Open-loop controller tuning for \tilde{L}_{22} .

(b) Open-loop controller tuning for \tilde{L}_{32} .

Fig. 4.7. Open-loop controller tuning for the baseflow controller.

The controllers both achieve a bandwidth of approximately 1 Hz. As a result, the coupling effects that are discussed in Section 4.2.3 are limited. In Fig. 4.6 and 4.7, the tuning process of the SISO controllers for the R5C20 lung is shown. Each open-loop of (4.14) and the corresponding controller is shown in Fig. 4.6, 4.7a, and 4.7b. The controllers are designed to achieve low-frequency reference tracking up to 1 Hz. In the next section, stability of the MIMO system is proven.

4.3.2 MIMO stability

This section describes a generalized Nyquist stability test for the MIMO system in Fig. 4.4 with the decentralized controller design in (4.15). To achieve MIMO closed-loop stability the following theorem from [19, Theorem 4.9] is applied.

Theorem 4.3.1 ([19]) *Let P_{ol} denote the number of open-loop unstable poles in L . The closed-loop system with loop transfer function L and negative feedback is stable if and only if the Nyquist plot of $\det(I + L)$*

- i) makes P_{ol} anti-clockwise encirclements of the origin, and*
- ii) does not pass through the origin.*

Due to the open-loop stability of the system, as described in Section 2.2, there is no need for anti-clockwise encirclements in the first condition. The second condition ensures that the the

system is well-posed, i.e., a unique solution exists. Theorem 4.3.1 is used to prove that the SISO controller designs from the previous section do not destabilize the complete MIMO system. First, the closed-loop stability of each individual SISO loop is analyzed.

Fig. 4.8 shows the SISO Nyquist diagrams of \tilde{L}_{11} for four lungs, which are the same lungs as shown in Fig. 4.4. The grey disc is a visual tool to ensure that the systems achieve the desired robustness, using a modulus margin of 6 dB. Notice that the controller design of C_{11} is very conservative. This is done to obtain a less aggressive controller with a low bandwidth of 1 Hz to prevent coupling effects as discussed in Section 4.2.3. Fig. 4.9a and 4.9b show the SISO Nyquist diagrams of \tilde{L}_{22} and \tilde{L}_{32} , respectively. Due to the switching condition in (2.34), the system switches between the outputs Q_{exp} and Q_{out} , and consequently, between the two Nyquist diagrams in Fig. 4.9. It can be seen that the open-loop for Q_{out} , i.e., \tilde{L}_{32} , limits the performance of the controller C_{22} .

Using SISO Nyquist theory, it is possible to conclude that a SISO closed-loop system is stable when the open-loop is stable and the system does not encircle the (0,-1) point, see [24]. From

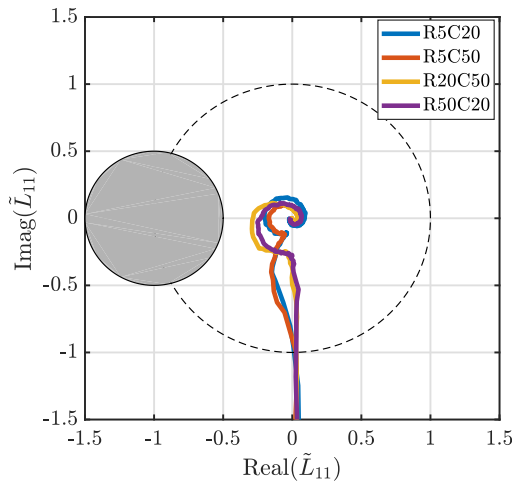
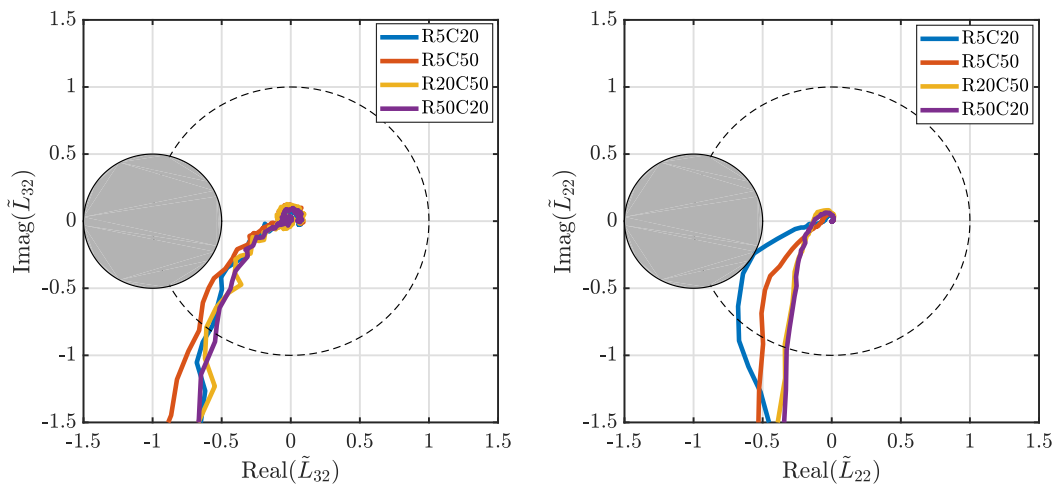


Fig. 4.8. Nyquist diagram of the open-loop transfer function \tilde{L}_{11} , i.e., from u_1 to p_{aw} .



(a) Nyquist diagram of the open-loop transfer function \tilde{L}_{22} , i.e., from u_2 to Q_{exp} .

(b) Nyquist diagram of the open-loop transfer function \tilde{L}_{32} , i.e., from u_2 to Q_{out}

Fig. 4.9. Two SISO open-loop systems that both use the controller C_{22} . Depending on the switching condition in (2.34), the left or the right Nyquist diagram is active.

the SISO Nyquist diagrams in Fig. 4.8 and 4.9 it is concluded that all SISO loops are closed-loop stable. However, this is not sufficient to guarantee stability of the full MIMO system. The reason for this is that the designed SISO controllers can still destabilize each other due to the cross terms G_{12} , G_{21} , and G_{31} in (4.4). To prove stability of the closed-loop MIMO system, the generalized Nyquist test in Theorem 4.3.1 is applied. Stability of the closed-loop MIMO system is proven by analyzing the MIMO open-loop system L , which is defined as

$$L = CG = \begin{bmatrix} C_{11} & 0 & 0 \\ 0 & C_{22} & 0 \\ 0 & 0 & C_{22} \end{bmatrix} \begin{bmatrix} G_{11} & G_{12} \\ G_{21} & G_{22} \\ G_{31} & G_{32} \end{bmatrix} = \begin{bmatrix} C_{11}G_{11} & C_{11}G_{12} \\ C_{22}G_{21} & C_{22}G_{22} \\ C_{22}G_{31} & C_{22}G_{32} \end{bmatrix} \quad (4.16)$$

Due to the switching outputs Q_{exp} and Q_{out} , the system in (4.16) is split in two separate MIMO systems:

$$L_{Q_{exp}} = \begin{bmatrix} C_{11}G_{11} & C_{11}G_{12} \\ C_{22}G_{21} & C_{22}G_{22} \end{bmatrix} \quad (4.17)$$

$$L_{Q_{out}} = \begin{bmatrix} C_{11}G_{11} & C_{11}G_{12} \\ C_{22}G_{31} & C_{22}G_{32} \end{bmatrix} \quad (4.18)$$

Stability under switched outputs will be discussed in Section 4.4. Let us for now assume that the system does not switch, in order to study closed-loop stability for the two separate MIMO systems during steady-state phase.

Closed-loop stability of each separate MIMO system is proven using generalized Nyquist stability theory for the open-loop systems $L_{Q_{exp}}$ and $L_{Q_{out}}$. The MIMO system is closed-loop stable if $\det(I + L_{Q_{exp}})$ and $\det(I + L_{Q_{out}})$ do not encircle the origin. Fig. 4.10 shows the MIMO generalized Nyquist for the four lungs. As can be seen, none of the MIMO open-loops encircle the origin which means that the each individual MIMO system for Q_{out} and Q_{exp} is closed-loop stable with the proposed decentralized controller C .

Although the closed-loop stability is proven for both closed-loop MIMO systems, it does not guarantee stability during the transient phases of the breathing cycle, i.e., phase I and III in Fig. 1.4a. During those phases the flow and pressure deviate too far from the identified models. As a result, the system behavior is partially unknown during those phases and extensive testing is required to 'guarantee' stability under various operation conditions. Furthermore, the closed-loop stability of the two individual MIMO systems in (4.17) and (4.18) does not a priori guarantee stability of the output switched MIMO system, see [25, p. 19]. The next section discusses the closed-loop stability of the output switching system.

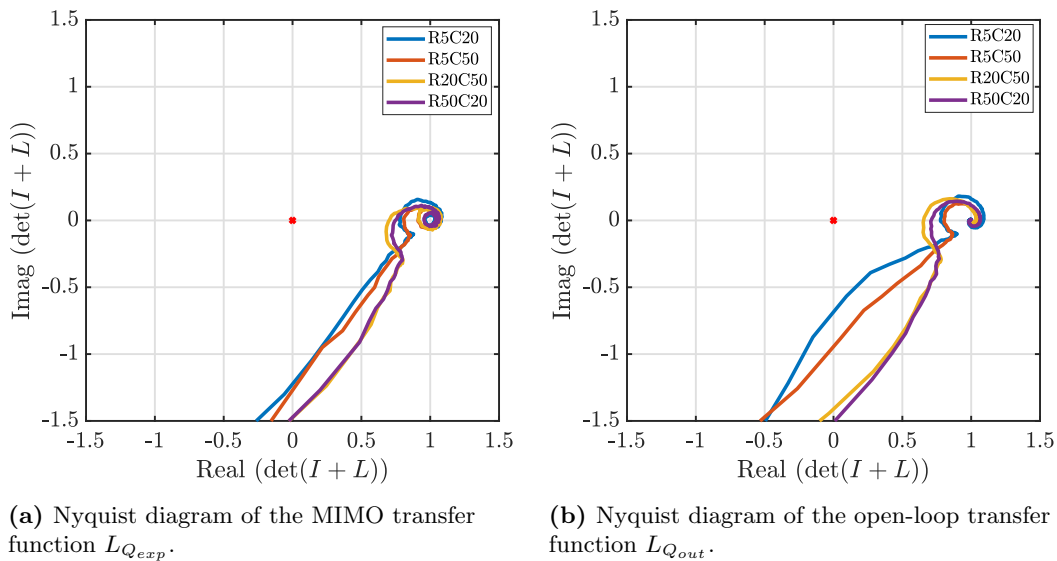


Fig. 4.10. Two MIMO open-loop systems which are used to prove MIMO closed-loop stability.

4.4 Stability under switched output signals

In the previous section, it is concluded that each MIMO sub-system in (4.17) and (4.18) is closed-loop stable during the steady-state phases II and IV. However, this does not guarantee closed-loop stability under switching, see [25, p. 19]. The switching condition is explained in Section 2.3, and defined in (2.34). In this section, stability of the switched closed-loop system is analyzed using the linearized model in (4.1).

First, in Section 4.4.1, the linearized closed-loop switched model is defined. Based on this model, the stability under switching outputs is discussed in Section 4.4.2 for two different switching scenarios.

4.4.1 Linearized closed-loop dynamics

To analyze the stability of the switching system, the linearized state-space model of (4.1) is considered. For ease of notation, the linearized system state p_{lung} is renamed x_l . The open-loop linearized system is written in a state-space format as

$$G_l = \begin{cases} \dot{x}_l &= \mathbf{A}_1 x_l + \mathbf{B}_1 u \\ y &= \mathbf{C}_1 x_l + \mathbf{D}_1 u \end{cases}, \quad (4.19)$$

in which \mathbf{A}_1 is the linearized state matrix, \mathbf{B}_1 is the linearized input matrix, \mathbf{C}_1 is the linearized output matrix, and \mathbf{D}_1 is the linearized feedthrough matrix. As a result of the output switch in (2.34), the output y is defined as

$$y = \begin{cases} \begin{bmatrix} p_{aw} \\ Q_{exp} \end{bmatrix} & \text{if } \phi = Q_{exp}, \\ \begin{bmatrix} p_{aw} \\ Q_{out} \end{bmatrix} & \text{otherwise.} \end{cases} \quad (4.20)$$

A more detailed description of the switching condition ϕ is found in Section 2.3. The output switching condition in (4.20) is combined with the linearized state-space model in (4.19), which results in

$$G_l = \begin{cases} \dot{x}_l &= \mathbf{A}_1 x_l + \mathbf{B}_1 u \\ y &= \begin{cases} \mathbf{C}_{11} x_l + \mathbf{D}_{11} u & \text{if } \phi = Q_{exp}, \\ \mathbf{C}_{12} x_l + \mathbf{D}_{12} u & \text{otherwise} \end{cases} \end{cases} \quad (4.21)$$

The designed decentralized controller in (4.11) is rewritten to a state-space structure, which results in

$$C = \begin{cases} \dot{x}_c &= \mathbf{A}_c x_c + \mathbf{B}_c e \\ u &= \mathbf{C}_c x_c \end{cases}, \quad (4.22)$$

where x_c is the controller state, u is the input vector, and e is the error vector. Due to the output switch in (4.20), the error vector e switches analogous to the output vector. The error vector is defined as

$$e = \begin{cases} \begin{bmatrix} p_{target} - p_{aw} \\ Q_{bf} - Q_{exp} \end{bmatrix} & \text{if } \phi = Q_{exp}, \\ \begin{bmatrix} p_{target} - p_{aw} \\ Q_{bf} - Q_{out} \end{bmatrix} & \text{otherwise.} \end{cases} \quad (4.23)$$

The closed-loop dynamics of the linearized system are obtained by combining the switched system and the controller state-space models using a cascade interconnection, see [18, p. 8]. This interconnection combines the switched linearized model G_l in (4.21) with the controller C in (4.22), which results in the following closed-loop dynamics:

$$\text{Closed loop} = \begin{cases} \dot{x}_l = \mathbf{A}_1 x_l + \mathbf{B}_1 \mathbf{C}_c x_c \\ \dot{x}_c = \begin{cases} \mathbf{A}_c x_c + \mathbf{B}_c (r - \mathbf{C}_{11} x_l - \mathbf{D}_{11} \mathbf{C}_c x_c) & \text{if } \phi = Q_{exp}, \\ \mathbf{A}_c x_c + \mathbf{B}_c (r - \mathbf{C}_{12} x_l - \mathbf{D}_{12} \mathbf{C}_c x_c) & \text{otherwise,} \end{cases} \end{cases} \quad (4.24)$$

where $r = [p_{target} \quad Q_{bf}]^T$. In addition, u is replaced with $\mathbf{C}_c x_c$. Restructuring this closed-loop system results in

$$\begin{bmatrix} \dot{x}_l \\ \dot{x}_c \end{bmatrix} = \begin{cases} \underbrace{\begin{bmatrix} \mathbf{A}_1 & \mathbf{B}_1 \mathbf{C}_c \\ -\mathbf{B}_c \mathbf{C}_{l1} & \mathbf{A}_c - \mathbf{B}_c \mathbf{D}_{l1} \mathbf{C}_c \end{bmatrix}}_{\mathbf{A}_{c11}} \begin{bmatrix} x_l \\ x_c \end{bmatrix} + \underbrace{\begin{bmatrix} 0 \\ \mathbf{B}_c \end{bmatrix}}_{\mathbf{B}_{c11}} r & \text{if } \phi = Q_{exp}, \\ \underbrace{\begin{bmatrix} \mathbf{A}_1 & \mathbf{B}_1 \mathbf{C}_c \\ -\mathbf{B}_c \mathbf{C}_{l2} & \mathbf{A}_c - \mathbf{B}_c \mathbf{D}_{l2} \mathbf{C}_c \end{bmatrix}}_{\mathbf{A}_{c12}} \begin{bmatrix} x_l \\ x_c \end{bmatrix} + \underbrace{\begin{bmatrix} 0 \\ \mathbf{B}_c \end{bmatrix}}_{\mathbf{B}_{c12}} r & \text{otherwise.} \end{cases} \quad (4.25)$$

This closed-loop system is simplified as

$$\dot{x} = \begin{cases} \mathbf{A}_{c11} x + \mathbf{B}_{c11} r & \text{if } \phi = Q_{exp}, \\ \mathbf{A}_{c12} x + \mathbf{B}_{c12} r & \text{otherwise,} \end{cases} \quad (4.26)$$

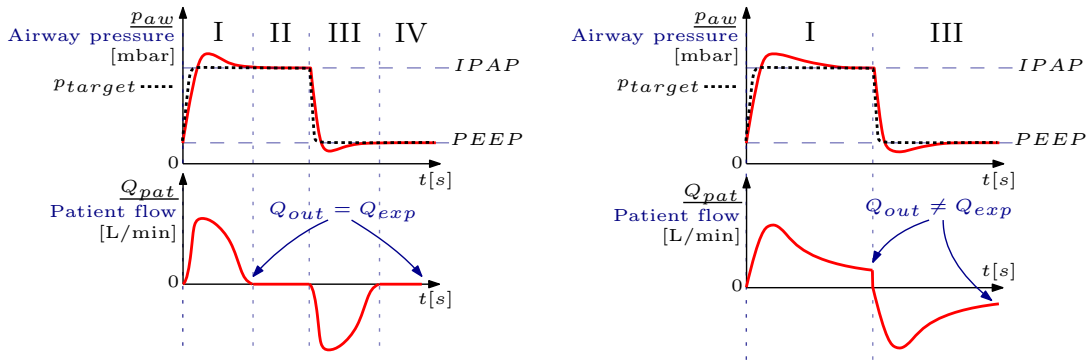
where $x = [x_l \quad x_c]^T$. The closed-loop state matrices \mathbf{A}_{c11} and \mathbf{A}_{c12} are Hurwitz, because of the stability of each linear MIMO closed-loop system in (4.17) and (4.18), respectively. Stability is proven using the Generalized Nyquist theorem in Section 4.3.2. However, due to the switching condition for e in (4.23), closed-loop stability for the switched system is not guaranteed. In the next section, two different switching scenarios are defined for the closed-loop switching system in (4.26).

4.4.2 Switching scenarios

Due to the switching condition for e in (4.23), there are two possible switching scenarios for this system, which depend on the lung characteristics. The two scenarios are defined as:

- e is continuous, which occurs when the switch is applied for a low resistance lung. The airway pressure p_{aw} and patient flow Q_{pat} for a low resistance lung are shown in Fig. 4.11a. During phase I, the stable controller ensures that $Q_{exp} \rightarrow Q_{bf}$ and $e \rightarrow 0$. The output switch occurs, as described in (4.23), at the moment when $Q_{out} = Q_{bf}$. At this moment, the ventilation system has reached a constant steady state and $Q_{pat} = 0$. Due to the conservation of flow in (2.6), it is concluded that $Q_{exp} = Q_{out}$. Consequently, the error vector e is continuous during the output switch.
- e is discontinuous, which occurs when the switch is applied for a high resistance lung. The airway pressure p_{aw} and patient flow Q_{pat} for a high resistance lung are shown in Fig. 4.11b. Due to the high resistance of the lung, the flow going in and out of the lung is lower compared to the low resistance lung. In this case, the lung does not reach phase II or phase IV, but instead jumps from phase I to phase III. In other words, it skips the constant steady-state phases II and IV. During phase I, the stable controller still ensures that $Q_{exp} \rightarrow Q_{bf}$ and $e \rightarrow 0$. At the moment of the output switch the system is not yet in steady state, which means that there is still air flowing into the lungs of the patient, i.e., $Q_{pat} \neq 0$. Due to the conservation of flow in (2.6), it is concluded that $Q_{out} \neq Q_{exp}$ at the moment of the output switch. As a result, e experiences a discontinuity when switching from Q_{exp} to Q_{out} and vice versa.

For the low resistant lung, i.e., e is continuous, the system switches the outputs during the transition from phase I to phase II, and again during the transition from phase IV to phase I. This means that the output switch occurs when the system transitions from a constant steady state to a transient state, or vice versa. During the transient state, the linearized model in (4.26) is not valid. However, an assumption is made regarding the switching location. Let us assume that at the switching location, there exists a very small area δ , where the transient phase changes to a constant steady-state phase. Within this area δ , the linearized model is assumed to be valid. Using this assumption, a conclusion is made regarding the closed-loop stability of the switched system for a low resistant lung scenario.



(a) Low resistant lung with a continuous switching error e . (b) High resistant lung with a discontinuous switching error e .

Fig. 4.11. Two different types of lungs. A low resistant lung (left) reaches the steady-state phases II and IV. a high resistant lung (right) does not reach a steady state. From phase I it jumps directly to phase III.

Due to the asymptotically stable controller C , the sub-systems \mathbf{A}_{c11} and \mathbf{A}_{c12} are Hurwitz. This means that the error e converges to zero for each output configuration. When the output switch is applied, the system does not experience a discontinuity at e , because $Q_{bf} = Q_{exp} = Q_{out}$, which means that e remains at zero, see Fig. 4.11a. As a result, the closed-loop dynamics in (4.25), do not contain any switching dynamics and it is concluded that the switched system is closed-loop stable for this scenario.

For the high resistant lung, i.e., e is discontinuous, it is not possible to analyze closed-loop stability using the linearized model, because the output switch occurs during the transient phases I and III. During those phases, the linearized model is no longer valid, and no accurate analytical model is available for the patient-hose-valve system. Consequently, it is not possible to conclude about closed-loop stability of the switched system for high resistance lungs. An extensive experimental case-study is shown in Chapter 5 to validate the stability and performance of the designed feedforward and feedback controllers.

4.5 Summary

This chapter described the motivation and design process of a decentralized feedback controller for the patient-hose-valve system. First, the motivation for a decentralized controller is provided. In addition, the need for identification experiments is explained. Then, a linear MIMO FRF of the system is acquired. Thereafter, a decentralized feedback controller is designed based on the identified MIMO systems, while also taking the RGA of the system into account for a suitable controller bandwidth. Stability of the proposed controller is proven using a generalized Nyquist test. MIMO switching stability in steady state is analyzed using the closed-loop linearized state-space model. Several assumptions regarding switched system stability are made. However, these do not apply for all switching scenarios. In the next Chapter, the feedforward controller from Chapter 3 and the decentralized feedback controller from this chapter are tested using simulations and experiments.

Chapter 5

Simulations and experimental verification

In this chapter, the performance of the feedforward and feedback controllers from Chapter 3 and 4, respectively, are analyzed by means of a simulation and experimental case-study. This is the fourth and final sub-objective of Section 1.4. First, in Section 5.1, the performance measures are defined for the ventilation system. Thereafter, in Section 5.2, the feedforward controller design without feedback is tested in simulations and experiments. In section 5.3, the decentralized feedback controller in combination with the feedforward controller is tested in simulation and experiments. After that, in Section 5.4, the proposed control strategy is compared to the state-of-practice control solution. Finally, in Section 5.5, the chapter is summarized.

5.1 Performance measure and use-case description

This section describes the measure of performance of the proposed controller design. During ventilation, the following performance criteria are defined:

- Minimize the p_{aw} overshoot during the inspiration phase I. A pressure overshoot may cause over-extension of the lung tissue which causes ventilation induced lung injuries [2].
- Minimize the p_{aw} undershoot during the expiration phase III. Pressure undershoot may result in a drop in lung pressure. If the lung pressure is too long too low during expiration, it might cause alveolar collapsing [2]. Frequent alveolar collapsing during mechanical ventilation causes lung damage over time.
- Baseflow tracking is desired in all phases of the breathing cycle. However, during phase I and III, the pressure tracking performance is more important, because this guarantees that the patient is sufficiently ventilated.
- A baseflow overshoot must be prevented as much as possible for two reasons. The first reason is that a baseflow overshoot might result in an undesired pressure ripple due to the physical connection. The second reason why baseflow overshoot must be prevented is that, hospitals often use the baseflow target Q_{bf} to calculate the usage of O_2 . Overshoot of Q_{bf} results in more O_2 usage than predicted. A baseflow undershoot, however, is less critical, because it results in less O_2 usage. As a result, the hospital calculations are too conservative which is not a problem.

To analyze the performance of the feedforward and feedback controller, the controllers are analyzed for a breathing cycle of four seconds. In more detail, the inspiration phase, i.e., phase I and II in Fig. 1.4a, takes two seconds in total. After that, two seconds are used for the expiration phase, i.e., phase III and IV in Fig. 1.4a. For each measurement, PEEP and IPAP are set to 5 and 20 mbar, respectively. The baseflow target Q_{bf} is set to 3 L/min for the complete breathing cycle. For each controller analysis, the performance for four different lungs are evaluated. The four lungs

are: R5C20, R5C50, R20C50, and R50C20. These lungs are also used for the feedback controller design process in Chapter 4.

The controllers are experimentally tested using the same set-up with the ASL 5000 breathing simulator as explained in Section 4.2.1. In the next section, the simulation and experimental results of the feedforward controller are analyzed.

5.2 Verification of the feedforward controller

This section shows the simulation and experimental results of the feedforward controller design from Chapter 3. Note that this means that there is only feedforward and no feedback applied to the system. In more detail, Section 5.2.1 shows the simulation results and Section 5.2.2 shows the experimental results of the feedforward controller.

5.2.1 Feedforward controller: simulation results

This section analyzes the simulation results of the feedforward controller without feedback. The feedforward controller is implemented first without feedback to assess its performance. The simulation model that is used for the controller verification is equal to the state-space model in (2.25)-(2.29). R_{hose1} and R_{hose2} are both set to 1.02 mbar s/L. In addition, the experimentally obtained model for the expiration valve in Section 3.3, is implemented as R_{exp} .

Fig. 5.1 shows the results of the feedforward controller in simulation for one breathing cycle of four seconds. The top figure shows the p_{aw} tracking performance and the bottom two figures together show the baseflow tracking performance. As explained in Section 1.3.3, the baseflow target is split between Q_{exp} and Q_{out} according to the switching condition (2.34). The switching effect of Q_{exp} and Q_{out} is visualized in the bottom two figures using the solid and dashed lines. If a line is solid, then it is actively used as a baseflow control signal. When a line is dashed, then it is not actively controlled.

During the inspiration phase in Fig. 5.1, i.e., up until $t=2s$, it can be concluded that the feedforward controller shows a good p_{aw} tracking performance. The rise-time from PEEP to IPAP is achieved within one second for all lungs. No overshoot is observed as well. The baseflow tracking during the inspiration phase shows a good performance as well. Only a very small undershoot is observed for all lungs at the start of the inspiration phase, i.e., at $t=0.1s$. However, as soon as the system reaches a steady state, the expiration flow converges to the correct baseflow target for all lungs.

At the start of the expiration phase, i.e., at $t=2s$, the airway pressure drops from 20 to 5 mbar, which allows the patient to exhale the used air. As can be seen, p_{aw} shows a very slow pressure decrease for all lungs. This effect is caused by the R_{exp} model that is used for the simulation. As described in Section 3.3, the model for R_{exp} is obtained in a constant steady state, i.e., it only depends on u_1 and u_2 . However, during transient phases, R_{exp} also depends on the lung pressure p_{lung} , which helps to push open the expiration valve during expiration. This phenomenon is not taken into account for the modeling process of R_{exp} . As a result, the pressure decrease that is observed in the top figure is solely generated by the inputs u_1 and u_2 . For the experimental verification process, the pressure decrease is expected to be much faster. Due to the slow pressure decrease, the system does not reach a new constant steady state before the breathing cycle is finished, hence there is no baseflow for any lung during the expiration phase. The flow discontinuity at $t=2s$ for the R20C50 and R50C20 lung is caused by the output switch (2.34). R20C50 and R50C20 lungs are considered high resistant lungs. As explained in Section 4.4.2, high resistant lungs experience a discontinuity during the output switch from Q_{exp} to Q_{out} .

From the simulation of the feedforward controller it can be concluded that, due to the limited model accuracy of the valve model R_{exp} , it is challenging to analyze the exact performance of the feedforward controller. In the next section, the experimental case-study for the feedforward controller is presented.

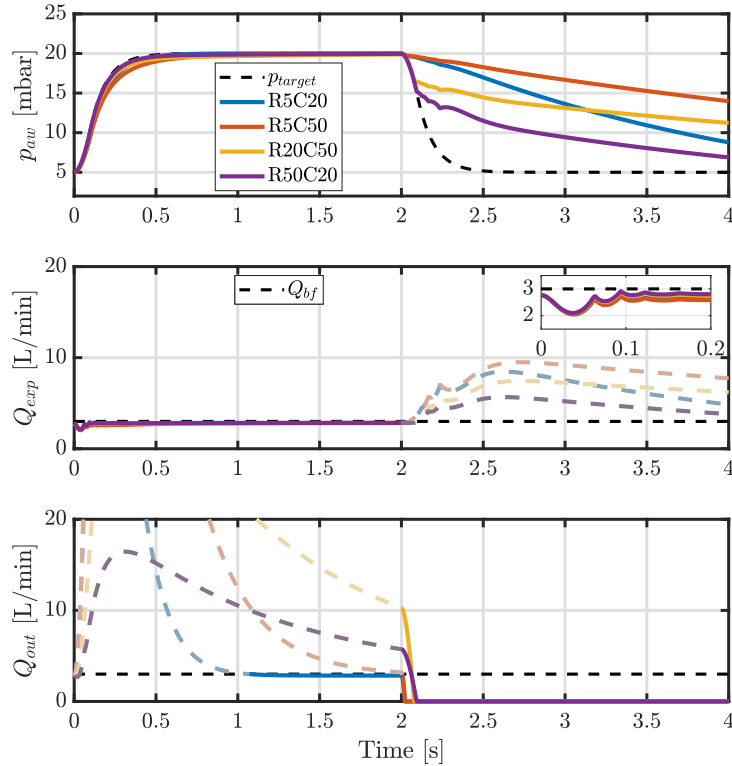


Fig. 5.1. Simulation of the patient-hose-valve system with feedforward controller. The airway pressure shows a slow response during the expiration phase after $t = 2s$. Consequently, the baseflow level is not achieved for Q_{out} after $t = 2s$ in the bottom figure.

5.2.2 Feedforward controller: experimental results

In this section, the proposed feedforward controller is applied to the experimental set-up. Fig. 5.2 shows the experimental results of a four second breathing cycle.

During the inspiration phase, the pressure tracking performance for p_{aw} shows the same rise-time compared to the simulation results in Fig. 5.1. It can be observed that the C50 lungs show a slightly slower response compared to the more stiffer lungs, i.e., the C20 lungs. In addition, a slight overshoot is observed for the R5C20 lung which is caused by the combination of a low resistance and a low compliance. This combination results in more pressure and flow oscillations compared to the other lungs. The bottom two figures in Fig. 5.2 shows the baseflow tracking performance of the experimental set-up for Q_{exp} and Q_{out} . During the inspiration phase, it can be observed that the baseflow target is achieved for the R5C20 and R5C50 lung as soon as each lung reaches a steady state. The time before each lung reaches a constant steady state depends on the value of R_{aw} and C_{lung} . Lungs with a high resistance and high compliance take longer to reach a steady state. Note that the R20C50 and R50C20 lungs are the slowest lungs and Q_{out} does not reach a steady state before the inspiration phase ends, i.e., before $t=2s$. The response of the stiffer lungs R5C20 and R5C50 during the inspiration phase shows that the feedforward controller reaches the baseflow target Q_{bf} independently of the patient type. Note that if the inspiration time would be longer, the R20C50 and R50C20 lung also achieve the desired baseflow level.

During the expiration phase, the airway pressure decrease is much faster compared to the simulation result in Fig. 5.1, due to the exhaled air of the patient that pushes open the expiration valve. As a result, more flow leaves the expiration valve, which allows the pressure inside the hose system to decrease much faster. This faster pressure decrease, however, causes a pressure overshoot for all lungs at approximately $t=2.5s$. As described in Section 5.1, this pressure overshoot

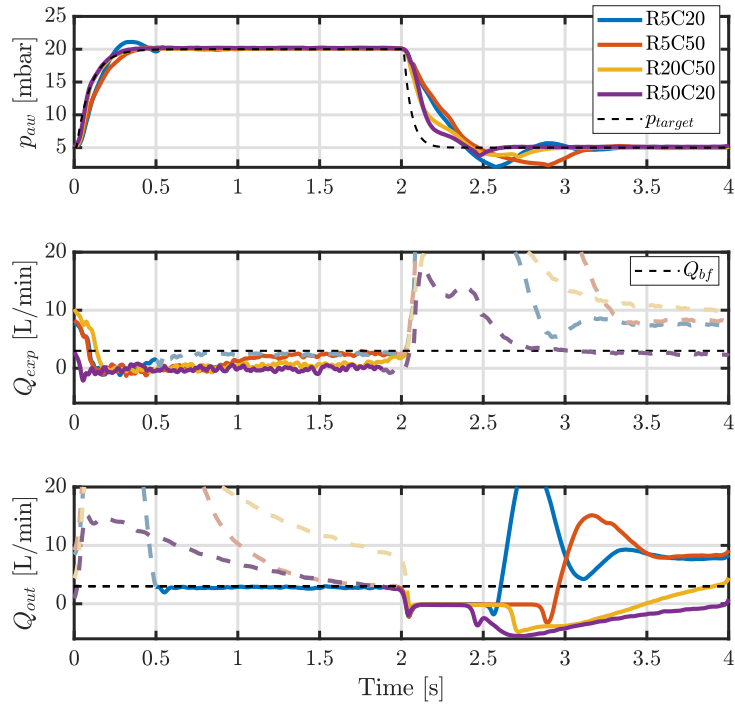


Fig. 5.2. Experimental test of the system with feedforward controller. The airway pressure shows a much faster response during after $t = 2s$ compared to the simulation results. The baseflow target is achieved for Q_{exp} as soon as each lung reaches a constant steady state. The poor performance of the baseflow tracking in the bottom figure after $t = 2s$ is caused by the hysteresis effect of the expiration valve and the slow constant steady-state convergence.

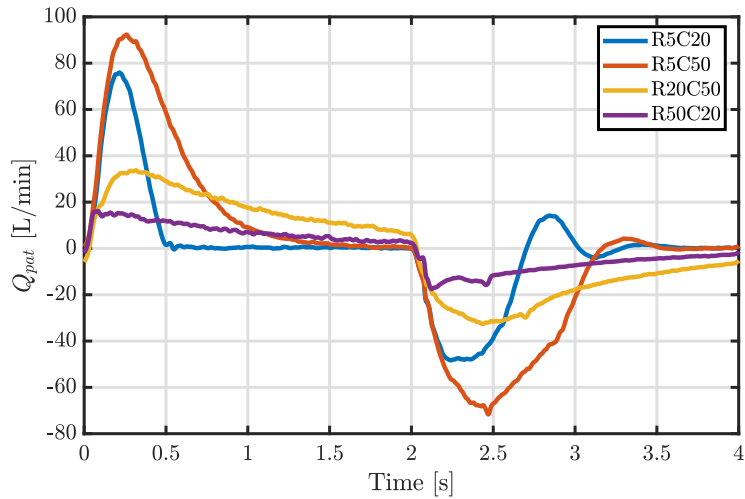


Fig. 5.3. Patient flow Q_{pat} for four lungs when the feedforward controller is applied in experiments.

is undesired during this phase of the breathing cycle. During the expiration phase the output flow Q_{out} shows a large baseflow error for all lungs in the bottom figure of Fig. 5.2. The main reasons for this effect are:

- The hysteresis effect of the piezo valve causes a steady-state error for the $R5C20$ and $R5C50$ lungs which is not included in the feedforward controller, see Section 3.3.
- The lungs with a high resistance, i.e., $R20C50$ and $R50C20$, are still not in steady state when the breathing cycle is finished at $t = 4s$. As a result, air is still flowing from the lungs and the correct baseflow target is not achieved. Fig. 5.3 shows the patient flow for each lung when the feedforward is applied. As can be seen, the patient flow of the $R20C50$ and $R50C20$ lung do not reach zero at the end of the expiration phase.

The negative output flow in the bottom figure of Fig. 5.2 is caused by the check valve. This check valve ensures that flow from the patient does not enter the inspiration hose, i.e., $Q_{out} > 0$. However, this check valve always has a small leak, which explains the negative blower output flow.

From the experimental case-study it is concluded that feedforward controller without feedback does not achieve a desirable performance. The main performance limitations are:

- Slow baseflow response during the inspiration phase for lungs with a high resistance.
- Poor pressure and baseflow tracking during the expiration phase.
- Significant steady-state baseflow errors at the end of the expiration phase, due to the hysteresis effect of the piezo valve and slow response of the lungs with a high resistance, see Fig. 5.3.

To improve the performance of the ventilation system, a decentralized feedback controller is added to the feedforward controller, as explained in Chapter 4. The following section shows the simulation and experimental results of the decentralized feedback controller in combination with the feedforward controller.

5.3 Verification of the feedback controller

This section shows the simulation and experimental results of testing the decentralized feedback control strategy from Chapter 4 in combination with the feedforward controller from Chapter 3. First, in Section 5.3.1, the simulation results are analyzed. Thereafter, in Section 5.3.2, the proposed control strategy is experimentally verified.

5.3.1 Feedback controller: simulation results

In this section, the feedforward and feedback controller are combined and tested using simulations. Fig. 5.4 shows the result of the feedback and feedforward controller for a breathing cycle of four seconds.

During the inspiration phase, it can be concluded that the implementation of feedback control improves the p_{aw} tracking performance by reducing the rise-time for all lungs. In addition, there is no overshoot for any lung. The baseflow tracking performance during the inspiration phase also shows that Q_{exp} is almost perfectly maintaining a baseflow, with only a very small undershoot at $t=0.1s$.

During the expiration phase, there is almost no p_{aw} overshoot in the top figure. For the baseflow tracking problem, the same switching effect from Q_{exp} to Q_{out} is observed for the $R20C50$ and $R50C20$ lung, which is the same as in Fig. 5.1. After $t=2s$, when the airway pressure decrease is initiated, each lung experiences a drop in baseflow. Almost all lungs drop to zero flow for a few tenths of a second, which is inevitable due to the fast pressure decrease and the delay in the system. Due to the build-up of the baseflow integrator action, a baseflow overshoot is seen for all lungs at $t=2.5s$. The highest overshoot is observed for the $R5C50$ lung. This transient behavior is only present for approximately 0.5 seconds. After $t=3s$, all lungs have converged to the desired baseflow target Q_{bf} . In the next section, the same control strategy is applied to the experimental set-up.

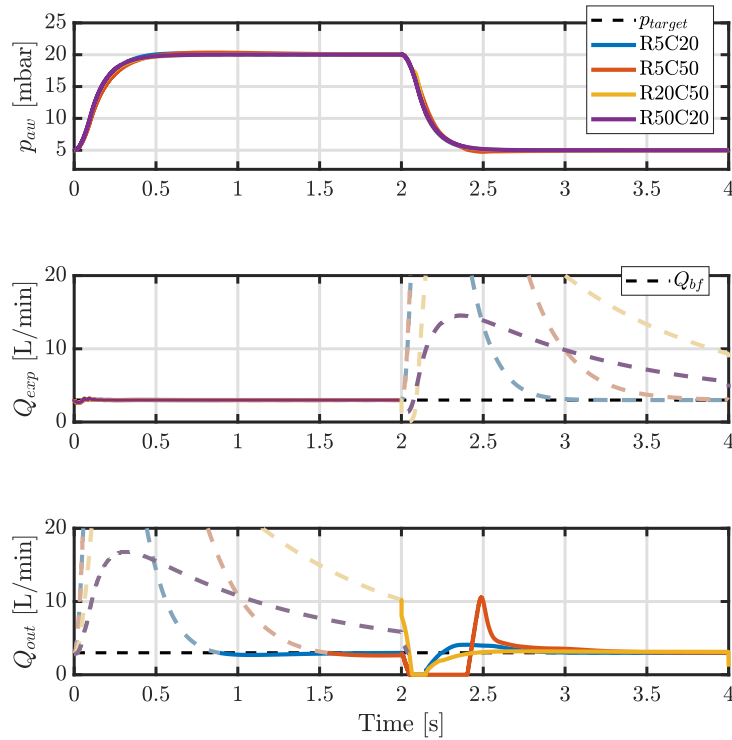


Fig. 5.4. Simulation of the patient-hose-valve system with feedforward and feedback controller. The airway pressure shows almost perfect tracking. The baseflow tracking shows some transients behavior between $t = 2s$ and $t = 2.5s$. After that, perfect tracking is achieved in the bottom figure.

5.3.2 Feedback controller: experimental results

In this section, the decentralized feedback controller in combination with the feedforward controller is tested experimentally. Fig. 5.5 shows the experimental results of the feedback and feedforward controller for the four seconds.

During the inspiration phase, a slight airway pressure overshoot is observed for the R5C20 and R5C50 lungs at approximately $t=0.4s$. The baseflow tracking performance for Q_{exp} is improved for the R20C50 and R50C20 lungs up until $t=2s$. However, the baseflow tracking performance has not improved for the R5C20 and R5C50 lungs. The R5C50 lung shows an undershoot which is explained later in this section.

During the expiration phase, the pressure decrease for p_{aw} is slightly faster. However, this comes at the cost of a significant airway pressure overshoot for all lungs at approximately $t=2.7s$. The baseflow tracking of Q_{out} during the expiration phase shows two very high flow peaks of approximately 30 L/min for the R5C20 and R5C50 lungs. The cause of those peaks is explained at the end of this section. These peaks are not allowed, because this increases the O_2 usage of the mechanical ventilation system significantly which conflicts with the performance requirements in Section 5.1. In addition, the baseflow overshoot causes p_{aw} pressure ripples which need to be corrected for by the pressure controller.

The generally poor performance of the combined feedback and feedforward controller is explained by analyzing the airway pressure error $e_{p_{aw}}$ and the baseflow error e_{bf} in Fig. 5.6. The numbers in the figure show a chain of events that explains the poor performance of the control strategy. The chain of events in Fig. 5.6 is described as:

1. The steep pressure drop during the expiration phase, i.e., at $t=2s$, causes a significant p_{aw} error signal due to the slow response of the feedback controller. This error signal results in a build-up of the integrator state of the C_{1fb} controller.
2. The built-up integral action of the C_{1fb} controller for p_{aw} generates a significant overshoot at $t=2.5s$.
3. The negative pressure error $e_{p_{aw}}$ is compensated for by creating a positive blower pressure u_1 . This pressure generation automatically results in a significant increase in blower output flow Q_{out} . This flow increase results in the large baseflow tracking error e_{bf} , see Fig. 5.6.

The flow undershoot for the R5C50 lung at $t=1.7s$ is also a result of the significant baseflow error of the previous breathing cycle. It is concluded that the implementation of a feedback controller in combination with the feedforward controller induces integrator overshoot effects which cause an undesired performance. In the following section, the feedback and feedforward controller combination is compared to the state-of-practice control solution.

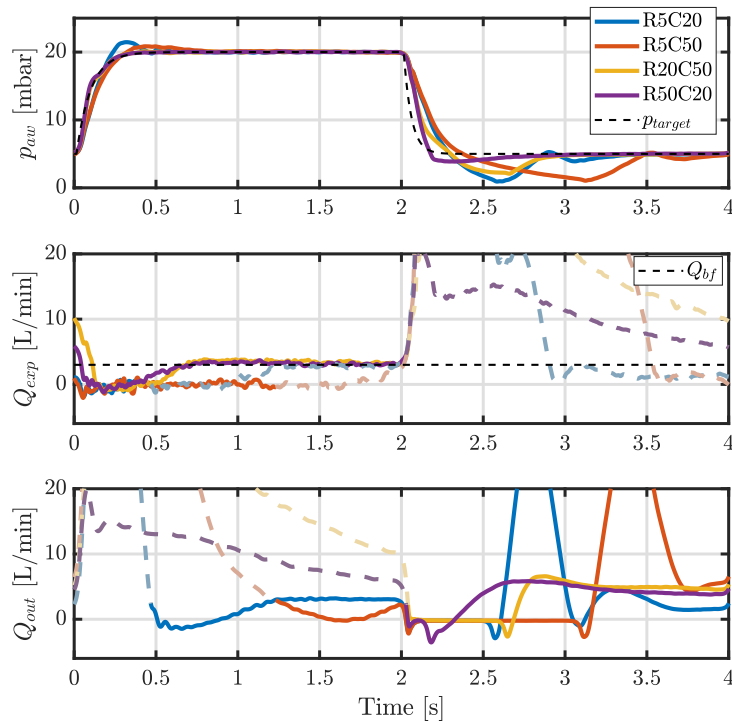


Fig. 5.5. Experimental test of the system with feedforward and feedback controller. The p_{aw} overshoot after $t = 2.5s$ causes significant flow overshoot for Q_{out} .

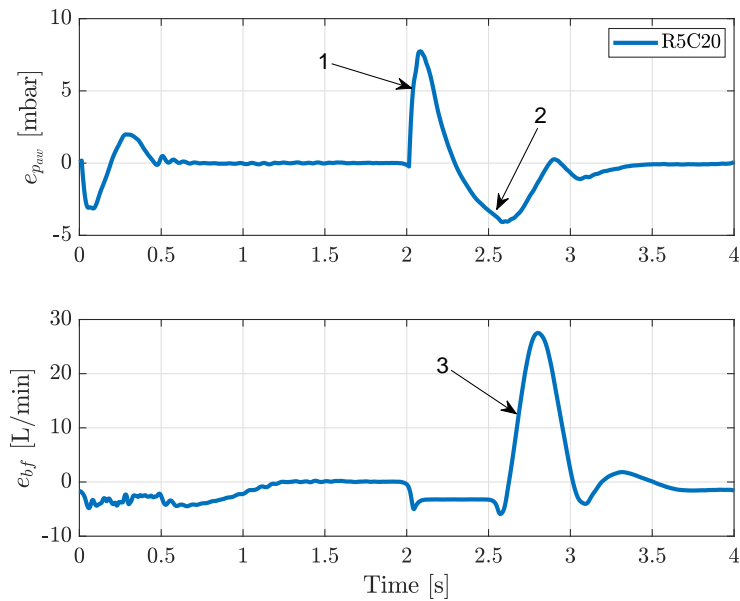


Fig. 5.6. Error signals of the objectives for p_{aw} and Q_{bf} . The numbers indicate a chain of events which causes the poor performance of the proposed control strategy. The pressure error in 1 results in an overshoot effect of the integral control action in 2. This overshoot effect also influences the baseflow behavior in 3.

5.4 State-of-practice control compared to the proposed controller design

In this section, the designed controller of this project is compared to the state-of-practice control solution. The state-of-practice controller is currently used for the produced mechanical ventilation systems of DEMCON Macawi. The controller is designed solely using identification experiments, and uses switching controllers, gain scheduling, and triggers to optimize its performance.

Fig. 5.7 shows the proposed feedforward and decentralized feedback controller in comparison with the state-of-practice controller. For a clear comparison, the controllers are only compared for the R5C20 lung.

During the inspiration phase, it is concluded that the p_{aw} tracking performance is improved. A slightly reduced overshoot is observed at $t=0.3s$ for the proposed controller design. In addition, the settling time of p_{aw} to converge to 20 mbar is similar for both controllers. The baseflow tracking performance during the inspiration phase shows a slower rise-time than the state-of-practice control solution at $t=1s$.

During the expiration phase after $t=2s$, both the pressure and baseflow tracking performance is much worse than the state-of-practice controller. The airway pressure shows a larger overshoot, and the baseflow overshoot is also much higher (30 L/min compared to 14 L/min).

Although the proposed controller of this work does not outperform the state-of-practice controller, it does provide a suitable foundation to build upon for a more insightful controller design. An insightful controller design minimizes the use of resets and gain scheduling, which requires expert knowledge of the ventilation system. This is also part of the sub-objectives in Section 1.4. Multiple recommendations are available to improve the controller performance. In Chapter 6 a collection of these recommendations is presented for the proposed control strategy. However, these recommendations cause a trade-off between controller complexity and performance.

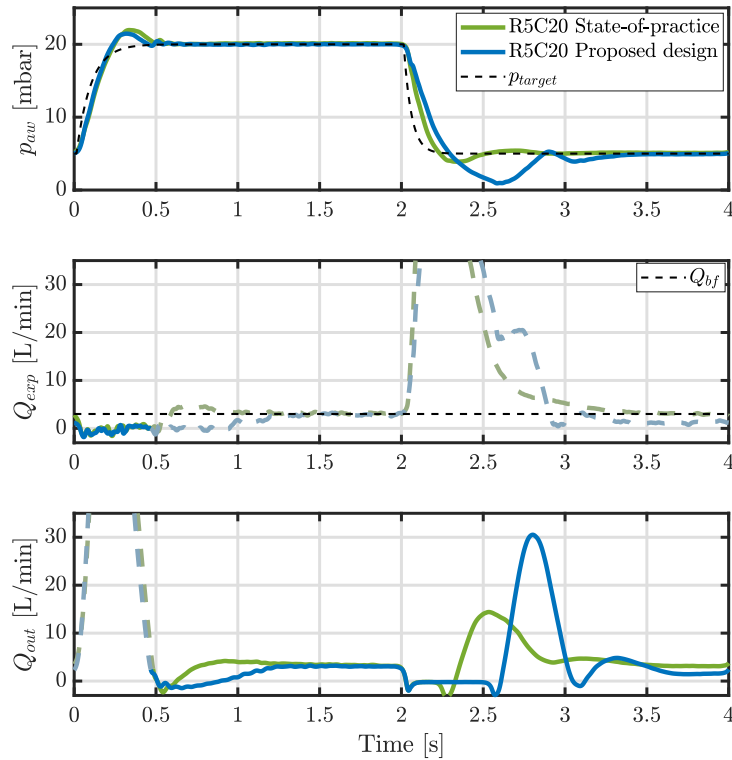


Fig. 5.7. Experimental comparison between the state-of-practice controller and the proposed control solution. The main limitations of the proposed controller design are the pressure overshoot at $t = 2.6s$ in the top figure and the baseflow overshoot at $t = 2.7s$ in the bottom figure.

5.5 Summary

This chapter presented the simulation and experimental results of the feedforward and feedback control strategy of this thesis. It is concluded that the feedforward controller on its own does achieve the desired steady-state targets for pressure and baseflow. However, the rise-time is still too slow for all lungs. During the expiration phase, the non-linear hysteresis effect limit the performance of the feedforward controller. This introduces a significant steady-state error and a long settling time. Thereafter, the feedback controller is implemented on top of the feedforward controller. Although the baseflow tracking performance is improved for lungs with a high resistance, it induces significant pressure and baseflow overshoot during the expiration phase. Finally, it is concluded that the proposed control solution does not outperform the state-of-practice control solution. However, it does provide a suitable foundation for a more insightful controller design without the use of resets and gain scheduling, which require expert knowledge on ventilation systems. In the next chapter, the conclusions and recommendations regarding this thesis are provided.

Chapter 6

Conclusions and Recommendations

In this work, a feedforward and feedback control strategy are proposed for a MIMO mechanical ventilation system with patient. The main goal of the mechanical ventilation system during the pressure-controlled ventilation cycle is to track a desired airway pressure trajectory and to maintain a baseflow through the hose system. The control problem is challenging, because of the physical interaction between inputs and outputs, and the large variety in the unknown patient dynamics. In this thesis, a control strategy has been proposed to improve the pressure and baseflow tracking performance with respect to the state-of-practice control solution. First, in Chapter 2, a non-linear state-space model has been created for the patient-hose-valve system. Thereafter, in Chapter 3, a steady-state feedforward control strategy is proposed. In Chapter 4, a decentralized feedback controller is designed based on experimentally identified linearized MIMO system dynamics. Finally, in Chapter 5, the feedforward and feedback control strategy have been tested in simulation and in an experimental case-study.

In Section 6.1, the main conclusions of this master thesis are presented. Thereafter, in Section 6.2, several recommendations are presented for future research to improve the performance of the designed controller.

6.1 Conclusions

In section 1.4, the main research objective is presented. This objective is divided into several sub-objectives. The main results of this thesis are used to discuss each sub-objective separately. Thereafter, all sub-objectives are combined to derive a thorough conclusion for the main research objective.

- *Derive a dynamical model of the breathing hose system, expiration valve, and patient, which is suitable for a controller design.*

In Chapter 2, a non-linear state-space model is derived for the patient, hose system, and expiration valve. This model is used to gain insight in the dynamics of the MIMO ventilation system. Thereafter, in Chapter 3, the state-space model is extended with an experimentally obtained expiration valve model. The derivation of this model shows that the inputs and outputs are coupled in a non-linear way. The system is proven to be open-loop stable for bounded inputs and has a unique steady-state solution. As a result, the steady-state dynamics of this model are proven to be accurate and are therefore used for an effective feedforward control strategy. However, for perturbations around this steady state, the state-space model is not accurate enough. As a result, the feedback controller is designed independently of the state-space model.

The mechanical ventilation system has two main control objectives: a pressure and flow control objective. The flow objective is to maintain baseflow during the whole breathing cycle. However, it is physically impossible to constantly measure baseflow at one location in the hose system. This

is due to the conflicting objectives of filling the patient's lungs with air and maintaining a baseflow target at the same time. As discussed in Section 2.3, the baseflow target problem is solved by implementing a switching control strategy which uses the expiration flow and blower outlet flow to achieve a fully defined baseflow target during the whole breathing cycle. During phase I, baseflow is maintained at the expiration valve, and during the phase II, III, and IV, baseflow is maintained near the blower, see Fig. 1.4a.

- *Using the dynamical model, establish a well-defined feedforward control strategy which takes the pressure and flow coupling into account.*

A feedforward control strategy is derived, using the dynamical model of Chapter 2. This feedforward controller is designed to compensate for all known and fixed components of the mechanical ventilation system, i.e., the hose system and expiration valve. Using this strategy, it is possible to derive a feedforward control strategy that is independent of the unknown patient dynamics.

The feedforward controller is derived using a steady-state solution of the dynamical model and the inverse expiration valve model. The feedforward controller provides the desired feedforward inputs to control the system during the steady-state phases of the breathing cycle, i.e, phase II and IV in Fig. 1.4a. The accuracy of the feedforward controller during the transient phases is limited, because the system deviates too far from a steady-state operating point. However, the asymptotically stable dynamics and the unique steady-state solution ensure that the system converges to the correct steady-state pressure and baseflow level.

- *Design a feedback controller that controls the large variety of unknown patient dynamics, and attenuates unknown disturbances. Minimize the use of triggers, resets, and gain scheduling to obtain a controller design which is insightful and easy-to-use for control engineers.*

The feedback controller is designed using a decentralized feedback strategy in Chapter 4. This controller is designed without the use of the non-linear state-space model of Chapter 2, because this model is not suitable to simulate perturbations around a steady-state operating point. In addition, the expiration valve model is only accurate for constant inputs.

To design a suitable feedback controller without the state-space model, a linear MIMO system is identified using FRF measurements of the experimental set-up. Consequently, the decentralized feedback controller is tuned based on those identified linearized MIMO transfer functions. Although closed-loop stability of the system with output Q_{exp} and Q_{out} is proven separately, the stability of the closed-loop system with switching dynamics is not guaranteed. A switching stability analysis is performed which guarantees stability for certain switching scenarios. In addition, overall switching stability of the designed controller is verified experimentally by extensive testing.

As discussed, the controller consists of a steady-state feedforward controller and a decentralized feedback controller. These control strategies are relatively straight-forward in control engineering practice and operate without the use of ventilation-related events or triggers. As a result, the proposed controller design is deemed easy-to-use, and a more insightful solution compared to the state-of-practice controller.

- *Experimentally test the designed controller.*

In Chapter 5 the feedforward and feedback controller are tested by means of a simulation and an experimental case-study. From the experiments it is concluded that the control solution is not yet suitable to improve the performance of the state-of-practice control solution. The feedforward control strategy shows promising results in steady state. However, the addition of the decentralized feedback controller does not achieve the desired performance improvements, compared to the state-of-practice control strategy. The lack of performance is the result of modeling uncertainties and unpredictable highly non-linear dynamics during the transient phases I and III of the breathing cycle. These non-linear effects, such as, the hysteresis effect of the piezo valve and the unknown patient dynamics, are not fully taken into account during the controller design process. As a result, the proposed control strategy does not outperform the state-of-practice control solution.

Using the conclusions of each sub-objective, it is possible to draw a conclusion regarding the main objective. The main objective is defined as:

- *Design a controller for a mechanical ventilation system with expiration valve to improve both pressure and baseflow tracking performance, by taking into account the coupling between pressure and flow in the design process.*

The experimental case-study has shown that the designed controller of this work is not yet a suitable control strategy to outperform the state-of-practice control solution. This is caused by the significant amount of model uncertainty of the state-space model, and unpredictable non-linear dynamics which are not incorporated in the controller design process. Although the proposed control strategy is not suitable to improve the pressure and baseflow tracking performance of the state-of-practice control solution, it is easy-to-use for control engineers, and provides a more insightful controller foundation for future control research for this application.

Possible performance improvements are available and are briefly discussed in the following section. In addition, it is most likely possible to apply elements of the proposed control structure, such as, the steady-state feedforward controller, to the state-of-practice control solution to improve its performance.

6.2 Recommendations

In this section, recommendations are presented which can be used to improve the performance of the controlled system in future research. First, in Section 6.2.1, the lack of model accuracy is discussed and a possible improvement is suggested for future research. Thereafter, in Section 6.2.2, a reset integrator for C_{1fb} is suggested to reduce the pressure and flow overshoot during the expiration phase. Finally, in Section 6.2.3, a pressure bound is suggested for C_{2fb} to reduce the build-up effect of the integrator during the transient phases of the breathing cycle, which results in an improved baseflow performance during the expiration phase. The recommendations in Section 6.2.2 and 6.2.3 are motivated using experimental results.

6.2.1 Improved model accuracy

This section describes how the performance of the controlled ventilation system can be improved by increasing the model accuracy. Due to the limited model accuracy, the exact coupling between inputs and outputs is not properly defined in the state-space model in (2.25)-(2.29) for the transient phases I and III of the breathing cycle, see Fig. 1.4a. This limited model accuracy also limits the available controller design choices and their performance.

The main model accuracy limitation is due to the expiration valve resistance model R_{exp} . As described in Section 3.3, the model is only obtained in a constant steady state, which means that it solely depends on the constant inputs u_{1ss} and u_{2ss} . In reality, however, the expiration valve resistance heavily depends the patient effort as well. The patient flow during expiration influences the pressure just before the expiration valve, i.e., p_{exp} , and thus the expiration valve resistance R_{exp} . In addition, the hysteresis effect of the piezo valve is also not taken into account, which causes a significant steady-state error for the feedforward controller. Due to these model limitations, the feedback controller needs to compensate for many unknown disturbances, which limits the performance of the complete ventilation system.

A possible future research objective is to derive a suitable dynamic model for the expiration valve and the hysteresis effect, depending on u_1 , u_2 , and p_{exp} . An improved model helps to gain insight in the transient behavior of the ventilation system during phase I and III. As a result, a more thorough control strategy (possibly non-linear) can be derived to control this transient behavior.

6.2.2 Reset integrator for C_{1fb}

As described in Section 5.3.2, one of the main causes of the poor controller performance is due to the integrator build-up of the p_{aw} controller, i.e., C_{1fb} . The integrator build-up effect is shown in blue in the top figure of Fig. 6.1. As can be seen, the steep pressure drop at $t=2s$ causes a pressure overshoot at $t=2.6s$. As described in Section 5.3.2, this causes a chain of events which also causes a large baseflow overshoot in the bottom figure of Fig. 6.1.

A possible solution for this build-up effect is to apply a reset integrator to C_{1fb} . The main idea of a reset integrator is to reset the internal state of the integral controller to zero when a predefined condition is fulfilled [26]. For this control problem, a suitable reset condition might be $p_{aw} < PEEP$ during the expiration phase. Using this reset condition, the build-up effect of the feedback controller is prevented.

Fig. 6.1 shows the comparison between the proposed feedback controller from this thesis with and without an additional reset during experiments. It is concluded that the implementation of a reset integrator significantly reduces the p_{aw} overshoot during the expiration phase, i.e., at $t=2.6$ s. Due to the coupling effect between pressure and flow, the reduced p_{aw} overshoot also reduces the baseflow overshoot of Q_{out} during the expiration phase at $t=2.7$ s. In addition, the reduced baseflow overshoot results in a faster settling time of the baseflow target at $t=3.5$ s for Q_{out} . This effect also translates to the next breathing cycle. It is observed that during the inspiration phase at $t=1$ s, the baseflow rise-time is slightly faster compared to the controller without a reset. However, this faster rise time results in a minor baseflow overshoot.

In general, it can be concluded that the implementation of a reset integrator for C_{1fb} gives promising results. Although this solution is relatively easy to implement in the proposed controller design, further research should indicate if this reset integrator is stable in every scenario. In addition, this reset complicates the overall controller design. A trade-off must be made regarding improving performance and control structure simplicity.

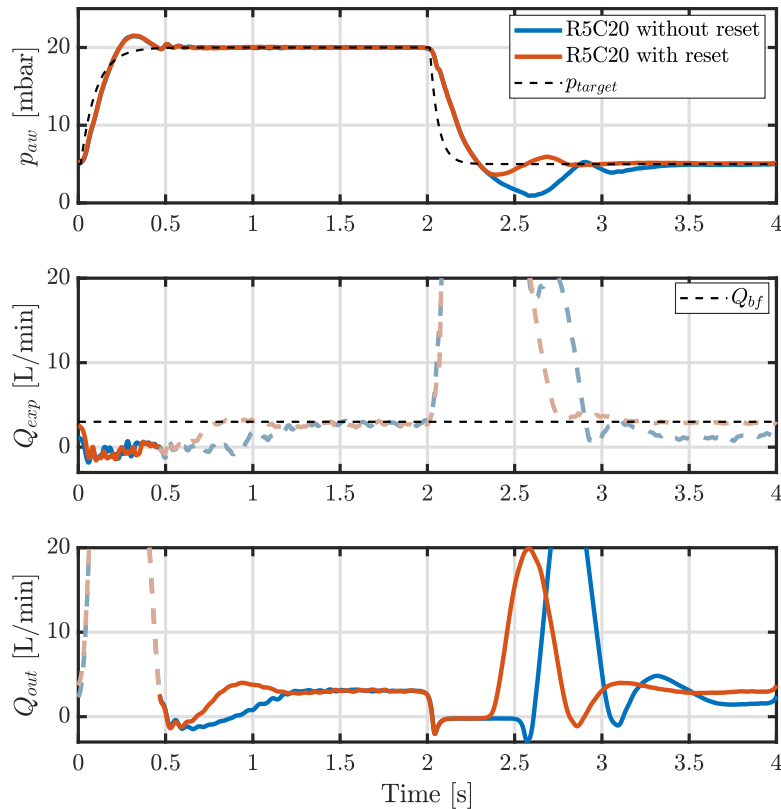


Fig. 6.1. Experimental implementation of a reset integrator for the designed control strategy. Adding a reset integrator prevents an airway pressure and baseflow overshoot.

6.2.3 Pressure bound for C_{2fb}

In this section, an improvement for the C_{2fb} feedback controller is presented. This improvement is based on a pressure error bound and is analyzed using the experimental set-up.

A limitation of the feedback controller is caused by the coupling effect between pressure and flow during phase III of the breathing cycle, see Fig. 1.4a. During this phase, it is very challenging to track baseflow using Q_{out} due to the slow response of the C_{2fb} feedback controller. This is also observed in Fig. 5.5 between $t=2s$ and $t=2.5s$. During this phase, the baseflow integrator in C_{2fb} is still building up to achieve the desired baseflow level. This integrator build-up effect is shown in blue in the middle figure of Fig. 6.2. As depicted, the integrator signal u_{2fb} builds up from $t=2s$ up until $t=2.5s$ without any baseflow generation at Q_{out} in the bottom figure. Due to this build-up effect, a flow overshoot occurs at $t=2.8s$, which results in a long settling time for Q_{out} to converge to the baseflow target Q_{bf} for the remainder of the expiration phase.

A solution for this problem is to stop the integrator build-up effect of C_{2fb} during the expiration phase, i.e., when the pressure error $e_{p_{aw}}$ is high. To achieve this, a pressure error bound is defined as $\nu = |e_{p_{aw}}|$, in which ν is a positive tunable parameter. This bound can be applied to the C_{2fb} controller as follows:

- If $|e_{p_{aw}}| > \nu$, i.e., during large pressure errors in phase III, the internal state of the integrator for C_{2fb} is frozen. In other words, the integrator input is zero.
- If $|e_{p_{aw}}| < \nu$, the internal integrator state is updated again.

Using this strategy, the main result is that the baseflow controller does not build up when the pressure error exceeds the pressure error bound ν , i.e., during the expiration phase III. The results are shown in Fig. 6.2. In this figure, the feedback with feedforward controller is compared with a C_{1fb} reset and a pressure bound on C_{2fb} and the same controller without the bound and

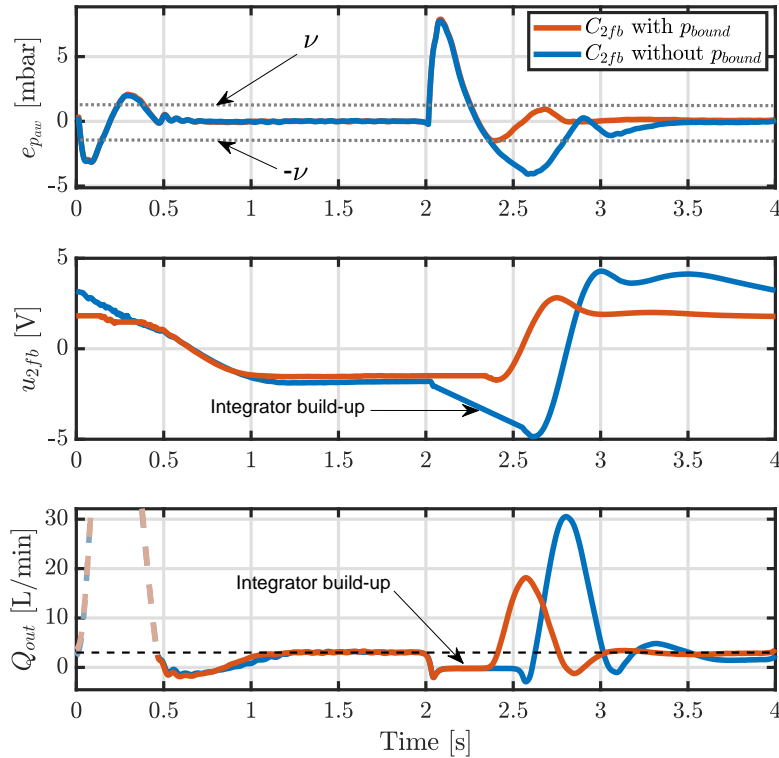


Fig. 6.2. Experimental implementation of a pressure error bound ν to prevent integrator build-up for u_{2fb} .

reset. As depicted in the top figure, the pressure bound is chosen as $\nu = 1$. It is observed that u_{2fb} freezes as soon as the pressure error exceeds the bound at $t=2s$. As a result, the bottom figure shows that the baseflow overshoot for Q_{out} during expiration is reduced from 30 to 18 L/min. In addition, the settling time is reduced as well and a small final baseflow error is achieved.

Fig. 6.3 compares the state-of-practice control solution with the proposed control solution with reset and pressure error bound. During the inspiration phase, the pressure tracking performance is slightly better than the state-of-practice solution. The baseflow tracking is slightly worse, but it does not show any overshoot compared to the state-of-practice solution. During expiration, the proposed solution shows a slightly slower pressure drop. The pressure overshoot at $t=2.4s$ is similar for both solutions. The baseflow tracking controller shows a slightly higher flow overshoot at $t=2.6s$. However, the settling time at $t=3s$ is improved.

It is concluded that this proposed solution results in a similar performance compared to the state-of-practice control solution. This solution is also easy to implement. However, future research should indicate if this solution does not induce instability. In addition, this strategy induces another ventilation related event to the proposed controller design which conflicts with the intuitive controller design objective.

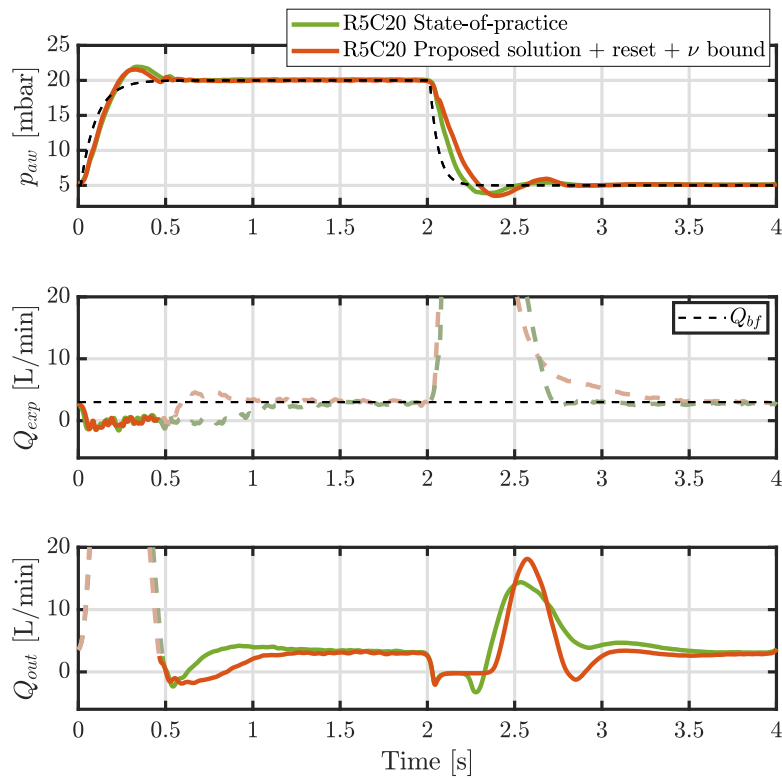


Fig. 6.3. Experimental comparison between the proposed controller design with pressure error bound ν and reset, and the state-of-practice control solution.

Bibliography

- [1] Macawi DEMCON. [Online] <https://www.macawi.com>, 2019.
- [2] L. Gattinoni, E. Carlesso, P. Cadringer, F. Valenza, F. Vagginelli, and D. Chiumello. Physical and biological triggers of ventilator-induced lung injury and its prevention. *European Respiratory Journal, Supplement*, 22(47):15–25, 2003.
- [3] D Carney, J DiRocco, and G Nieman. Dynamic alveolar mechanics and ventilator-induced lung injury. *Critical Care Medicine*, 33(3), 2005.
- [4] M.A. Warner and B. Patel. Mechanical Ventilation. In *Benumof and Hagberg’s Airway Management*, pages 981–997.e3. Elsevier Inc., third edition, 2013.
- [5] R.L. Chatburn. Classification of Ventilator Modes : Update and Proposal for Implementation. *Respiratory care*, 52(3):301–323, 2007.
- [6] J. H. T. Bates. *Lung mechanics*. Cambridge University Press, 2009. ISBN 9780521509602.
- [7] R.L. Chatburn. Engineering principles applied to mechanical ventilation. pages 406–410, 2004.
- [8] D. W. Guillaume and M. Borrello. Simulating gas flow through the exhalation leg of a respirator’s patient circuit. *Journal of Biomedical Engineering*, 13(1):77–82, 1991.
- [9] Y. Li. Investigation on dynamics of the flow control unit in ventilator systems and its fundamental performance limitations. In *Proceedings of the American Control Conference*, pages 2181–2186, Portland, OR, USA, 2005. IEEE.
- [10] M. Borrello. Modeling and control of systems for critical care ventilation. In *Proceedings of the American Control Conference*, pages 2166–2180, Portland, OR, USA, 2005. IEEE.
- [11] O. Smal, B. Raucent, and H. Jeanmart. Fluid flow modelling of a micro-valve. *International Journal for Simulation and Multidisciplinary Design Optimization*, 3(2):356–362, 2009.
- [12] M. Scheel, T. Schauer, A. Berndt, and O. Simanski. Model-based control approach for a CPAP-device considering patient’s breathing effort. *IFAC-PapersOnLine*, 50(1):9948–9953, 2017.
- [13] B. Hunnekens, S. Kamps, and N. van de Wouw. Variable-Gain Control for Respiratory Systems. *IEEE Transactions on Control Systems Technology*, PP:1–9, 2018.
- [14] M. Scheel, A. Berndt, and O. Simanski. Iterative learning control: An example for mechanical ventilated patients. *IFAC-PapersOnLine*, 28(20):523–527, 2015.
- [15] J. Reinders, F. Heck, B. Hunnekens, T. Oomen, and N. van de Wouw. Online hose calibration for pressure control in mechanical ventilation. In *Proceedings of American Control Conference*, Philadelphia, PA, USA, 2019.
- [16] J. Mohammadpour and C. W. Scherer. *Control of Linear Parameter Varying Systems with Applications*. Springer, New York, 1st edition, 2012. ISBN 9781461418320.

-
- [17] N. van de Wouw, E. Lefeber, and I. Lopez Arteaga, editors. *Nonlinear systems: Techniques for Dynamical Analysis and Control*. Springer, 2017. ISBN 978-3-319-30356-7.
- [18] Joao P. Hespanha. *Linear Systems Theory*. Princeton University Press, 2009. ISBN 9780691140216.
- [19] S. Skogestad and I. Postlethwaite. *Multivariable Feedback Control: Analysis and Design*. Wiley, second edition, 2005. ISBN 978-0-470-01167-6.
- [20] H. K. Khalil. *Nonlinear Systems*. Prentice Hall, 3th edition, 2002. ISBN 978-1-29203-921-3.
- [21] H. Nijmeijer and A. van der Schaft. *Nonlinear Dynamical Control Systems*. Springer, 1990. ISBN 9780387972343.
- [22] M. Steinbuch, R. Merry, M. Boerlage, M. Ronde, and M. van de Molengraft. Advanced Motion Control Design. *W. S. Levine (Ed.), The Control Handbook, Control System Applications, Second edition*, pages 27–1–27–25, 2010.
- [23] R. Pintelon and J Schoukens. *System Identification: A Frequency Domain Approach*. John Wiley & Sons Inc., Hoboken NJ, 2nd edition, 2012. ISBN 9780470640371.
- [24] G. Franklin, J. D. Powell, and A. Emami-Naeini. *Feedback Control of Dynamic Systems*. Pearson, 7th edition, 2015. ISBN 9780136019695.
- [25] D. Liberzon. *Switching in Systems and Control*. Springer Science+Business Media, LLC, 2003. ISBN 9781461265740.
- [26] M. F. Heertjes, K. G.J. Gruntjens, S. J.L.M. Van Loon, N. Kontaras, and W. P.M.H. Heemels. Design of a variable gain integrator with reset. In *Proceedings of the American Control Conference*, volume July, pages 2155–2160, Chicago IL, 2015.

Appendix A

Steady-state solution

In this chapter, the constant steady-state solution of the patient-hose-valve system in (2.25)-(2.29) is derived, which shows that during a constant steady state, $p_{aw} = p_{lung}$ and $Q_{pat} = 0$.

The constant steady-state solution is achieved by setting $\dot{p}_{lung} = 0$. As a result, the state equation of (2.25) changes to

$$\bar{p}_{lung} = -\mathbf{A}^{-1}(u_{ss})\mathbf{B}(u_{ss})u_{1ss}, \quad (\text{A.1})$$

in which \bar{p}_{lung} is the constant lung pressure, $\mathbf{A}(u_{ss})$ is the state matrix in a constant steady state, and $\mathbf{B}(u_{ss})$ is the input matrix in steady state. The equation in (A.1) describes the constant steady-state solution of the lung dynamics. Substituting the matrices $\mathbf{A}(u_{ss})$ and $\mathbf{B}(u_{ss})$ results in

$$\bar{p}_{lung} = \frac{R_{hose2} + R_{\xi}(u_{ss})}{R_{hose1} + R_{hose2} + R_{\xi}(u_{ss})}u_{1ss}. \quad (\text{A.2})$$

It is concluded from (A.2), that the constant steady-state lung dynamics only depend on the expiration valve resistance and hose resistances, and that the patient parameters R_{aw} and C_{lung} are not present. Hence, the constant steady-state solution is patient independent.

To show that during a constant steady state $p_{aw} = p_{lung}$, (A.1) is inverted, which results in

$$u_{1ss} = -\mathbf{B}^{-1}(u_{ss})\mathbf{A}(u_{ss})\bar{p}_{lung}. \quad (\text{A.3})$$

The constant steady-state output solution for p_{aw} is described by

$$p_{aw} = \mathbf{C}_{\mathbf{p}}(u_{ss})\bar{p}_{lung} + \mathbf{D}_{\mathbf{p}}(u_{ss})u_{1ss}. \quad (\text{A.4})$$

Substituting the constant steady-state lung dynamics from (A.3) in (A.4) results in

$$p_{aw} = \mathbf{C}_{\mathbf{p}}(u_{ss})\bar{p}_{lung} - \mathbf{D}_{\mathbf{p}}(u_{ss})\mathbf{B}^{-1}(u_{ss})\mathbf{A}(u_{ss})\bar{p}_{lung}. \quad (\text{A.5})$$

Next, it is possible to fill in the state-space matrices from (2.26)-(2.29). The equation in (A.5) then simplifies to

$$p_{aw} = \bar{p}_{lung}. \quad (\text{A.6})$$

From this equation it is concluded that during a constant steady-state, i.e., $\dot{p}_{lung} \rightarrow 0$, the airway pressure p_{aw} and lung pressure p_{lung} equalize. Consequently, the patient flow Q_{pat} is reduced to zero. Due to the asymptotically stable open-loop dynamics for bounded inputs in Section 2.2, it is concluded that the system with constant inputs will always achieve this constant steady state.

Appendix B

LUT experiment for the expiration valve

This chapter describes the derivation of a Look Up Table (LUT) for the expiration valve resistance R_{exp} .

B.1 Purpose

The purpose of this experiment is to obtain a more realistic expiration valve resistance model R_{exp} , by means of a LUT. This LUT provides insight in the dynamics of the expiration valve, and is used as part of the steady-state feedforward controller in Chapter 3. The LUT is derived in steady state, such that it only depends on two parameters, i.e., u_1 and u_2 . As a result, the proposed LUT is only accurate during steady-state operation of the mechanical ventilation system and patient. In the following section, the experimental set-up is briefly described.

B.2 Set-up

For the LUT experiment, the following items are required:

- Bonemine ventilation module
- Inspiration hose
- Expiration hose
- Membrane actuated expiration valve
- Seal (To close off the patient entrance of the hose).
- dSPACE setup
- Laptop

Fig. 3.4 shows a schematic drawing of the proposed set-up. The hose system is closed off at the patient side which means that all generated flow from the blower is equal to the flow that leaves the system, i.e., $Q_{out} = Q_{exp}$. In the following section, the measurement method is described.

B.3 Method

In this section, the method of obtaining a LUT is explained in detail. The LUT is accurate during steady state operation of the system, i.e., $Q_{pat} = 0$. As a result, it is possible to derive a two dimensional look up table which estimates R_{exp} as:

$$R_{exp} = f(u_1, u_2). \quad (\text{B.1})$$

The following steps are applied to derive a LUT for R_{exp} :

1. Set the blower pressure u_1 to a constant value.
2. Ramp down the piezo voltage u_2 from 24 to -24 Volt ($u_2 \downarrow$).
3. Ramp up the piezo voltage u_2 from -24 to 24 Volt ($u_2 \uparrow$).
4. Q_{exp} and p_{exp} are averaged to eliminate a maximum error due to hysteresis, as explained in Section 3.3. The following averaging equations are used:

$$\tilde{p}_{exp} = \frac{p_{exp}(u_2 \downarrow) + p_{exp}(u_2 \uparrow)}{2}, \quad \tilde{Q}_{exp} = \frac{Q_{exp}(u_2 \downarrow) + Q_{exp}(u_2 \uparrow)}{2}, \quad (\text{B.2})$$

in which \tilde{Q}_{exp} and \tilde{p}_{exp} are the averaged values of Q_{exp} and p_{exp} . Fig. B.1 shows an example of the hysteresis curve for a measurement of Q_{exp} .

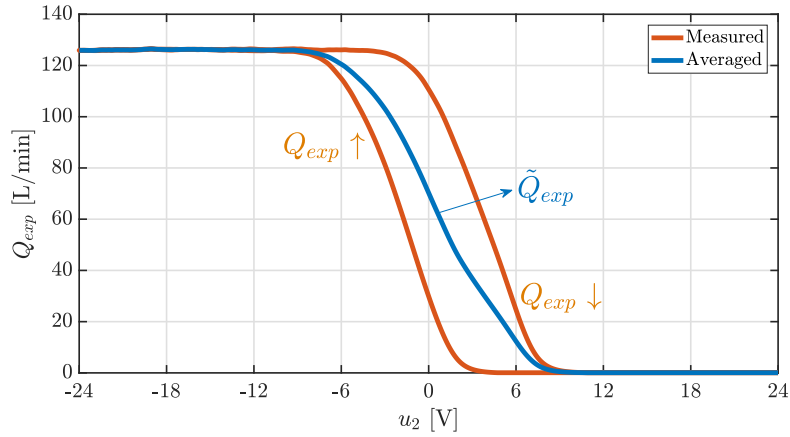


Fig. B.1. Hysteresis effect of the piezo valve.

5. Derive the average expiration valve resistance \tilde{R}_{exp} using:

$$\tilde{R}_{exp} = \frac{\tilde{p}_{exp}}{\tilde{Q}_{exp}} \quad (\text{B.3})$$

6. Step 1 to 5 is now repeated for several different constant values of u_1 to derive a 3d-surface for \tilde{R}_{exp} . The lowest value for u_1 is 2.5 mbar, which is increased with increments of 2.5 mbar up until 40 mbar.

B.4 Limitations

This section describes the limitations of the proposed LUT strategy for R_{exp} . The LUT is only valid during steady state which means that it is not accurate during the transient phases, i.e., phase I and III of the breathing cycle in Fig. 1.4a. As a result, when $Q_{pat} > 0$ then R_{exp} is estimated too high. When $Q_{pat} < 0$ then R_{exp} is estimated too low.

Appendix C

TU/e Code of Scientific Conduct

Declaration concerning the TU/e Code of Scientific Conduct for the Master's thesis

I have read the TU/e Code of Scientific Conductⁱ.

I hereby declare that my Master's thesis has been carried out in accordance with the rules of the TU/e Code of Scientific Conduct

Date

26-11-2019

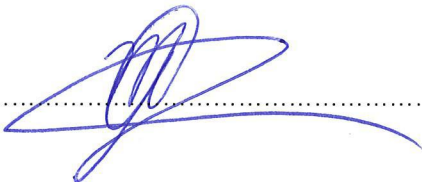
Name

MAS Geerven

ID-number

1020646

Signature



Submit the signed declaration to the student administration of your department.

ⁱ See: <https://www.tue.nl/en/our-university/about-the-university/organization/integrity/scientific-integrity/>

The Netherlands Code of Conduct for Scientific Integrity, endorsed by 6 umbrella organizations, including the VSNU, can be found here also. More information about scientific integrity is published on the websites of TU/e and VSNU